Targeting of hepatocytes

Using vector-conjugated liposomes:

evaluation of targeting strategies

INAUGURALDISSERTATION

zur

Erlangung der Würde eines Doktors der Philosophie

vorgelegt der

Philosophisch-Naturwissenschaftlichen Fakultät

der Universität Basel

von

Pascal Detampel

aus Riehen (BS)

Basel, 2013

Genehmigt von der Philosophisch-Naturwissenschaftlichen Fakultät

auf Antrag von

Prof. Dr. Jörg Huwyler

Prof. Dr. Stephan Krähenbühl

Basel, den 11.12.2012

Dekan Prof. Dr. Jörg Schibler

Originaldokument gespeichert auf dem Dokumentenserver der Universität Basel
edoc.unibas.ch

Dieses Werk ist unter dem Vertrag „Creative Commons Namensnennung-Keine kommerzielle Nutzung-Keine Bearbeitung 2.5 Schweiz“ lizenziert. Die vollständige Lizenz kann unter
creativecommons.org/licences/by-nc-nd/2.5/ch
eingesehen werden.

Namensnennung-Keine kommerzielle Nutzung-Keine Bearbeitung 2.5 Schweiz

---

Sie dürfen:

das Werk vervielfältigen, verbreiten und öffentlich zugänglich machen

Zu den folgenden Bedingungen:

Namensnennung. Sie müssen den Namen des Autors/Rechteinhabers in der von ihm festgelegten Weise nennen (wodurch aber nicht der Eindruck entstehen darf, Sie oder die Nutzung des Werkes durch Sie würden entlohnt).

Keine kommerzielle Nutzung. Dieses Werk darf nicht für kommerzielle Zwecke verwendet werden.

Keine Bearbeitung. Dieses Werk darf nicht bearbeitet oder in anderer Weise verändert werden.

- Im Falle einer Verbreitung müssen Sie anderen die Lizenzbedingungen, unter welche dieses Werk fällt, mitteilen. Am Einfachsten ist es, einen Link auf diese Seite einzubinden.
- Jede der vorgenannten Bedingungen kann aufgehoben werden, sofern Sie die Einwilligung des Rechteinhabers dazu erhalten.
- Diese Lizenz lässt die Urheberpersönlichkeitsrechte unberührt.

Die gesetzlichen Schranken des Urheberrechts bleiben hiervon unberührt.

Die Commons Deed ist eine Zusammenfassung des Lizenzvertrags in allgemeinverständlicher Sprache: http://creativecommons.org/licenses/by-nc-nd/2.5/ch/legalcode.de

Haftungsausschluss:
Die Commons Deed ist kein Lizenzvertrag. Sie ist lediglich ein Referenztext, der den zugrundeliegenden Lizenzvertrag übersichtlich und in allgemeinverständlicher Sprache wiedergibt. Die Deed selbst entfaltet keine juristische Wirkung und erscheint im eigentlichen Lizenzvertrag nicht. Creative Commons ist keine Rechtsanwaltsgesellschaft und leistet keine Rechtsberatung. Die Weitergabe und Verlinkung des Commons Deeds führt zu keinem Mandatsverhältnis.

Quelle: http://creativecommons.org/licenses/by-nc-nd/2.5/ch/ Datum: 3.4.2009

This work is dedicated to my wife Aurélie.

"Plus j'étudie la nature et plus je suis émerveillé par les travaux de Notre Créateur."

Louis Pasteur (1822-1895)

Table of Contents

Acknowledgements

First, I want to thank Prof. Dr. Jörg Huwyler for not only giving me the chance to work on this fascinating topic, but also for his consistently encouraging manner how to interpret my results and teaching me not being too critical with myself. I have learned so much from him and it is one of the biggest privileges having him as a supervisor from a scientific and interpersonal point of view.

Next, I want to thank Prof. Dr. Stephan Krähenbühl for supporting the project from the beginning on. His feedback was always a very enriching and important part of my thesis, and without him the project would not have been possible. Additionally, I appreciated the chance of becoming an "external" member of his team, which gave me the opportunity to interact with many of his group members. Hence, I am very grateful to Karin Brecht, in helping me to get the cell culture started, and Jamal Bouitbir, for introducing me to histology techniques and proofreading my thesis. But also Réjane Morand, Swarna Maseneni, Anja Zahno, and all the other members of the Clinical Pharmacology and Toxicology group who aided me a lot at various tasks. Furthermore, I had the possibility to build up a personal relationship with Massimiliano Donzelli and Beatrice Vetter.

I also want to thank Prof. Dr. Alex Odermatt who agreed to take the role as a chairman in my PhD defense committee. Further, he actively supports the interaction between our groups, and in this context, I want to express my gratitude to Balazs Legeza for involving me into his project and the valuable discussions and help from Thierry Da Cunha.

Looking back to the time in the lab in the Pharmazentrum, I am very thankful for the pleasant working atmosphere that we had. Especially the relationships with Le-Ha Dieu and Helene Kettiger, with whom I spent most of my lab time, were growing to deep friendships. Thank you. Further, I am also grateful for the enjoyable time with the other team members, particularly Susanne Schenk, Vimalkumar (Vimal) Balasubramanian, André Ziegler, Stefan Winzap, Marine Camblin, Stefan Jenzer and all the other members of the group in the Rosental.

I appreciated to share my daily lab life with Carla Kirchhofer and Urs Duthaler from the Swiss Tropical and Public Health Institute, with whom I spent the time at the Rosental and in the

Pharmazentrum. In this context, I also want to mention especially Mireille Vargas, who helped me a lot in the preparation of the *in vivo* experiments and Isabel Meister.

Getting the chance to hand over the research project to a successor is a privilege and an appreciation of the achieved work. But having Dominik Witzigmann as a PhD follower, who is not only highly motivated but has already a great scientific working attitude, is something special. Therefore, I am looking forward to the next months, during which we will spend a lot of time together in the lab. Thank you also for giving me valuable inputs to the final draft of this thesis.

Furthermore, I want to thank the people from the FHNW in the Rosental and especially Georg Imanidis, Berndt Joost, Martin Kuentz, Fabienne Thoenen, Michael Lanz, Martin Cavegn, Martin Studer, Venkateshwar (Venky) Rao Nalluri, Yvonne Arnold, and Daniela Stoller, Claudia Escher, René Prétôt, Peter Spies, and many more. I really enjoyed working with you.

A special thanks goes also to Christina Erb and Evelyne Rudin for not only helping in various administrative duties, but also for their support beyond their normal daily tasks.

Regarding my pharmacokinetic studies, I want to thank Mareike Beck from DSM and Martin Schmutz from the FHNW for the great collaboration.

I do not want to miss to thank Christiane Kluba, Simon Kleeb, and many others, who I have not mentioned, for various valuable interactions during my PhD thesis project.

This work was financially supported by the Senglet Foundation. In particular, I want to thank their president Dr. Beat Disler for the uncomplicated handling of the sponsorship.

Last but not least, I want to thank my family-in-law and especially Anne for supporting me during the last few months. But most notably, I am so grateful to my wife, Aurélie, for her endless patience and encouragement, not only during my thesis. When I frequently and miserably failed to come home at the promised time, she only questioned if the topic of my PhD would not be better described by the title “space-time distortion”. Thank you for your infinite love.

Abbreviations

7-AAD, 7-aminoactinomycin D

ABC, accelerated blood clearance

AF, asialofetuin

ApoE, apolipoprotein E

ASGPR, asialoglycoprotein receptor

ASGPR-1/2, asialoglycoprotein receptor subunit 1 and 2

AUC, area under the concentration-time curve

BBB, blood-brain barrier

BSA, bovine serum albumin

CDR, complementarity determining regions

CF, 5(6)-carboxyfluorescein

CF-NHS, 5(6)-carboxyfluorescein N-hydroxysuccinimide ester

Chol, cholesterol

CLSM, confocal laser scanning microscopy

DIC, differential interference contrast

DSPC, 1,2-distearoyl-sn-glycero-3-phosphocholine

DSPE, 1,2-distearoyl-sn-glycero-3-phosphoethanolamine

DSPE-CF, 1,2-dioleoyl-sn-glycero-3-phosphoethanolamine-N-(carboxyfluorescein) (ammonium salt)

DSPE-PEG(2000), 1,2-distearoyl-sn-glycero-3-phosphoethanolamine-N-[methoxy(polyethylene glycol)-2000] (ammonium salt)

DSPE-PEG(2000)-Mal, 1,2-distearoyl-sn-glycero-3-phosphoethanolamine-N-[maleimide(poly-ethylene glycol)-2000] (ammonium salt)

DSPE-Rho, 1,2-dioleoyl-sn-glycero-3-phosphoethanolamine-N-(lissamine rhodamine B sulfonyl) (ammonium salt)

EDTA, ethylenediaminetetraacetic acid

EPR, enhanced permeability and retention

Gal, D-galactose

GalNAc, N-acetyl- D-galactosamine

GM_1, monosialotetrahexosylganglioside

HBV, hepatitis B virus

HCV, hepatitis C virus

HCC, Hepatocellular carcinoma

HPLC, high-performance liquid chromatography

IgG, Immunoglobulin G

kDa, kilo dalton

KCR, Kupffer cell receptor

LED, light-emitting diode

LUV, large unilamellar vesicles

mAb, monoclonal antibody

MLV, multilamellar vesicles

PBS, phosphate buffered saline

PDI, polydispersity index

PEG, polyethylene glycol

PFA, paraformaldehyde

QD, quantum dot

RES, reticulo-endothelial system

ROI, regions of interest

RPE, R-phycoerythrin

rpm, rounds per minute

SDS-PAGE, sodium dodecylsulphate-polyacrylamide gel electrophoresis

STPP, stearyl-triphenylphosphonium bromide

SUV, small unilamellar vesicles

TLC, thin layer chromatography

Summary

The need for specific targeting strategies towards hepatocytes stems from the lack of efficient therapeutic options to treat numerous serious liver diseases. Moreover, various genetic disorders, such as α1-antitrypsin deficiency and hemophilia A and B, are depending on an efficient gene delivery to defined cells, such as hepatocytes, preferentially avoiding viral vectors. Since the asialoglycoprotein receptor is primarily expressed by liver parenchymal cells, it offers a potential target for a cell specific delivery system.

First, the binding of various vectors was analyzed, using the human hepatocellular carcinoma cell line HepG2 as an *in vitro* model. While the uptake of D-galactose as a monomer was non-specific, the glycoprotein asialofetuin was analyzed as an alternative vector, which represents the desialated derivative of fetuin, containing multi-antennary galactose-terminating glycan residues. Next to a pronounced cellular accumulation, the uptake was markedly inhibited in the presence of an excess of free asialofetuin, indicating specific endocytosis through the asialoglycoprotein receptor. Therefore, asialofetuin was selected as an ideal vector for the further development of a drug delivery system targeting liver parenchymal cells.

Asialofetuin was covalently attached to pegylated liposomes, yielding a highly monodisperse preparation with a particle size below 100 nm. A subsequently incubation with HepG2 cells resulted in a specific endocytosis of the vesicles, providing an experimental proof of concept for targeting hepatocytes *in vitro*. The delivery and intracellular accumulation in HepG2 cells were investigated by incorporating various organic dyes and fluorescent semiconductor nanocrystals, also known as quantum dots, into liposomes. The cellular uptake of asialofetuin-conjugated liposomes, loaded with quantum dots, resulted in a bright fluorescent signal, which was impaired by the need for a specific photoactivation prior to fluorescence analysis. Despite their challenging optical properties, quantum dots are valuable fluorochromes for further optimization of drug targeting strategies.

Finally, a proof of principle for a hepatocyte specific delivery was provided *in vivo*, by intravenously injecting rats with asialofetuin-conjugated and pegylated liposomes, which were taken up by the liver parenchymal cells. In contrast, accumulation in hepatocytes was reduced by co-injecting free asialofetuin and conventional liposomes were uniquely engulfed by Kupffer cells.

Summarized, asialofetuin-conjugated pegylated liposomes represent a novel approach, combining desialated glycoproteins, which exhibit a high affinity towards the asialoglycoprotein receptor, with long circulating vesicles, for a specific targeting of liver parenchymal cells. This concept represents a most promising strategy for a hepatocyte specific drug delivery system and gives the opportunity for further studies, such as the isolated utilization of glycans only, to avoid immunogenic reactions.

These targeting strategies can be used to deliver drugs to diseased tissues or organs within our body. This reflects our interests to modulate the pharmacokinetics of drugs using specific formulation strategies. Two additional pharmacokinetic investigations of pharmaceutical relevant substances were published in peer-reviewed journals. One study addresses the risk of physical drug interactions of ceftriaxone with calcium in human plasma, and the second one discusses the interaction potential of high doses of resveratrol with various cytochrome P450 isoenzymes. These studies are presented in the section “Appendix”, to separate them from the drug targeting approach of hepatocytes using liposomal formulations.

1. Introduction

This section will provide arguments why drug targeting strategies are needed to deliver drugs to the liver and in particular to the hepatocyte. Technical possibilities, such as the use of liposomal carriers, are discussed. Additionally, the use of quantum dots, as a new tracer for *in vitro* and also for a potential optimization tool *in vivo*, is outlined.

1.1. Targeting of the liver

The liver is a central organ, responsible among others for metabolism, detoxification, bile production, protein synthesis, storage, hormone synthesis, and hosting parts of the mononuclear phagocyte system. The functional units are built up as liver lobules, which transport the blood from the portal vein and the hepatic artery through the sinusoids to the central vein (Figure 1, panel A). Hepatocytes, making up about 80% of the cells in the liver, are separated from the blood stream by the space of Disse and hepatic sinusoidal endothelial cells (Figure 1, panel B), which build up an endothelium with fenestrae of approximately 100 to 150 nm (Thews et al. 1999; Pathak et al. 2008; M. Tanaka et al. 2011).

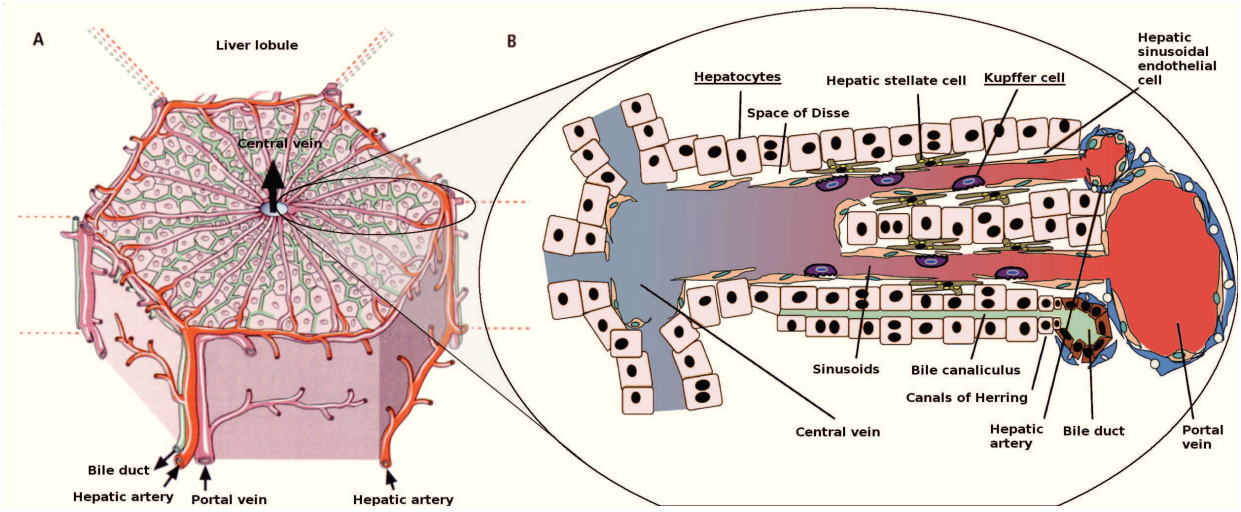

Figure 1: Schematic representation of a liver lobuli and the architecture of sinusoids. The blood from the portal vein and the hepatic artery flows through the sinusoids to the central vein. Sinusoidal endothelial cells form a fenestrated layer, which allows only small particles (< 150 nm) to pass from the blood flow into the space of Disse and to reach hepatocytes. In contrast, Kupffer cells are located in the sinusoids and have directly access to the blood flow. Adapted from Thews et al. 1999; Tanaka et al. 2011

Hepatocytes are taking over many of the above-mentioned functions of the liver and with their variety of metabolizing enzymes, they are primarily responsible for clearing many drugs (Testa & Krämer 2006). Intestinal absorbed substances are transported via the portal vein to the liver and in many cases are extensively metabolized at this site, which belongs to the so-called first-pass effect. Therefore, hepatocytes are often exposed to high amounts of drugs, due to their natural function without any targeting system. Developing strategies to deliver drugs to the liver, and especially to hepatocytes, raises the question about the therapeutic need, when these cells metabolize most of the xenobiotics anyway. Hence, it can appear to be superfluous to evaluate specific drug-delivering systems to hepatocytes.

This view stands in contrast to the inadequate treatment options for many liver diseases. While the incidence rates for hepatic diseases are constantly increasing over the past decades, the pharmacotherapies, which are available today, are often insufficient (Poelstra et al. 2012).

In general, the maximum amount of pharmaceutical substances that can be administered is limited by adverse side effects, caused by the drug at non-diseased tissue. Delivery of compounds to specific cells (in our case to hepatocytes) would increase the local drug concentration, while decreasing systemic toxic effects. Especially in cancer, an increased local concentration of chemotherapeutical drugs does not only minimize side effects, but can also result in an improved survival rate (Pérez-López et al. 2007). For example, exclusively delivering anti-tumor drugs and cytokines, like doxorubicin for hepatocellular carcinoma (HCC) to diseased cells would open new therapeutic possibilities.

In addition to conventional drugs, targeting systems are explored as well for gene therapy for various medical indications like genetic disorders, metabolic deficiencies, cancer, and viral infections. In particular genetic diseases affecting hepatocytes could be cured, if specific delivery and stable integration of exogenous DNA in hepatocytes was possible. Although various viral vectors, like adenovirus and retrovirus, demonstrate sufficient transfection efficiency, their clinical use is hampered by safety concerns (Hacein-Bey-Abina et al. 2003). Additionally, these and other viral vectors result in a non-specificity to hepatocytes and therefore causing side effects like

immunogenic responses. Although some promising strategies based on viral vectors are investigated in the clinics for gene delivery, alternative strategies for safer vectors with a high efficiency are needed (Campos & Barry 2007; Petrus et al. 2010; Haisma & Bellu 2011).

Non-parenchymal cells in the liver are therapeutic targets in several other hepatic diseases, such as acute liver inflammation, liver fibrosis, liver cirrhosis, and primary biliary cirrhosis. Drug delivering strategies and current approaches for these cells are reviewed elsewhere (Popov & Schuppan 2009; Poelstra et al. 2012).

1.1.1. Hepatocytes

Hepatocytes, which build up the parenchyma of the liver, exhibit a highly polarized structure with a basolateral (sinusoidal) membrane towards the sinusoids, an apical side constituting the bile canaliculi, next to a lateral surface connecting adjacent cells. Beside their major role in metabolism, they produce a large number of serum proteins, and in case of injury their production of inflammatory mediators contribute to the pathologic cascade of liver fibrosis (J. Wu & Zern 2000). Additionally, the liver parenchymal cells are affected in various liver diseases. Hepatitides can be caused by infectious diseases (such as viral, bacterial, protozoal, parasitic, fungal, and algal) or non-infectious diseases (alcohol-, toxin-, and drug-induced, autoimmune, ischemic, inherited). The two viral pathogens HBV and HCV are able to cause a chronic hepatitis, which leads to fibrosis and after some point to cirrhosis (Herzer et al. 2007). Conclusively, hepatocytes are important targets, especially in chronic viral hepatitis caused by HBV and HCV (L. C. Casey & W. M. Lee 2012; Lampertico & Liaw 2012), nonalcoholic steatohepatitis (Siebler & Galle 2006), and HCC (Aravalli et al. 2012), where treatment options are limited and often insufficient.

Moreover, genetic disorders like Wilson's disease, α1-antitrypsin deficiency, and hereditary hemochromatosis are examples of diseases where specific delivery of genes would open new therapeutic possibilities in healing these defects. Furthermore, hepatocytes could potentially be

used as a surrogate “host” to express and segregate proteins in additional genetic disorders like hemophilia A and B, where clotting factors VIII and IX are missing. High expectations are set that hemophilia will be curable in the near future by gene therapy, as the disease is caused by the lack of only one protein. In addition, already minor amounts of secreted protein ameliorate symptoms in severe cases (Mannucci & Tuddenham 2001). Hepatocytes are selected in most studies as target cells for gene expression, due to their central role in protein synthesis and easy access to the blood circulation. Despite substantial progress using viral and non-viral vectors, major challenges are remaining (Petrus et al. 2010). For example, the use of viral vectors and unspecific transduction of various cell types can cause immunologic reactions, which prevents a successful treatment (Herzog & Dobrzynski 2004; Nathwani et al. 2011). Hence, it is a requirement to evade transfection of cells of the immune system, and especially the antigen-presenting cells, to avoid unwanted immunological responses towards the transgenic expressed proteins (Petrus et al. 2010). Therefore, specific targeting of suitable cells, like hepatocytes, with non-viral vectors is a promising step in successfully transferring this new treatment options to the clinics.

Next to viral vectors, such as adenovirus, lentivirus, and HBV, which are commonly used for gene delivery (Poelstra et al. 2012), various other strategies are investigated to target hepatocytes. Another approach is taking advantage of the natural presence of apolipoprotein E (ApoE) in the plasma, which can adsorb on to injected liposomes and lipid nanoparticles and triggers an uptake by the low-density lipoprotein (LDL) receptor (Yan et al. 2005; Akinc et al. 2010). A similar strategy, using ApoE-fragments on liposomes, is utilized to cross the blood-brain barrier for targeting the central nervous system (Hülsermann et al. 2009), which raises questions about the specificity of this method. The most prominent strategy to target hepatocytes is through the asialoglycoprotein receptor (ASGPR), which is particularly expressed on liver parenchymal cells and exhibits a high affinity to terminal D-galactose (Gal) and N-acetyl-D-galactosamine (GalNAc) residues of glycans from glycoproteins. Recently, monoclonal antibodies were raised against the receptor and coupled to toxins to target hepatocytes (Trahtenherts & Benhar 2009; X. Zhao et al. 2011). This approach has its weak point to be species specific, and therefore animal studies can only be transferred with

limitations to the situation in humans. Since the affinity of the antigen binding property, also known as complementarity determining region (CDR), of the antibody can easily suffer from various causes, such as protein denaturation and non-specific conjugation, coupling to nanoparticles and storage of these components are challenging. As an alternative to antibody targeting, different vectors are synthesized, mimicking endogenous ligands of the ASGPR, to target liver parenchymal cells by using terminal Gal, GalNAc, or various desialated glycoproteins.

1.1.2. Structure of the asialoglycoprotein receptor and targeting strategies

The human ASGPR receptor is built up of two different subunits, each with an apparent molecular mass of approximately 41 kDa (J. Wu et al. 2002) and a sequence identity of 54%. These subunits are composed of 291 and 311 amino acids, with an unglycosylated molecular weight of 33 and 35 kDa, respectively (Uniprot.org 2012a; Uniprot.org 2012b). While both subunits contain carbohydrate recognition domains, the first subtype is responsible for endocytosis and the second one is in charge of an exclusively transport to the basolateral membrane. The functional receptor preferentially forms a 2:2 heterotetramer on the cell membrane (Fuhrer et al. 1994; Bider et al. 1996).

The ASGPR belongs to the group of C-type lectins (Ca^{2+}-dependent), binding to terminal Gal or GalNAc of glycoproteins, after sialic acid has been removed. Terminal sialic acids on glycan residues of proteins serve as an “expiry date”, and removal of this terminal sugar marks the protein for recycling. An example is the endogenous glycoprotein plasma fibronectin, which is produced and secreted by hepatocytes, and finally gets recycled after the sialic acid is cleaved from the glycan residue (Morell et al. 1971; Rotundo et al. 1998). The receptor is highly expressed on mammalian hepatocytes and presented on the sinusoidal membrane. Therefore, the receptor is regarded as an ideal structure for liver-specific targeting (Stockert 1995; J. Wu et al. 2002). However, small amounts of ASGPR have been detected in a subpopulation of activated primary T cells (J.-H. Park et al. 2006), in renal proximal tubular epithelial cells (Seow et al. 2002), on

human sperms (Harvey et al. 2000), and on thyrocytes (Marinò & McCluskey 2000). While primary rat hepatocytes have approximately 550 000 ASGPR per cell, HepG2, a cell line derived from a human liver parenchymal carcinoma, presents a reduced amount of about 225 000 receptors per cell (Popielarski et al. 2005).

The receptor is associated with some infectious diseases in humans. For example, the uptake of Marburg viruses is triggered by this receptor (Becker et al. 1995), while its role for HBV uptake is discussed controversially (Stockert 1995; De Meyer et al. 1997). In rats, hyperphosphorylation of ASGPR was detected after chronic ethanol exposure, leading to an impaired receptor mediated endocytosis of hepatocytes (McVicker et al. 2000).

The binding affinity of the ASGPR is around 30 times higher for GalNAc compared to Gal and binding of bi-antennary, and tri-antennary glycan residues are two and four orders of magnitude stronger compared to mono-antennary glycans, respectively (Connolly et al. 1982; Schwartz 1984). Tetra-antennary glycoproteins, like the human asialoorosomucoid, bind with an additional 10-fold higher affinity to the isolated human ASGPR compared to the tri-antennary protein asialofetuin (AF) (Baenziger & Maynard 1980). This additional increase in binding affinity results *in vivo* only in slightly faster uptake behavior (Clarenburg 1983). After clathrin-mediated endocytosis, the receptor releases its cargo in the acidic endosome and is transported back to the membrane, while the endosome fuses with the lysosome, where the ligand is degraded (Schwartz 1984). Similar sugar binding affinities between various mammalian species make this receptor an ideal target to develop drug delivery strategies specifically for hepatocytes.

Alternatives to natural occurring monosaccharides were developed, with a twofold increase in affinity compared to GalNAc (Stokmaier et al. 2009). Another approach using chemical synthesis to optimize ASGPR binding is to use β-linked GalNAc coupled to a tri-antennary backbone (Khorev et al. 2008). A possible combination of these strategies may result in a promising synthetic and specific vector towards ASGPR, although the chemical synthesis can be challenging.

The ASGPR is present on the plasma membrane in the majority of differentiated HCC, which makes it a potential target for antitumor drugs (Trerè et al. 1999). Although this approach could optimize current antineoplastic treatments, which lack any specificity, it cannot distinguish between healthy and malign liver parenchymal cells. Nevertheless, specific drug delivery to liver parenchymal cells through the ASGPR is viewed as an opportunity for an improved treatment of HCC (X. Zhao et al. 2011).

1.1.3. Kupffer cells

Targeting of hepatocytes is often equalized with an accumulation in the liver (Poelstra et al. 2012). But many nanoparticles are taken up unspecifically in the liver by Kupffer cells, and therefore it is crucial to distinguish which cell type is reached. Although Kupffer cells are making up less than 10% of the cells in the liver, they represent 80 to 90% of macrophages of the body (Bertrand & Leroux 2012). Next to their essential role in protecting the body from pathogens like viral particles, Kupffer cells are also responsible for engulfing various drug delivery vesicles, especially after they have been opsonized by antibodies or components of the complement system. Therefore, vesicular drug targeting strategies to hepatocytes need to circumvent an uptake by Kupffer cells. To prevent an uptake of drug carriers by the reticulo-endothelial system (RES), which also includes Kupffer cells, the surface of the particles are sterically stabilized with polyethylenglycol (PEG) polymers (pegylated). The reduced clearance results in an increased circulation half-life (Malam et al. 2009), which is a prerequisite for an active drug targeting strategy. The use of pegylated liposomes will further be discussed in section 1.2.2.

Next to an unspecific opsonization, negatively charged particles can be taken up through the scavenger receptor by Kupffer cells. Especially the classes A, B (CD36), and D (CD68) are regarded to play a prominent role in clearing anionic particles (Moghimi & Hunter 2001). In particular, liposomes with a high amount of the anionic phospholipid phosphatidylserine, which

mimics apoptotic or damaged cells, are recognized by the scavenger receptors of macrophages (Sambrano & Steinberg 1995). Therefore, strong anionic lipid mixtures have to be avoided.

Kupffer cells in the rat carry another relevant receptor, the so-called Kupffer cell receptor (KCR), which is not functionally expressed in humans. Like the ASGPR on hepatocytes, it exhibits a preference for glycoproteins with terminal Gal and GalNAc. But in contrast to the ASGPR, multiple separate glycan residues, rather than multi-antennary oligosaccharides on glycoproteins, result in a higher affinity (Fadden et al. 2003).

Another strategy to evade an uptake of phagocytic activity of Kupffer cells is the inhibition with methyl palmitate at non toxic concentrations (P. Cai et al. 2005). Although this concept might work *in vitro*, it is questionable if co-administration of liposomes with methyl palmitate results in a reduced uptake of particles by macrophages *in vivo*. A different approach is taken by depleting macrophages, including Kupffer cells, by delivering clodronate encapsulated in liposomes (Van Rooijen & Sanders 1996). This method significantly reduces the unwanted phagocytic effect of Kupffer cells and opens up a timeframe of about one week, until new macrophages start to repopulate the liver and the spleen (Van Rooijen et al. 1990). Although liposomal clodronate is well tolerated in clinical trials in patients with rheumathoid arthritis (Barrera et al. 2000), other non-toxic strategies circumventing Kupffer cells are favored, which do not bear the risk of impairing the host-defense.

1.2. Drug delivery

Many pharmacotherapies are limited by an insufficient delivery of therapeutic concentrations at the diseased tissue due to limited aqueous solubility, poor pharmacokinetic properties, or by side-reactions caused by toxic effects on healthy organs and tissues. Therefore, various approaches, such as liposomal delivery, have been explored to optimize pharmaceutical formulations to overcome these limitations.

1.2.1. Liposomes

Liposomes are vesicles composed of a mixture of lipids forming a lipid bilayer surrounding an inner aqueous phase. They usually are made up from phospholipids, from natural or artificial sources, and cholesterol forming multilamellar vesicles (MLV), large unilamellar vesicles (LUV), and small unilamellar vesicles (SUV) depending on their size and structure, after hydrating in an aqueous media (Figure 2).

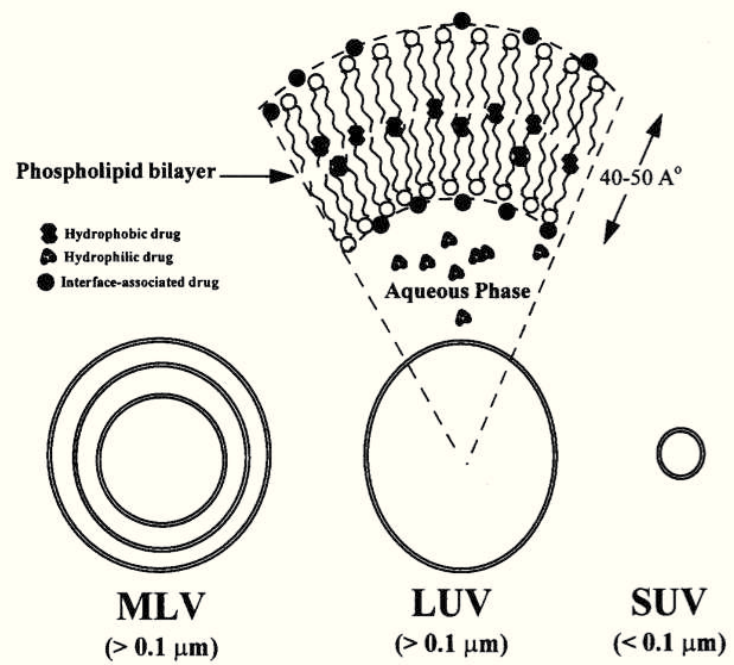

Figure 2: Schematic illustration of different types of liposomal formulations. Membranes are built up of bilayers containing different phospholipids and cholesterol. Mulitlamellar vesicles (MLV) consist of several layers of phospholipids, while larger unilamellar vesicles (LUV) and small unilamellar vesicles (SUV) are composed of only one layer. The particle size of SUVs are considerably smaller (< 100 nm) compared to LUVs. Adopted from Sharma et. al. 1997

In the last three decades, liposomal formulations were explored to achieve higher drug concentrations specifically at diseased locations. Generally, the concept is to load drugs in the lipid bilayer or in the inner aqueous phase, depending on their lipophilicity, and by passive or active accumulation of the vesicles at the desired tissue. It is commonly agreed that SUV bear the highest potential for drug targeting strategies. Intravenously applied MLV and LUV are substantially larger in particle size, which hinders them to extravasate and accumulate into tissue or tumors, resulting in a preferentially uptake by the RES (A. Sharma & U. S. Sharma 1997). Formulations of SUV can be prepared by extrusion, sonication, microfluidization of MLV or LUV (Mozafari 2010). The membrane is composed of phospholipids and cholesterol, which makes liposomes biocompatible, non-toxic, non-immunogenic, and biodegradable, while protecting the loaded drug from quick degradation in the blood plasma. The lipid composition and cholesterol content are responsible for *in vitro* and *in vivo* stability in terms of retention of the loaded cargo. Elevated cholesterol content, up to 50%, result in a higher liposome stability after intravenous or intraperitoneal administration in mice (Kirby et al. 1980). Loading of the drug in the inner liposomal compartment is either accomplished at the beginning of the preparation by passive entrapment through hydrating the dried lipid mixture with the drug of choice dissolved in an aqueous phase, or by active loading after vesicle preparation through a pH or ion gradient. An excellent example for an active loading is the antitumor drug doxorubicin, which can be incorporated inside of the liposomes with an efficiency as high as 98%, which exceeds its normal aqueous solubility by far. Thereby, doxorubicin, which is an amphipathic weak base, is entrapped inside the liposome either after being protonated, resulting from a lower pH inside the vesicle (pH gradient), or by precipitation with sulfate ions after creating an ammonium sulfate gradient, where in exchange the ammonium ion can diffuse across the liposomal membrane (Mayer et al. 1986; Haran et al. 1993). An example for a drug incorporated into the lipid membrane is the substance amphotericin B, which is used against systemic fungal infections. Liposomal formulation of the drug increases its therapeutic efficacy while reducing systemic toxicity, such as cardio- and nephrotoxicity (Szoka et al. 1987; Tiphine et al. 1999; Adler-Moore & Proffitt 2002). Because liposomal formulations are only to some extent chemically and physically stable due to oxidation of phospholipids, leakage of

the encapsulated solute, and liposome aggregation, they can be stabilized by various techniques, whereas lyophilization is the usual choice to ensure long-term stability (C. Chen et al. 2010). Examples of FDA and EMA approved drug formulations using conventional liposomes are amphotericin B (sold as AmBisome® from Gilead) as a representative for a drug associated within the lipid bilayer of the liposome, doxorubicin (sold as Myocet® by Elan Pharmaceuticals), daunorubicin (sold as DauoXome® from Galen), and cytarabine (sold as DepoCyt® from Skye, Enzon, and Mundipharm) as typical substances entrapped in the aqueous phase inside the vesicles.

Liposomal formulations are not only used as a drug delivery vehicle, but are also utilized as vaccine adjuvants to increase immunogenicity. The influenza vaccines Inflexal V® or the vaccine against HAV Epaxal® are representatives which are available on the market. These systems can be superior compared to inactivated or attenuated vaccines, because they can lead to a strong humoral and cell-mediated immune response without the risk of reverting to a virulent form. Henriksen-Lacey et al. have reviewed the recent advantages and prospects of these liposomal vaccine delivery systems (Henriksen-Lacey et al. 2011).

1.2.2. Reduced reticulo-endothelial system clearance and passive targeting

Intravenously applied particles are in general subjected to a fast clearance, caused by the RES. First trials in humans with non-coated liposomal doxorubicin resulted in a preferential uptake by macrophages in the liver and the spleen, which questioned a further clinical development of these types of formulations (reviewed in (Barenholz 2012)). Therefore, strategies have been developed to reduce the uptake by the phagocytic system and to prolong the plasma half-life of these vesicles. The most prominent approach is the use of linear or branched polyethylene glycol (PEG) chains attached to the surface of nanoparticles. The discovery of these sterically stabilized liposomes was initiated after the observation that PEG coupled to proteins are non-immunogenic and avoided by the RES (Abuchowski et al. 1977). This effect led to the development and approval of several

pegylated proteins, where the modified surface enabled their therapeutic utilization by reducing the clearance in the kidney through an increased hydrodynamic volume, preventing immunogenicity, reduction of protein aggregation, and increasing thermal stability of the folded protein (reviewed in (Pasut & Veronese 2012)). In addition, several other strategies were investigated to modify the liposomal surface, like the use of monosialo-tetrahexosylganglioside (GM_1) or hydrogenated phosphatidylinositol (HPI), but comparative studies resulted in a superior effect of PEG-liposomes (Allen & Hansen 1991; Gabizon et al. 1993). Pegylation and further optimization of liposomal doxorubicin leads to a 5 to 10 times longer half-life of the drug, resulting in an approximately 300-fold higher area under the concentration-time curve (AUC) and a potential increased accumulation in the tumor tissue, compared to the free compound (Gabizon et al. 2003). A higher drug concentration in tumors can be achieved if the cancerous tissue is penetrated with porous blood vessels where the nanoparticle can extravasate and accumulate. This observation was termed as enhanced permeability and retention (EPR) effect and first described for larger proteins (Matsumura & H. Maeda 1986). The use of PEG-liposomes was advanced significantly by the development and regulatory approval of doxorubicin loaded pegylated liposomes (sold as Doxil® from Johnson & Johnson (US market) and as Caelyx® from Janssen-Cilag (outside the US)). A second PEG-liposomal formulation with loaded cisplatin is in evaluation by the authorities (Lipoplatin® from Regulon).

Repeated injection of pegylated liposomes can decrease the circulation time of the drug dramatically (Ishida et al. 2003), an effect named accelerated blood clearance (ABC). This observation is attributed to the occurrence of PEG specific IgM antibodies, leading to a complement activation and therefore to a faster clearance from the blood stream (Ishida et al. 2006). Additionally, the loaded cargo is of importance, since doxorubicin does not show this behavior in a relevant manner, in contrast to other cytotoxic substances like topotecan (Ma et al. 2012). Although these effects are not completely understood, this observation hints to the fact that even pegylated liposomes interact with the immune system. It is still unknown if these effects can

be prevented by attaching specific targeting vectors to the liposomal surface, which trigger a fast uptake into specific cells and reduce the blood circulation time.

While passively targeting tumors with pegylated liposomes, alone or in combination with a second cytostatic, has become a first-line therapy in various oncological indications, some tumors cannot be treated effectively with this approach. For example, pegylated liposomes with doxorubicin are not effective against HCC (Halm et al. 2000). Therefore, additional strategies are warranted to target these tumors.

1.2.3. Active targeting and combination with nanocarriers

An increasing number of various therapeutic antibodies, which bind to diseases specific cells or proteins, have been approved in the past years by the regulatory authorities (reviewed by (Imai & Takaoka 2006)). These new biologicals have revolutionized treatments in several cancerous and non-cancerous indications through their specific binding. Examples are the anti-CD20 monoclonal antibody rituximab against lymphoma (sold as Mabthera® from Roche) and the anti-TNFα monoclonal antibody infliximab against rheumatoid arthritis (sold as Remicade® from MSD). An additional step is to conjugate monoclonal antibodies with a pharmaceutical active substance, such as a drug, a toxin, or a radioactive compound, either for treatment or imaging purposes (Schnell et al. 2002; Pasquetto et al. 2011). For example, a recent clinical study indicates a beneficial effect of monoclonal anti-CD22 antibodies coupled to exotoxin A from *Pseudomonas aeruginosa* in patients with hairy cell leukemia (Kreitman et al. 2012). Although these new therapeutical constructs are still in clinical trials, it is expected that they amplify the efficacy of several treatments through a specific binding of cellular targets combined with a high pharmacological potency.

A limitation of this approach is that only one or very few molecules can be coupled to a single antibody. Therefore, attaching antibodies to nanoparticles, like liposomes (immunoliposomes), opens up the possibility to increase delivery of therapeutic active substances at specific targets,

and hence increase efficacy. The specific binding affinity of an antibody ensures targeting of selective cellular structures, while the coupled liposome can transport high amounts of drugs or genes, which are in addition protected inside the vesicle from premature degradation. In combination with long circulating liposomes, an even higher accumulation of drugs at the target cell population or organ might be achievable.

Active liposomal targeting can even be used to cross cellular membranes, like the blood-brain barrier (BBB), to deliver daunomycin to the rat brain. Most intravenous applied drugs are unable to traverse the BBB, which makes treating diseases in the brain with pharmaceutical substances challenging. For example, the monoclonal antibody against the rat anti-transferrin receptor (OX26) was coupled to liposomes, which enabled these vesicles to undergo transcytosis across the BBB and to deliver their cargo to the brain (Huwyler et al. 1996). Endocytotic uptake of OX26-immunoliposomes has also demonstrated to be able to circumvent efflux transporters of the ATP-binding cassette B (ABCB) family, such as the P-glycoprotein (P-gp or ABCB1) receptor, which is also known as multi-drug resistant protein 1 (MDR1), due to its ability to permit cancer cells to become resistant to various antineoplastic drugs. This effect was demonstrated *in vitro* on P-gp expressing RBE4 cells using OX26-immunoliposomes loaded with digoxin or daunomycin, which are P-gp substrates (Huwyler et al. 2002; Schnyder et al. 2005). Therefore, specific endosomal uptake of liposomes can be a strategy to overcome multidrug resistances of tumors, which have shown in the past a poor response rate to various chemotherapeutic drugs (Gottesman 2002).

While for some therapeutic substances an endosomal uptake is sufficient to achieve a cellular effect, others need to circumvent lysosomal degradation and specific intracellular delivery. Especially acid labile drugs need to circumvent endosomal and lysosomal inactivation, and DNA for gene targeting requires additional access to the nucleus or mitochondrial compartment for an efficient transfection. In the endosome, the pH decreases to approximately 6.0, which can be utilized in different liposomal formulations to escape into the intracellular compartment. One approach uses pH sensitive lipids, such as N-palmitoyl homocysteine, oleic acid,

cholesterylhemisuccinate, dioleoylsuccinylglycerol, or dipalmitoylsuccinylglycerol, which stabilize the liposomal bilayer at neutral pH, but fuse with other adjacent membranes in a mildly acidic environment, like it is present in endosomes (Connor & Huang 1986; Drummond et al. 2000). The fusion of the liposomal bilayer with the endosomal membrane results in a release of the cargo into the cytoplasm. A second approach takes advantage of a conformation change of membrane permeabilizing peptide, which takes place below a pH of 6.4 and that can be attached to the liposomal surface (Midoux et al. 1998). In contrast to the previous method, the latter approach preserves intact vesicles and can be used for subsequent intracellular delivery. For nuclear targeting, specific peptides, such as the simian virus 40 (SV40) or the M9 domain from the heterogeneous nuclear ribonucleoprotein A1 (hnRNPA1), can be attached to the liposomal surface (Aronsohn & Hughes 1998; Subramanian et al. 1999). An example for a successful cell targeting, combined with an endosomal escape and nucleus delivery, was recently achieved with lipid coated porous silica beats *in vitro* in a HCC model (Ashley et al. 2011). For intracellular targeting of hydrophobic molecules towards mitochondria, stearyl-triphenyl-phosphonium bromide (STPP) is incorporated into the lipid mixture of liposomes. STPP interacts with the mitochondrial membrane and can increase the ability to induce apoptosis of cytostatic substances, such as the retinoic acid receptor (RAR) γ activator CD437, by acting directly on mitochondria (Weissig 2012).

Despite intensive research with conjugated liposomal formulations, only very few clinical studies were conducted up to today. Compared to a plethora of various clinical trials in different stages with immunoconjugates, where antibodies are attached to pharmaceutical drugs, toxins, or radioactive substances (reviewed in (Pasquetto et al. 2011)), hardly any clinical studies are reported for immunoliposomes. To date, only two clinical phase I trials are known in the scientific community. The first study was conducted in patients with metastatic stomach cancer with F(ab′)2 fragments of a human monoclonal antibody GAH, which is derived from a screening of hybridomas against solid tumors of various types, coupled to pegylated liposomes and loaded with doxorubicin (S. Hosokawa et al. 2004; Matsumura et al. 2004). In this small study, the maximum tolerated dose of doxorubicin was lower compared to the pegylated but non-targeted liposomal formulation, and

no tumor response was visible. A second trial was recently presented, where monoclonal antibodies against the epidermal growth factor receptor (EGFR) were attached to doxorubicin containing pegylated liposomes (Mamot et al. 2012) and applied in patients with various solid tumors ((University Hospital Basel, Switzerland 2012) Toyama Meeting Basel 2012). Although the presented data are promising, further details about the tolerability and efficacy are awaited to be published.

The small number of performed clinical trials is also an expression of the technical hurdles that have to be overcome to prepare clinical applicable immunoliposomes. These challenges include difficulties in formulating stable liposomal constructs and immunogenicity of not humanized antibodies (Pasquetto et al. 2011). Further, coupling antibodies to liposomes in a reproducible manner and subsequent characterization can be challenging in a lab environment, but transferring these techniques to industrial scale is another hindrance. Although the two conducted clinical trials demonstrated that these obstacles can be overcome at least in a small-scale setup, alternative strategies, leading to more robust and better characterizable constructs, are warranted.

1.2.4. Liposomal targeting of the asialoglycoprotein receptor

In regard of the limitations of antibody-conjugated liposomes, monosaccharides, or residues from glycans may represent valuable alternatives to target oligosaccharide binding receptors on cell membranes. For drug delivery to hepatocytes, the ASGPR is the receptor of choice, which binds terminal Gal or GalNAc of residues from glycoproteins.

Using Gal coupled directly to cholesterol, in combination with pegylated phospholipids of various lengths, results in a preferred uptake by hepatocytes in contrast to non-parenchymal cells in mice. A pegylated chain length of 350 Da produces a higher uptake ratio of liver parenchymal cells to non-parenchymal cells (PC/non-PC) compared to PEG2000, due to steric hindrance of the longer PEG-chain (Managit et al. 2003). Using the shorter PEG length is a trade of, between the easier

accessibility of the Gal moiety and a length depending protecting effect of the PEG chain from the RES. A further development of this approach is the use of cleavable PEG2000 lipids, which enhances the circulation time while giving subsequent access to the underlying Gal residues (S. Wang et al. 2010). Although the published results of these two approaches cannot be directly compared, due to different experimental setups, a higher PC/non-PC ratio resulted in the former approach. Replacing surface bound Gal with GalNAc produces only a relatively weak uptake in HepG2 cells (Bernardes et al. 2010). The lack of pegylated surfaces of the former formulation raises additional doubts about a successful usability *in vivo*. A different approach is taken by coupling lactose to DSPE-PEG2000 residues through a reductive amination of the glucose moiety and subsequently binding to the PEG chain, which provides a terminal galactose (Morille et al. 2009). Although a significant transfection efficiency is obtained *in vitro*, specific *in vivo* targeting of hepatocytes is questionable, due to the relatively large particle size of 130 to 180 nm and the cationic zeta potential between + 5 to 26 mV. Next to the limitation of the diameter of fenestrations in the sinusoidal membrane of the liver, which is approximately 100 to 150 nm (Pathak et al. 2008), the uptake of galactosylated liposomes by the ASGPR is size-dependent and lies in the range of 70 and 90 nm (Rensen et al. 2001). Liposomal size is even more important for cellular uptake into hepatocytes than the presence of coupled Gal to the surface of the vesicles. Studies by Popielarski et al. in freshly isolated hepatocytes revealed that 50 nm methoxy-terminated nanoparticles are taken up to a greater extent compared to 140 nm Gal-terminated vesicles. Despite their Gal-coating, the latter nanoparticles primarily accumulate in Kupffer cells (Popielarski et al. 2005). In addition to the size of vesicles, the lipid mixture is of major importance. Murao et al. explored the *in vivo* uptake behavior in hepatocytes of 90 nm vesicles in regard of various ratios of 1,2-distearoyl-sn-glycero-3-phosphocholine (DSPC) to cholesterol (Chol) mixtures, while using a fixed amount of 5% (mol) galactosylated cholesterol. A combination of lipids of DSPC:Chol of 60:35 results in a PC/non-PC uptake ratio of 15 versus 0.78 for a mixture of 90:5, respectively (Murao et al. 2002). Exaggerating the density of attached Gal residues, such as 20% (mol) of the lipid mixture, leads again to a predominantly uptake by Kupffer cells (K. Shimada et al. 1997). The most favorable ratio in terms of liver PC/non-PC uptake results with an inclusion of 5% (mol)

galactosylated lipidis in a liposomal formulation (Managit et al. 2005a). Therefore, it can be stated that not only particle size, but also an increased cholesterol content of the lipid composition, as well as an optimal surface density of Gal residues, are critical for a hepatocyte specific targeting approach (Pathak et al. 2008).

Alternative approaches use naturally occurring glycoproteins as vectors, such as AF, which carry multiple Gal terminated bi- and tri-antennary glycans (Neue et al. 2011). The first utilization of AF associated liposomes was already reported in 1975 from Gregoriadis et al., when they described an increased liver uptake in the rat with fetuin-liposomes, compared to conventional liposomes or in the presence of an excess of free AF (Gregoriadis & Neerunjun 1975). Interestingly, they also described a first preparation of immunoliposomes by just mixing polyclonal and unpurified Immunoglobulin G (IgG) with sonicated vesicles, which resulted *in vitro* to a weak but significant specific uptake of the target cells. Despite the increased liver uptake of AF-liposomes, the majority of the controls accumulated also in the liver, indicating a prominent unspecific uptake by Kupffer cells. The major unspecific binding in the liver was confirmed by the group of Tsuchiya, while they used vesicles with an approximative size of 500 nm and incorporated AF covalently bound to palmitic acid into the lipid mixture (Tsuchiya et al. 1986). Subsequent studies using smaller liposomes in the range of 130 nm resulted in a preferential uptake by hepatocytes (Hara et al. 1987). Further *in vitro* investigations by the group revealed a greater accumulation in PC compared to non-PC with an increased amount of Chol content in the AF-liposomes (Hara et al. 1988), and delivery of γ-interferon resulted in a pharmacological effect in a HBV model (Ishihara et al. 1991). Wu et al. conformed in mice the preferential liver accumulation of AF-liposomes and demonstrated an augmented protective effect of vitamin E loaded AF-liposomes on hepatocytes after CCl_4-induced acute liver injury (J. Wu et al. 1998).

For a gene targeting strategy, transfection of hepatocytes is achieved with cationic AF-liposomes *in vitro* (Hara et al. 1995a) or *in vivo* after injection into the portal vein in mice (Hara et al. 1995b). Including the fusogenic lipid dioleoylphosphatidylethanolamine (DOPE) in the lipid mixture

enhances the transfection efficiency of hepatocytes *in vitro* (Hara et al. 1996). A combination of cationic liposomes with protamine or γ-cyclodextrin results in an increased transfection efficacy in mice (Arangoa et al. 2003; Motoyama et al. 2011). At least *in vitro*, mixing liposomes loaded with DNA (ie. lipoplex) and unbound AF results in a transfection of HepG2 cells (Tros de Ilarduya 2010). It should be noted that most of these reports published *in vitro* data only, since pharmacokinetic of these cationic particles is not favorable for a hepatocyte specific targeting. *In vivo* studies, using AF-liposomes, were unable to produce a constant protein expression for a clinical benefit in an α1-antitrypsin deficient mouse model (Dasí et al. 2001). While the binding and uptake behavior of AF-liposomes on hepatocytes is promising, transfection efficiency is still poor, due to a suboptimal liposomal formulation strategy of DNA with lipids, resulting mostly in large cationic structures with a disappointing pharmacokinetic behavior *in vivo*.

The use of bovine AF as a vector for drug delivery includes the limitation of utilizing an immunogenic compound. To avoid this effect, two possibilities are obvious. Substituting the bovine AF with the human analogue alpha-2-HS-glycoprotein, or cleaving the required tri-antennary glycans from the peptide backbone and using only these small non-immunogenic oligosaccharide residues as a vector. Fragmentation of the AF protein backbone, isolation of the correct glycan-peptide fragments, and incorporation into liposomes was first described with the intention to study carbohydrate-based recognition systems and membrane tagging in plant cells (Warren & Fowler 1982). First experiments in rats with AF glycan-petides incorporated into liposomes led to a fast liver accumulation, although it was only slightly increased compared to control vesicles (Banno et al. 1983). Many years later, this approach was picked up again and peptide fragments of AF bearing tri-antennary glycans were coupled to various fatty acids. Incorporation into liposomes indicated a specific uptake *in vitro*. Preliminary *in vivo* results pointed to an increased liver uptake without further intrahepatic localization (Kallinteri, Papadimitriou, et al. 2001; Kallinteri, Liao, et al. 2001).

In comparison, other glycoproteins were used with variable success for targeting hepatocytes through the ASGPR. For example, various soybean-derived sterylglucosides (Shimizu et al. 1996), arabinogalactan from the plant *Larix occidentalis* (T. Tanaka et al. 2004), human asialorosomucoid (A. Singh et al. 2010), and the hydrophobic polysaccharide pullulan from the fungus *Aureobasidium pullulans* (Guhagarkar et al. 2010).

While the published results of AF-liposomes vary in view of hepatocyte uptake, specificity, and selectivity, due to different particle sizes and charges of the liposomal formulations, no approach is reported to date to attach AF on to the distal end of pegylated vesicles. Therefore, using AF attached to pegylated liposomes is a new and promising approach, since avoiding an uptake by the RES, including Kupffer cells, is a key issue in achieving a specific drug delivery system to liver parenchymal cells.

1.3. Quantum dots

To be able to follow and detect liposomal formulations in *in vitro* and *in vivo* experiments, fluorescent substances can be incorporated. Usually, organic dyes, like carboxyfluorescein or rhodamine B, are used, but their application is limited to a low photobleaching threshold and a broad emission spectra. Alternatives to these conventional dyes are quantum dots, which are composed of semiconductor nanocrystals. Compared to rhodamine, they are 100 times more resistant to photobleaching and 20 times as bright (Chan & Nie 1998). By tailoring their size, defined emission spectra from the blue to the red and even near infrared are possible, while the emission peak is very narrow and generally below 40 nm full-width at half-maximum (Figure 3)(Dabbousi et al. 1997). These properties permit tracking, uptake, and intracellular distribution of drug carriers in living cells, without the limitations of photobleaching after a prolonged time of observation. Further, the narrow emission spectra allows the simultaneous use of different fluorochromes, because the fluorescent signals can easily be distinguished from each other (Kosaka et al. 2009).

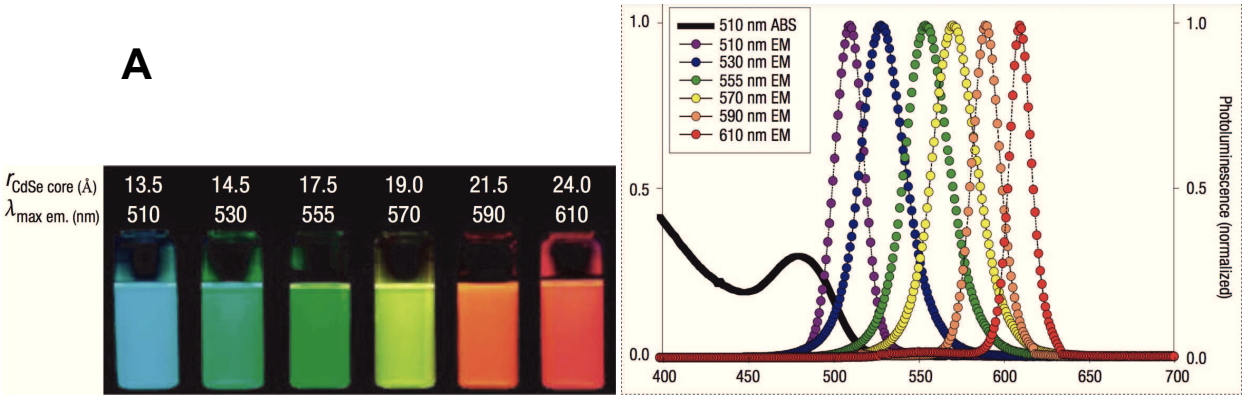

Figure 3: Picture and emission spectra of quantum dots. The colors of the quantum dots are depending on their nanocrystal size (panel A). All quantum dots can be excited at a single wavelength in the ultraviolet spectra (e.g. 400 nm) and fluoresce at their corresponding wavelength with a narrow emission peak (panel B). Note, Stokes shifts are much wider, compared to most organic fluorochromes (150 to 250 nm). Adopted from Medintz et al. 2005

The usage of quantum dots in combination with pharmacological active substances in liposomes would permit additional applications in treating various diseases. These theranostics, combining therapeutic and diagnostic capabilities, could be used for example to treat cancer cells with anti-neoplastic compounds in combination with imaging of an accumulation of the vesicles in the tumor tissue by following the fluorescent signal of incorporated quantum dots (W. T. Al-Jamal & Kostarelos 2011). At least in small animals like mice, tissue distribution and accumulation of quantum dots could be followed over time (Ballou et al. 2004). Therefore, quantum dots are promising alternatives to conventional dyes, and their bright and photostable properties might open new potential applications in biological systems.

2. Aim of Thesis

It was the aim of the present thesis to explore a drug delivery system that can ultimately be used *in vivo* to transport various therapeutic or diagnostic compounds specifically to liver parenchymal cells. This strategy was implemented by targeting the asialoglycoprotein receptor (ASGPR). Therefore, a vector-conjugated liposomal formulation was developed, which included the following objectives:

1. Evaluation of different targeting vectors, which are binding specifically to the ASGPR, by using the *in vitro* cell culture model HepG2 and technologies such as confocal laser scanning microscopy and flow cytometry.

2. Coupling of the vector to the distal end of maleimide-functionalized pegylated phospholipids. Characterization of the resulting liposomal formulations.

3. *In vitro* proof of principle by incubating vector-conjugated liposomes with HepG2 cells. The uptake was mediated by the ASGPR and was suppressed by adding a competitive inhibitor.

4. Evaluation of liposomal tracking and delivery of quantum dots (QD). Characterization of vector-conjugated liposomes loaded with QDs, and subsequently analysis of cellular uptake. Comparison of optical properties of QDs with organic dyes and evaluation of their usage to optimize drug targeting strategies.

5. *In vivo* proof of principle studies by injecting rats with vector-conjugated liposomes and the characterization of liver uptake. Special attention was paid to the difference between accumulation in liver parenchyma and phagocytosis by Kupffer cells.

6. Two additional projects in the section “Appendix” illustrate our interest in pharmacokinetics. They cover the formation of ceftriaxone precipitates in human plasma and the interaction potential of resveratrol with different cytochrome P450 isoenzymes.

3. Material and Methods

3.1. Materials

4-aminophenyl β-D-galactopyranoside, asiaolofetuin (AF, Lot. 069K7425V), 5(6)-carboxyfluorescein (CF), 5(6)-carboxyfluorescein *N*-hydroxysuccinimide ester (CF-NHS), Cholesterol, 2-iminothiolane (Traut's reagent), 5,5′ -Dithiobis(2-nitrobenzoic acid) (Ellman's reagent), poly-D-lysine hydrobromide (mol wt 70 000-150 000), paraformaldehyde (PFA), Hoechst 33342, 7-Amino-actinomycin D (7-AAD), Mowiol 4-88 and all other reagents were of analytical grade and obtained from Sigma-Aldrich (Buchs, Switzerland). The following lipids: 1,2-distearoyl-sn-glycero-3-phospho-choline (DSPC), 1,2-distearoyl-sn-glycero-3-phosphoethanol-amine (DSPE), 1,2-dioleoyl-sn-glycero-3-phosphoethanolamine-N-(carboxy-fluorescein) (ammonium salt) (DSPE-CF), 1,2-distearoyl-sn-glycero-3-phosphoethanolamine-N-[methoxy(polyethylene glycol)-2000] (ammonium salt) (DSPE-PEG(2000)), 1,2-distearoyl-sn-glycero-3-phosphoethanol-amine-N-[maleimide(poly-ethylene glycol)-2000] (ammonium salt) (DSPE-PEG(2000)-Mal), and 1,2-dioleoyl-sn-glycero-3-phosphoethanolamine-N-(lissamine rhodamine B sulfonyl) (ammonium salt) (DSPE-Rho) were purchased form Avanti Polar-Lipids (Alabaster, AL). QDot® 625 ITK were obtained from Invitrogen, Life Technologies (Zug, Switzerland). The monoclonal antibody against ASGPR subunit 1 and 2 (mouse anti-human ASGPR-1/2 IgG) was obtained from Santa Cruz Biotechnology (sc-166633, Santa Cruz, CA). R-phycoerythrin (RPE)-conjugated polyclonal goat anti-mouse F(ab')2 fragmented immunoglobulins (goat anti-mouse-RPE) were purchased from Dako (Baar, Switzerland). The modified Lowry protein assay kit and the CBQCA protein quantification kit were obtained from Pierce (Rockford, IL) and Molecular Probes (Eugene, OR), respectively, and used with bovine serum albumin or AF as a standard.

3.2. Fluorescent labeling of D-galactose

Fluorescent-labeled Gal was prepared by coupling N-hydroxysuccinimide ester from CF-NHS to galactose containing a primary amine (Hermanson 2008). Therefore, 4-aminophenyl β-D-galactopyranoside was incubated together with a 10-fold excess of CF-NHS in a $NaHCO_3$ buffer (50 mM, pH 8.0) for 60 min at room temperature. The reaction progress was monitored and the final product was purified by a binary Agilent HP 1050 series high-performance liquid chromatography system (HPLC, Agilent Technologies, Santa Clara, California). Analytes were detected by ultraviolet (UV) absorbance at 220 nm and 490 nm, using an Agilent diode array UV/Vis detector (Agilent Technologies). The injection volume was 30 µl and as a stationary phase a Nucleosil 100-5 C_8 reversed-phase column (particle size 5 µm, 125 mm x 2 mm I.D., Macherey-Nagel, Düren, Germany) was used. HPLC solvents were 70% MeOH (A) and 2% MeOH (B) in H_2O, and separation was achieved at a flow rate of 0.3 ml/min, using a linear gradient from 40% to 100% over 20 min, with respect to eluent A. Fractions containing Gal-CF were concentrated to dryness using a N_2 flow at room temperature to remove any organic solvent.

3.3. Fluorescent labeling of asialofetuin

AF was labeled with CF-NHS by crosslinking the N-terminus of the protein backbone or with ε-amines of lysine side chains (Hermanson 2008). Hence, AF was incubated together with a 10-fold excess of CF-NHS in a $NaHCO_3$ buffer (50 mM, pH 8.5) for 2 h on ice. Excess of CF-NHS was removed on a fast protein liquid chromatography (FPLC) system (Pharmacia 500, GE Healthcare, Glattbrugg, Switzerland or BioLogic DuoFlow System, Bio-Rad, Zürich, Switzerland) by size exclusion using a Sephadex G-50 fine column (1.6 cm x 20 cm, GE Healthcare) eluting with 0.01 M PBS (0.01 M phosphate and 150 mM sodium chloride), pH 7.2. Eluates were detected by UV absorbance at 280 nm and stored at -20°C. Final protein concentration was quantified using the modified Lowry protein assay, and the degree of labeling was calculated according to the spectrophotometric method described by Thermo Scientific (2009).

3.4. Liposomal preparation and characterization

Thiolation of proteins, and coupling to pegylated liposomes through maleimide functionalized lipids, was achieved as described previously (Huwyler et al. 1996). Thus, AF (2.7 mg, 60 nmol) was dissolved in a buffer containing 0.1 M phosphate and 1 mM EDTA, pH 8.0, and thiolated with a 200 times molecular excess of Traut's (2-iminothiolane) reagent for 1 h at room temperature. Thiolated AF was purified and concentrated in Amicon Ultra-4 centrifugal filter units, 10 kDa cut off (Millipore, Zug, Switzerland), with 0.1 M PBS containing 1 mM EDTA, pH 7.2. The amount of attached sulfhydryl groups was determined by Ellman's reagent at a wavelength of 412 nm, using a freshly prepared cystein solution as a standard.

In parallel, a mixture of lipids of DSPC (5.5 µmol), Cholesterol (4.5 µmol), DSPE-PEG(2000) (0.27 µmol), DSPE-PEG(2000)-Mal (0.06 µmol), and DSPE-Rho (0.04 µmol) or DSPE-CF (0.04 µmol) were dissolved in chloroform/methanol (2:1, v/v). For non-pegylated control liposomes, DSPE-PEG(2000) and DSPE-PEG(2000)-Mal were replaced by DSPE (0.33 µmol). The solution was evaporated by vacuum in a water bath at 60°C for 1 h to form a homogenous lipid film using a Rotavapor A-134 (Büchi, Switzerland). The lipid film was hydrated 10 min in 1 ml of 0.1 M PBS containing 1 mM EDTA, pH 7.2, using 3 g glass beats (diameter 5 mm) at 120 rpm in a water bath at 60°C. For passively loading carboxyfluorescein inside the liposomes, a solution of 5(6)-carboxyfluorescein was used for hydrating. The resulting multilaminar vesicles were subjected to five freeze-thaw cycles. Liposomes were extruded at 60°C five times through a 100 nm-pore-size polycarbonate membrane (Avanti Polar-Lipids, Alabaster, AL), followed by extrusion nine times through a 50 nm filter. For AF conjugation, the thiolated protein was mixed with liposomes and incubated overnight at room temperature. Conjugated liposomes were purified by size exclusion chromatography using a Superose 6 prep column (1.6 cm x 20 cm, GE Healthcare) eluting with 0.01 M PBS, pH 7.2. Average liposomal sizes and zeta potential were measured by dynamic and electrophoretic light scattering, respectively, using a Zetasizer Nano ZS (Malvern Instruments, Worcestershire, UK) or a Delsa Nano C (Beckman Coulter, Nyon, Switzerland). Preparations of

liposomes loaded with Quantum Dots (QDs) were performed with the following modifications. Lipids were hydrated in a 100 nM solution of QDots 625 ITK in 0.1 M PBS containing 1 mM EDTA, pH 7.2, and extrusion was performed five times through a 200 nm filter, followed by nine times through an 80 nm filter. The amount of AF coupled to liposomes was measured by the CBQCA protein quantification kit (Molecular Probes). Lipid content was either calculated by the AUC in the chromatogram from the size exclusion chromatography, corresponding to the liposomal fractions and recorded at an UV wavelength of 280 nm, or measured by a modified version from the Stewart assay (Stewart 1980), using DSPC as a standard. Thus, samples were incubated with chloroform and an aqueous 0.1 M ammonium ferrothiocyanate solution at a ratio of 1:1 (vol/vol), vortexed, and centrifuged at 300 g for 5 min at room temperature. Absorbance of the chloroform layer was measured at a wavelength of 485 nm.

3.4.1. Incorporation of phospolipids by the post-insertion method

Pegylated liposomes were prepared and purified as described above, and loaded with an aqueous solution of CF in either a non-self-quenching (3 mM) or a self-quenching (60 mM) concentration. DSPE-Rho (0.04 µmol) was dissolved in chloroform/methanol (2:1, v/v) and dried to form a homogenous lipid film by vacuum evaporation in a water bath at 60°C for 1 h. The lipid film was hydrated in 1 ml of 0.01 M PBS, pH 7.2, and thoroughly vortexed to form DSPE-Rho micelles. The concentration of the DSPE-Rho solution was kept above 1.5 µM, which was reported as the critical micelle concentration (CMC) for the more hydrophilic pegylated variants of DSPE (Ashok et al. 2004). The liposomal preparations were split up in equal amounts and were mixed with the corresponding fraction of DSPE-Rho micelles. Liposomes loaded with a non-self-quenching CF solution were incubated at 60°C between 0 min and 60 min., and liposomes loaded with a self-quenching CF solution were incubated for 70 min between 50°C and 80°C. Subsequent separation of liposomal and not incorporated DSPE-Rho lipids were achieved by size exclusion chromatography, using a Superose 6 prep column (1.6 cm x 20 cm, GE Healthcare) eluting with 0.01 M PBS, pH 7.2. The fluorescent signals of CF (excitation wavelength 488 nm, emission

wavelength 517 nm) and rhodamine B (excitation wavelength 559 nm, emission wavelength 583 nm) were analyzed for each preparation, using a SpectraMax M2e fluorometer (Molecular Devices, Sunnyvale, CA). Changes in liposomal size were measured by a dynamic light scattering using a Delsa Nano C (Beckman Coulter). For analyzing co-localization of fluorescence of CF and rhodamine B, diluted samples of liposomes were mounted in Prolong Gold antifade reagent (Gibco, Life Technologies, Zug, Switzerland) and sealed with nail polisher after drying. For mounting, a hair was added on the slide to facilitate focusing on the layer containing the liposomes. Slides were examined using an Olympus FV-1000 inverted confocal laser scanning microscopy (CLSM, Olympus, Hamburg, Germany), using a 60x PlanApo N oil-immersion objective (numerical aperture 1.40) with an optical resolution of 180 nm in the xy-plane and 700 nm in the z-plane.

3.5. Cell culture

HepG2 cells were kindly provided by Prof. Dietrich von Schweinitz (University Hospital Basel, Switzerland), and cultured at 37°C under 5% CO_2 and saturated humidity in DMEM low glucose (1 g/l) containing 10% fetal bovine serum (FBS), 0.1 mM Non-Essential Amino Acids (NEAA), 2 mM Glutamax, and 10 mM Hepes (all obtained from Gibco). Cells were confirmed to be free of mycoplasma (MycoAlert, Lonza, Rockland, ME).

3.6. Protein and lipid analysis

3.6.1. Plasma membrane isolation

HepG2 cells were homogenized in a Potter-Elvehjem homogenizer by 30 strokes in lysis buffer (10 mM Tris-HCl, 1 mM $MgSO_4$, 0.5 mM EDTA, Complete protease inhibitor mini (Roche Diagnostics, Rotkreuz, Switzerland), pH 7.4) and centrifuged at 1000 g for 10 min at 4°C. The pellet was resuspended in lysis buffer and subject to another passage of homogenization by 30 strokes and centrifuged at 1000 g for 10 min in 4°C. The supernatant of the first and second centrifugation were pooled and centrifuged at 75,000 g for 45 min at 4°C. The pellet was resuspended in storage buffer (50 mM Hepes, 5 mM $MgCl_2$, 1 mM $CaCl_2$, 0.1% BSA, 200 mM sucrose, pH 7.5) and stored at -20°C until use.

3.6.2. Western blot

Expression of ASGPR in the plasma membrane of HepG2 cells was studied by western blot analysis using a monoclonal antibody against ASGPR subunit 1 and 2. Sodium dodecylsulphate-polyacrylamide gel electrophoresis (SDS-PAGE) was performed with a Mini-Protean Tetra cell apparatus (Bio-Rad) using a Tris/glycine/SDS buffer (Bio-Rad). Plasma membrane from HepG2 cells and half the volume sample buffer (8% SDS, 40% glycerol, 0.25 M bromphenol blue, 400 mM DTT, Tris-HCl pH 6.8,) were mixed, incubated 5 min at 95°C and loaded on 12% Mini-Protean TGX Precast gels (Bio-Rad). After electrophoresis, proteins were transferred electrophoretically to 0.45 µm pore size nitrocellulose membranes (2.5 h at a constant voltage of 20 V) using a Mini Trans-Blot cell (Bio-Rad) and Tris/glycine buffer (Bio-Rad). The membranes were incubated for 2 h in blocking buffer (PBS containing 0.025% Tween 20 (PBS-T) and 5% powdered skimmed milk). Washed membranes were incubated in 2 µg/ml mouse anti-human ASGPR-1/2 IgG in PBS-T containing 1% BSA overnight at 4°C. Subsequently, washed membranes were incubated for 1 h at room temperature with horseradish peroxidase-conjugated goat anti-mouse IgG, at a dilution of 1:3000 (Bio-Rad), in PBS-T containing 1% BSA. Presence of ASGPR-1/2 was visualized by

incubation of the membrane 10 min at room temperature with the Opti-4CN-Kit (Bio-Rad) by colormetric detection.

3.7. *In vitro* uptake assay

3.7.1. Confocal laser scanning microscopy (CLSM)

HepG2 cells were cultured on poly-D-lysine coated cover slips (#1.5, Menzel, Braunschweig, Germany). Prior to incubation, cells were washed with warm D-PBS (Gibco) and pre-incubated for 1 h in DMEM low glucose without phenol red. For competition experiments, free AF or Gal were added to the medium during the pre-incubation period. Cells were incubated for 20 min with Gal-CF and AF-CF, and for 30 to 40 min with AF-PEG-conjugated liposomes at 4°C and 37°C. Nucleus counterstaining was performed by adding Hoechst 33342 (1 µg/ml) throughout the last 5 min of the uptake experiment. Cells were washed three times with cold D-PBS and fixed for 15 min with 2% PFA at 4°C. After an additional wash, slides were embedded in Prolong Gold antifade reagent (Gibco) and sealed with nail polisher after drying. Samples were analyzed with an Olympus FV-1000 inverted CLSM (Olympus), using a 60x PlanApo N oil-immersion objective (numerical aperture 1.40), and images were processed using either Imaris software (version 7.4, Bitplane, Zürich, Switzerland) or Gimp 2.8 software (GNU image manipulation program, http://www.gimp.org). Liposomes containing QDs were activated by light-emitting diodes (LEDs) with a wavelength of 400 nm (210 mW/cm^2) or 490 nm (190 mW/cm^2) (CoolLED 2012), using a pE-2 LED (CoolLED, Andover, UK) excitation system. Lambda scans of images containing QDs were performed with a fixed excitation wavelength of 488 nm and a variable emission between 550 nm and 700 nm, with a bandwidth of 10 nm and a step-size of 2 nm. Analyses of defined regions of interest (ROIs) were performed using the Olympus Fluoview software (version 3.1, Olympus).

3.7.2. Flow cytometry

Uptake experiments of Gal-CF, AF-CF, and competition studies were performed as described above. Cells were washed three times with cold D-PBS and detached using Accutase (Sigma-Aldrich), followed by centrifugation at 200 g for 5 min at 4°C and resuspended in staining buffer containing D-PBS, 2% fetal calf serum (FCS), and 0.1% NaN_3. For analyzing extracellular ASGPR, cells were incubated in staining buffer with mouse anti-human ASGPR-1/2 IgG (diluted 1:40) for 30 min at room temperature. After washing and centrifugation of the cells (200 g for 5 min at 4°C), they were incubated with goat anti-mouse-RPE (diluted 1:200) in staining buffer for 30 min at room temperature. For excluding apoptotic cells, 7-AAD (2 µg/ml) was added to the cell suspension at least 20 min prior to the analysis and 10 000 to 20 000 cells were analyzed per sample. Flow cytometry measurements were carried out using a FACSCalibur flow cytometer and the CellQuest software (Becton Dickinson, San Jose, CA), or using a CyAn ADP flow cytometer with Summit software (Beckman Coulter, Nyon, Switzerland). Final analysis of the data was performed with the Kaluza software (Beckman Coulter).

Remaining cells from flow cytometry experiments were washed, centrifugated (200 g for 5 min at room temperature), and fixed in 2% PFA for 10 min at room temperature. After washing and centrifugation (200 g for 5 min at room temperature), cells were mounted in Prolong Gold antifade reagent on a microscope slide. Samples were analyzed with an Olympus FV-1000 inverted CLSM (Olympus), using a 60x PlanApo N oil-immersion objective (numerical aperture 1.40).

3.8. Animal experiments

All animal experiments were carried out in accordance with local legislation on animal welfare. Male jugular vein catheterized CD rats (weighing 300 – 320 g) were obtained from Charles River Laboratories (L'Arbresle Cedex, France). Non-pegylated liposomes (nominal 3 µmol phospholipids / animal), AF-PEG-liposomes (nominal 3 µmol phospholipids / animal), free AF in 0.9% NaCl (7 mg / animal), or a carbon black solution (1 ml/kg body weight, diluted 1:9 using 0.9% NaCl, (Pelikan, Hannover, Germany)) were injected and animals were euthanized after 30 min using CO_2 inhalation. Liver tissue was frozen in cold isopentan (colled with liquid nitrogen) and cryosections of 10 µm were prepared. After drying the samples on Superfrost Plus Ultra G 90 microscope slides (Menzel), samples were washed with D-PBS and fixed with 2% PFA for 15 min at room temperature. Subsequent to washing, slides were counterstained with Hoechst 33352 (1 µg/ml) and mounted in Mowiol 4-88 / p-phenylenediamine (9:1, v/v). Samples were analyzed with an Olympus FV-1000 inverted CLSM (Olympus), using a 60x PlanApo N oil-immersion objective (numerical aperture 1.40), and pictures were processed using Gimp 2.8 software (GNU image manipulation program).

4. Results

4.1. Selection of a targeting vector using HepG2 as an *in vitro* model

Different compounds were explored for their capacity to target the ASGPR, with the intention to select an optimal vector to be used for the design of a hepatocyte specific drug delivery system.

4.1.1. Anti-asialoglycoprotein receptor type 1 antibody

The commercial mouse monoclonal anti-ASGPR-1/2 antibody from type IgG2b was raised against the full length of the first subunit of human ASGPR and can bind the extracellular domain of the receptor. In addition, the antibody cross reacts with the second subunit of the receptor, due to a partly identical amino acid sequence (Uniprot.org 2012c). To validate a sufficient expression of the receptor in the plasma membrane of the used *in vitro* cell culture model HepG2, the presence of ASGPR was confirmed by western blot analysis (Figure 4).

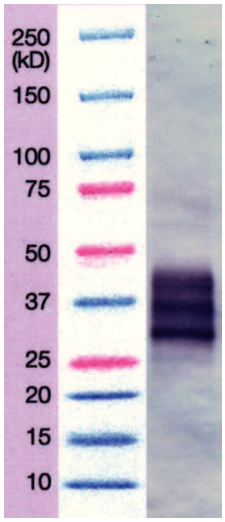

Figure 4: Western blot analysis of HepG2 plasma membrane with monoclonal anti-ASGPR-1/2 antibody. While the upper band corresponds to the mature receptor (approximately 41 kDa), the two lower bands are consistent with the first and second subunit of the ASGPR with an expected molecular weight of 33 kDa and 35 kDa, respectively.

Plasma membranes of HepG2 cells were obtained by sequential centrifugation and collecting the corresponding fraction. Gel electrophoresis and subsequent staining with the anti-ASGPR-1/2 antibody resulted in three bands in the range between 33 and 41 kDa, which can be assigned to the unglycosylated and the apparent molecular weight of glycosylated receptor.

4.1.1.1. Extracellular binding of anti-asialoglycoprotein receptor antibody

Extracellular binding to the ASGPR was confirmed by flow cytometry and by microscopy. For the analysis by flow cytometry, non-permeabilized HepG2 cells were stained with anti-ASGPR-1/2 mAb and subsequently labeled with a second antibody with RPE (Figure 5). A strong shift of the fluorescent signal by more than two logarithmic orders in magnitude was observed. A control with the secondary antibody was performed to validate the specificity of the signal. Apoptotic cells were excluded by gating the 7-AAD negative cell population.

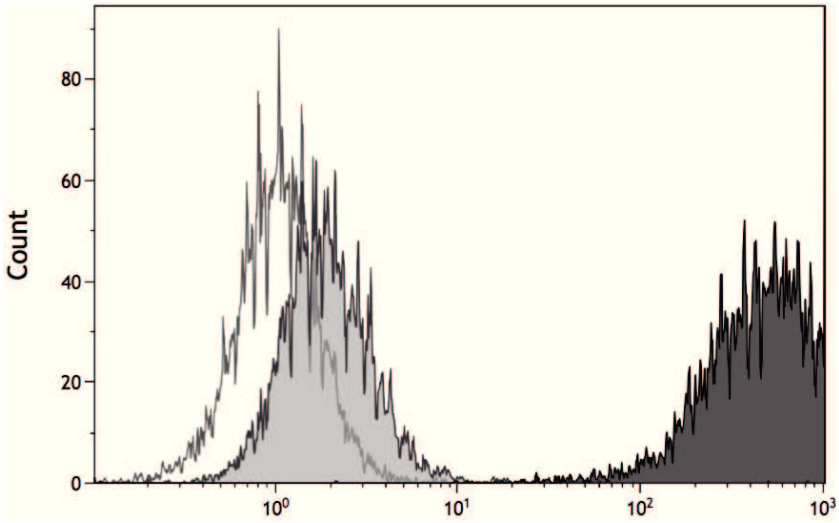

Figure 5: Flow cytometry of anti-ASGPR-1/2 antibodies on HepG2 cells. Cells were labeled with monoclonal mouse anti-ASGPR-1/2 and goat anti-mouse-RPE antibodies (black histogram). The white and gray histograms result from control cells and cells only labeled with secondary antibodies, respectively. Dead cells were excluded by gating 7-AAD negative cells only.

Samples remaining from flow cytometry experiments were subsequently fixed and further studied by CLSM (Figure 6). Therefore, detached cells were directly mounted on a cover slip, which resulted in a more rounded cell appearance compared to adherently attached cells exhibiting a

more stretched out shape (e.g. Figure 11). While living cells (7-AAD negative) displayed a homogeneous coverage of receptors on the cell membrane, almost no signal of membrane-bound ASGPR was obtained from apoptotic cells. Again, control samples only using the secondary antibody were produced to exclude any non-specific binding of the secondary antibody.

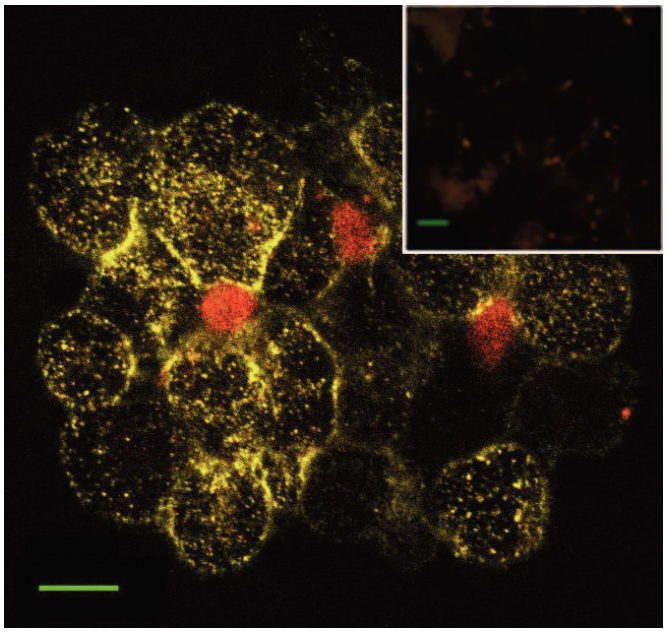

Figure 6: CLSM of anti-ASGPR-1/2 antibodies on HepG2 cells. ASGPR were labeled with monoclonal mouse anti-ASGPR-1/2 and goat anti-mouse-RPE antibodies (yellow). Nuclei of apoptotic cells were stained with 7-AAD (red). The insert presents the control experiment with secondary antibodies only. Scale bars represent 10 µm.

4.1.2. Galactose as a vector

Since terminal galactose residues of glycoproteins bind with a high affinity to the ASGPR on hepatocytes, the direct binding of galactose was investigated. To be able to study binding and uptake of the monosaccharide, a fluorescent dye was coupled. Therefore, 4-Aminophenyl β-D-galactopyranoside was attached to CF-NHS (Figure 7). The NHS reagent reacted with the nucleophilic nitrogen of the 4-Aminophenyl moiety with a release of the NHS leaving group, to form a stable amide bond, resulting in a fluorescent galactose (Gal-CF). An excess of the fluorescein-containing educt was used and the reaction progress was monitored by HPLC analysis. After a reaction time of 60 min, complete disappearance of the galactose-containing starting material was

observed and a double peak of Gal-CF, corresponding to the 5- and 6-position of the carboxylic function of CF, was obtained (data not shown).

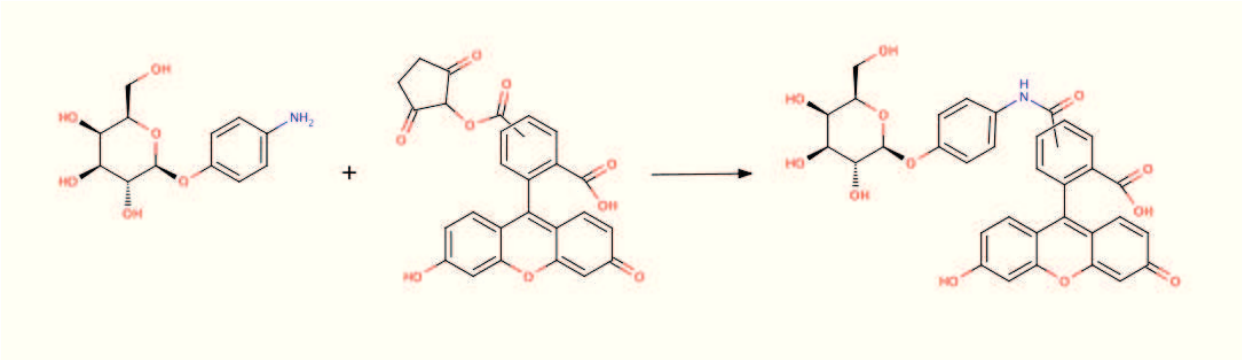

Figure 7: Schematic illustration of the coupling reaction of fluorescent galactose (Gal-CF). The modified monosaccharide 4-Aminophenyl β-D-galactopyranoside was conjugated to a 5(6)-carboxyfluorescein N-hydroxysuccinimide ester. The primary amine reacted with the NHS-Ester to form a stable amide bond.

Receptor binding was studied by CLSM (Figure 8) and flow cytometry (Figure 9). Under the microscope, fluorescence was detected at a concentration of 108 µM Gal-CF, while lower concentrations did not result in a signal (data not shown). Despite a clear sign of binding, no inhibition was possible with a 10-fold excess of unlabeled Gal or 90 µM AF (corresponding to 4 mg/ml), which is a well-known ligand for ASGPR with a high affinity.

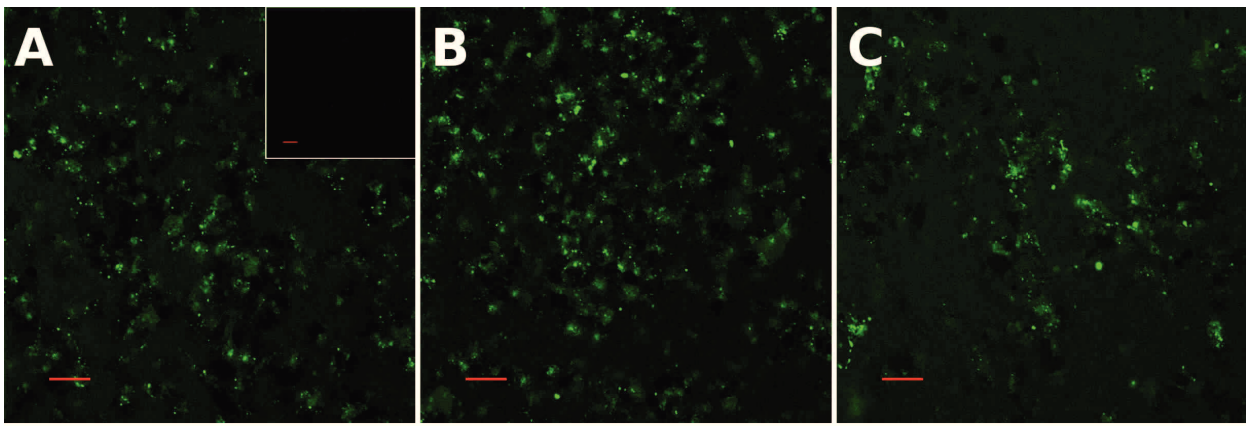

Figure 8: CLSM of fluorescent-labeled galactose (Gal-CF) taken up by HepG2 cells. A weak uptake could be observed at a concentration of 108 µM Gal-CF after 20 min (A). Competing with a 10-fold excess of free galactose was not inhibiting the uptake of Gal-CF (B). Only slight inhibition of Gal-CF uptake was detected in the presence of 90 µM free AF (C) The insert in panel A displays a control sample without Gal-CF. Scale bars represent 10 µm.

These results were confirmed by flow cytometry. While concentrations of 36 µM Gal-CF produced a 10-fold increase in the signal, only a weak shift of the fluorescent peak could be detected at a concentration of 3.6 µM. Also pre-incubation with unlabeled AF did not diminish the signal of Gal-CF on HepG2 cells.

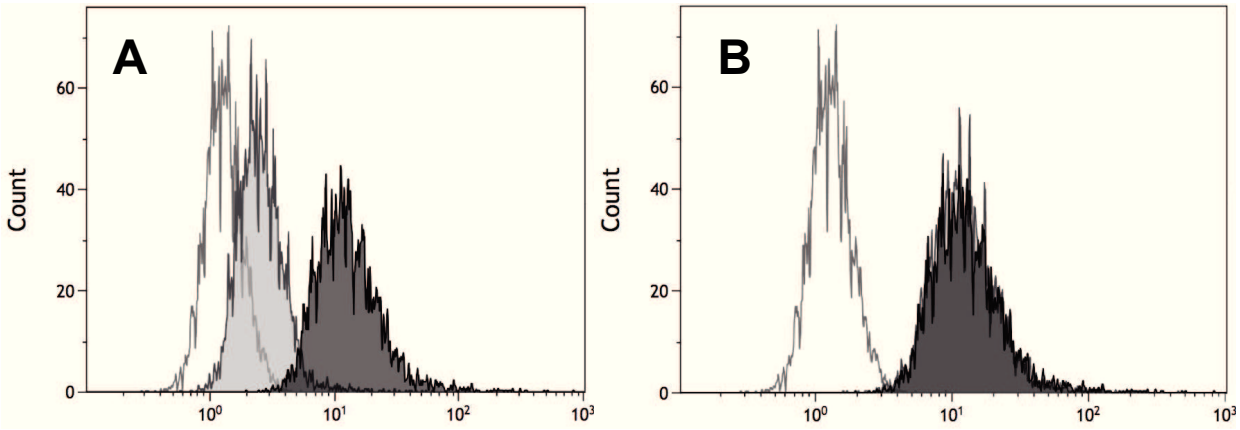

Figure 9: Flow cytometry analysis of fluorescent-labeled galactose (Gal-CF) on HepG2 cells. The black histograms represent cells incubated with 36 µM Gal-CF, while the white histograms show untreated cells (panel A and B). The gray histogram in panel A displays a concentration dependency of the signal, representing a 10-fold reduced amount of Gal-CF (3.6 µM). In panel B the gray histogram, which overlaps with the black histogram, compares inhibition of the signal in presence of 90 µM AF. Dead cells were excluded by gating 7-AAD negative cells only.

It can be stated that a binding occurred, but a specific uptake via ASGPR is questionable, since the signal cannot be inhibited with an excess of unlabeled Gal or AF.

4.1.3. Asialofetuin as a vector

Labeling of the desialated glycoprotein AF was done using CF-NHS. The NHS ester binds primarily to the α-amine at the N-terminus and the ε-amines of lysine side chains to form a stable amide bond (Hermanson 2008) (Figure 10). After purification by size exclusion chromatography, the degree of labeling was calculated to be in the range of 3.0 to 4.2 CF molecules per molecule of protein (Thermo Scientific 2009).

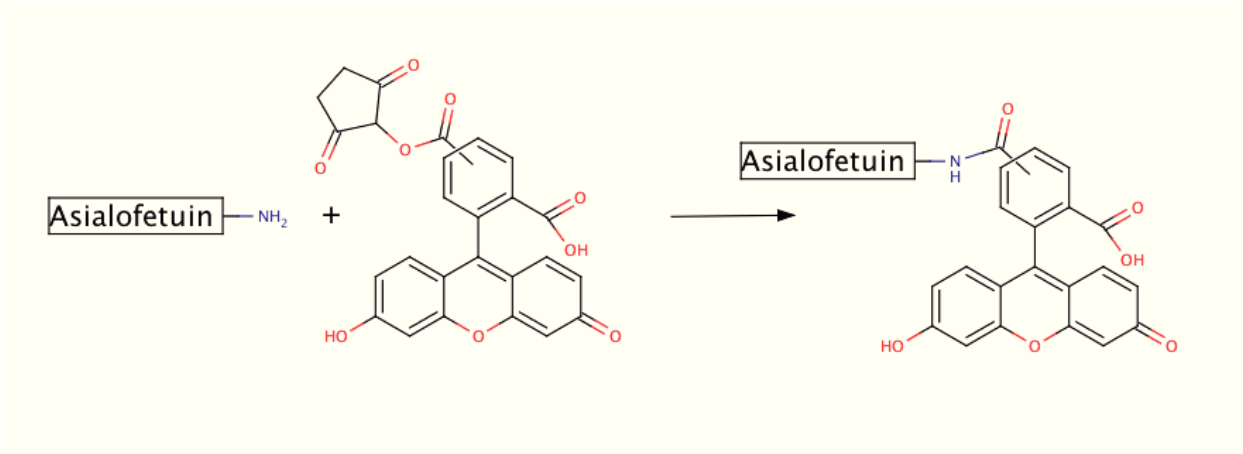

Figure 10: Schematic illustration of the coupling reaction of fluorescent asialofetuin (AF-CF). The N-terminus of the protein backbone or ε-amines of lysine side chains from asialofetuin reacted with 5(6)-carboxyfluorescein N-hydroxysuccinimide ester to form a fluorescent-labeled asialofetuin.

Incubating HepG2 cells with small concentrations of 0.23 µM fluorescent-labeled AF (corresponding to 10 µg/ml) resulted in a strong signal after an uptake period of 20 min (Figure 11). When cells were pre-incubated with unlabeled AF at a 100-fold higher concentration (23 µM), the uptake was virtually completely inhibited. Further, it should be noted that the green signal had a strongly point-shaped distribution and was clearly distinguishable from the greenish ubiquitous background fluorescence.

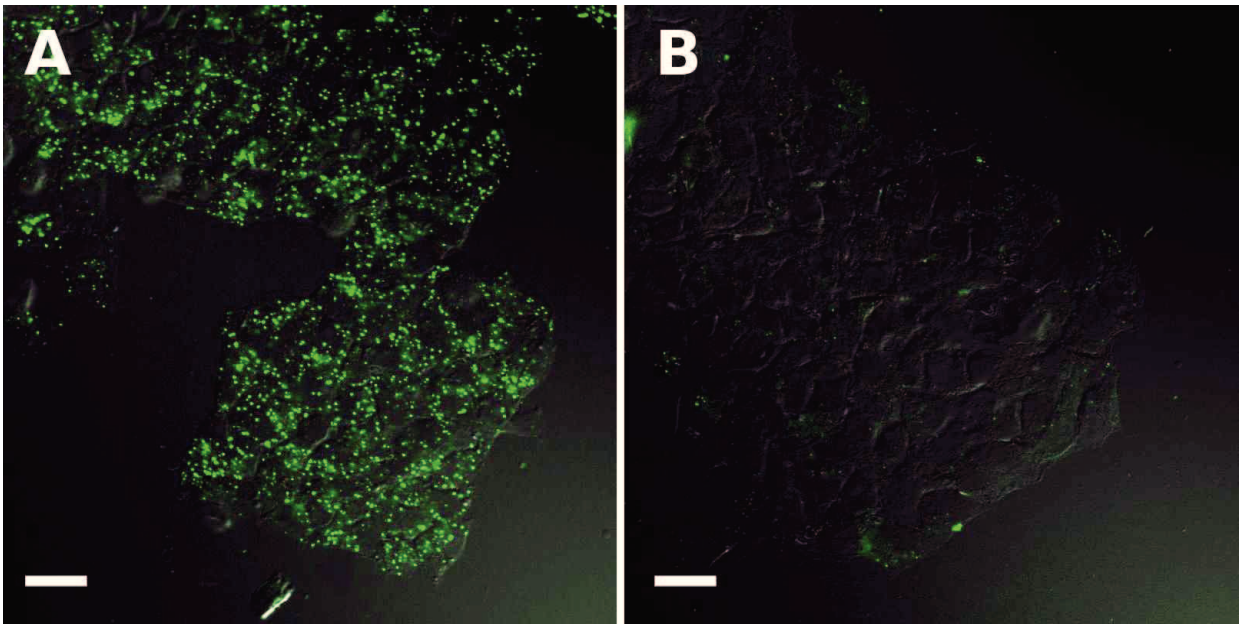

Figure 11: CLSM analysis of carboxyfluorescein-conjugated AF with HepG2 cells. HepG2 cells were incubated for 20 min with 0.23 µM carboxyfluorescein-coupled AF (panel A). Competitive inhibition of signals using 23 µM unbound AF (panel B). An overlay of carboxyfluorescein signal with DIC images of the cells is shown. Scale bars represent 20 µm.

Analysis with flow cytometry resulted in a similar outcome (Figure 12). While the fluorescent signal shifted by a factor of 10 in the presence of 0.23 µM AF-CF, a clear inhibition could be observed by pre-incubating the cells with 23 µM of unlabeled AF.

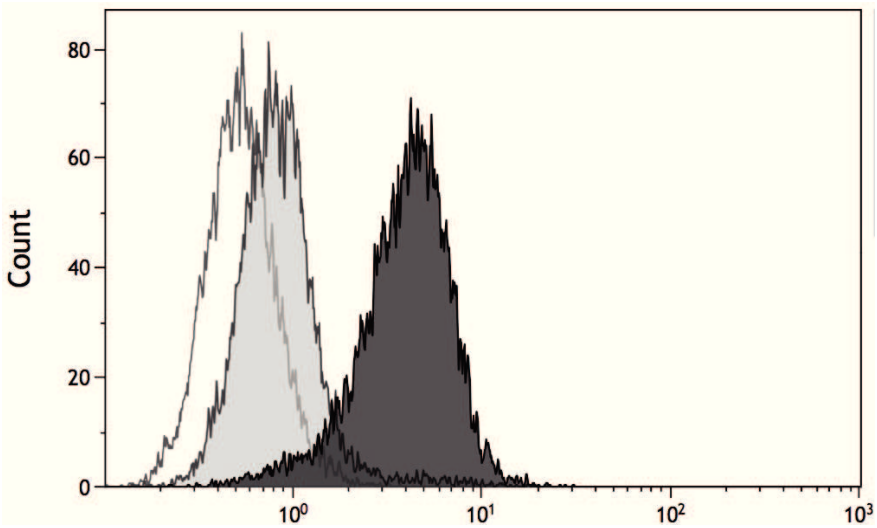

Figure 12: Flow cytometry analysis of carboxyfluorescein-conjugated AF with HepG2 cells. HepG2 cells were incubated for 20 min with 0.23 µM carboxyfluorescein-coupled AF (black histogram). Competitive inhibition of fluorescence using 23 µM unbound AF (gray histogram). Control cells are shown as white histogram. Dead cells were excluded by gating 7-AAD negative cells only.

In summary, the binding of AF-CF produced a distinct and strong binding signal at low concentrations. This signal was suppressed in presence of the free ligand. This finding stands in contrast with the binding of Gal-CF, which resulted in a weaker signal even at two logarithmic orders in magnitude higher concentrations.

4.2. Liposomal Preparation

After optimizing the vector for targeting ASGPR on the surface of hepatocytes, liposomes with different fluorescent cargos were produced to be able to investigate a specific delivery *in vitro* and *in vivo*. Functionalized and pegylated phospholipids were incorporated in the liposomal formulation and coupled to AF. Hence, the conjunction of the targeting vector AF with the vesicle was achieved after preparing the liposomes by coupling the thiolated vector with maleimide-containing phospholipids (Figure 13).

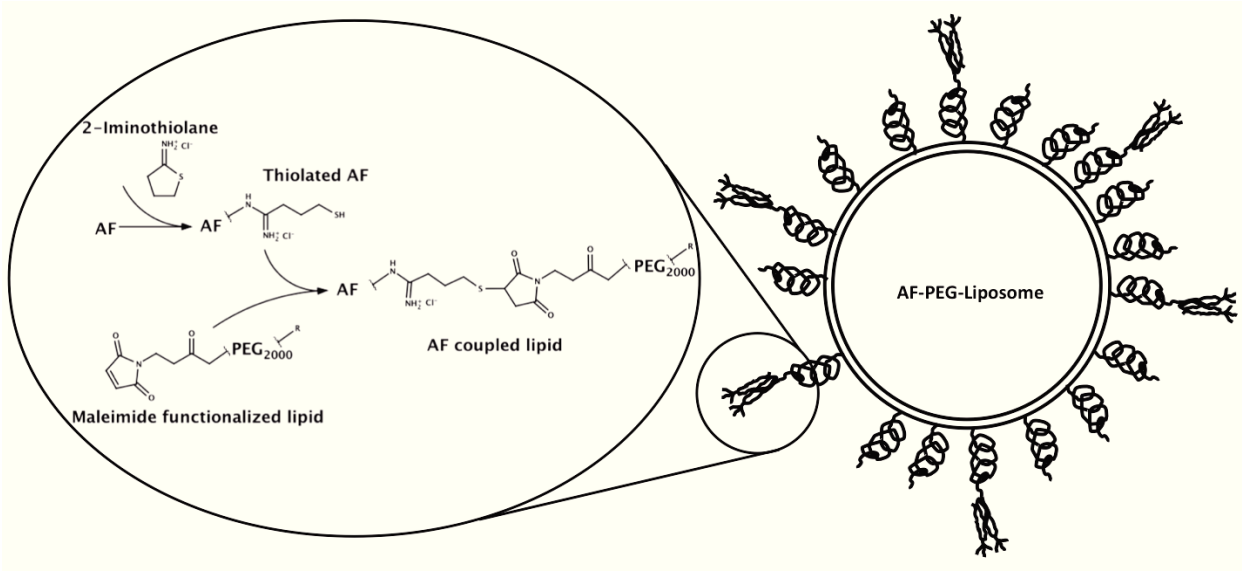

Figure 13: Schematic illustration of the bioconjugation of thiolated AF and maleimide-functionalized pegylated DSPE attached to liposomes. AF was thiolated with 2-Iminothiolane. In parallel, liposomes were prepared with maleimide-functionalized pegylated DSPE and thereafter conjugated to AF. Different cargos like QDs and carboxyfluorescein were loaded inside of the liposomes.

Liposomes were prepared by the extrusion method, using filters with a defined pore-size. Depending on the lipid mixture and the cargo, vesicles with a particle size in the range between 90 nm and 140 nm, with a moderate anionic zeta potential, were produced (Table 1). Adding small amounts of pegylated lipids to liposomes resulted in a significant smaller size, compared to their non-pegylated variants. Further, the addition of pegylated phospholipids facilitated considerably the force needed for the extrusion process, increased the steric stability, and was a prerequisite to achieve a specific targeting in the following *in vivo* experiments. Liposomes loaded with QDs were extruded through an 80 nm pore-size filter, because they were unable to pass through the smaller membrane of 50 nm, resulting in slightly larger vesicles. The narrow polydispersity index (PDI) of 0.06 of the pegylated formulations indicated a monodisperse size distribution. The produced liposomal formulations resulted in a remarkable shelf live when stored at 4°C. No increase in mean particle size and only a marginal larger PDI, but still monodisperse, was observed after storage for 14 months (data not shown).

For thiolation of AF, a molecular excess of 200-times of 2-iminothiolane was used. This resulted in an average of two sulhydryl groups per molecule of AF, which were analyzed by Ellman's reagent (Riddles et al. 1979) (data not shown). The amount of AF bound per vesicle was in the range of 30 to 270 molecules, based on the assumption that a 100 nm liposome contains approximately 80 000 molecules of phospholipids (Hansen et al. 1995). The coupling efficiency was on average 20% of the used thiolated AF.

Table 1: Characterization of prepared liposomes with different surface coating and cargo by dynamic and electrophoretic light scattering. Data represent mean ± SD; *n ≥ 5.

Formulation	Mean particle size (nm)	PDI	Zeta Potential (mV)
Control Liposomes	140 ± 38	0.141 ± 0.044	-13.7
PEG-Liposomes	89 ± 1	0.053 ± 0.001	-19.8 ± 8.5
AF-PEG-Liposomes*	97 ± 3	0.060 ± 0.032	-11.8 ± 4.6
AF-PEG-Liposomes / QD*	126 ± 10	0.060 ± 0.019	-13.1 ± 2.8

For the *in vitro* studies, the fluorescent marker carboxyfluorescein was loaded inside the liposomes as a solution (Figure 17, panel D), incorporated into the liposome membrane by using phospholipid-labeled dyes, or by attaching fluorescent-labeled and thiolated AF onto the liposomal surface (Figure 16, panel D). As an alternative to the classic dyes, quantum dots were incorporated as fluorescent markers (Figure 20, panel E)

4.2.1. Evaluation of the post-insertion method for labeling liposomes

The post-insertion method was investigated as an alternative strategy to incorporate (fluorescent or radioactive) tracers or vectors into the liposomal bilayer after preparing the vesicles. As a model compound, rhodamine B-conjugated phospholipids were hydrated in an aqueous buffer to form micelles. Subsequently, incubation with prepared liposomes under various conditions was investigated. With higher temperature and longer incubation time, the amount of rhodamine B-labeled phospholipids was increasing in the liposomal membrane. Liposomes were loaded with a

second dye, CF, as an internal standard to measure a possible loss of cargo during the incubation process (Figure 14).

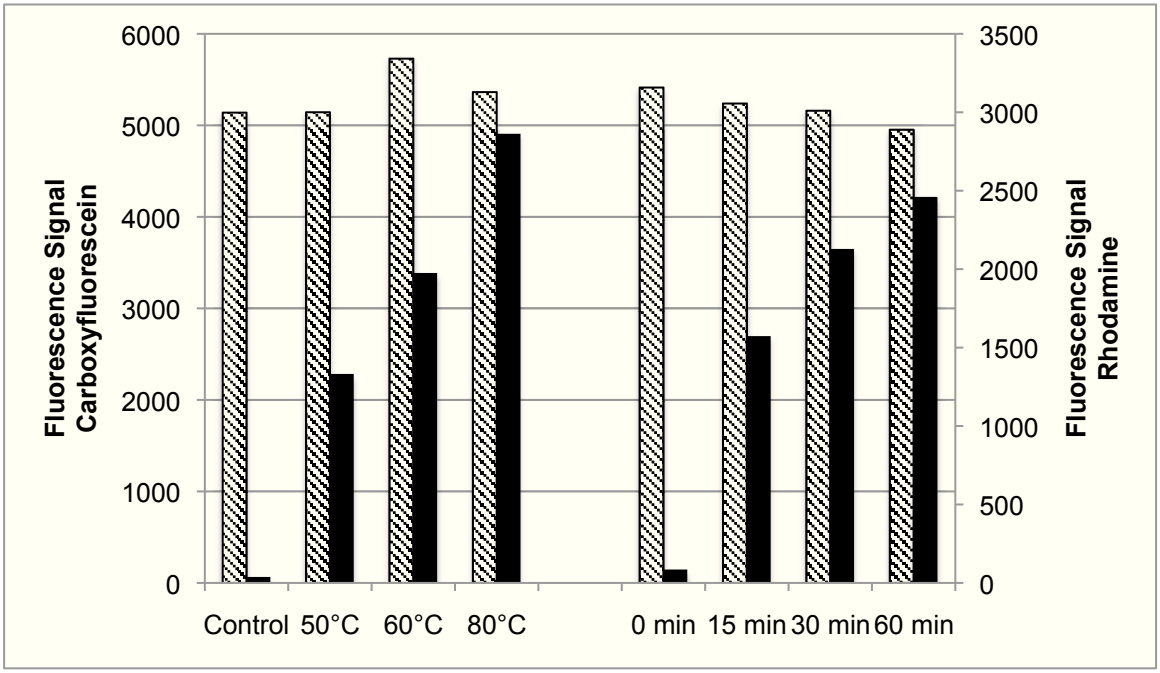

Figure 14: Incorporation of Rho-labeled phospholipids with the post-insertion method. Liposomes containing carboxyfluorescein as an internal standard (hatched bars) were incubated with rhodamine B-labeled phospholipids. The amount of rhodamine-labeled liposomes increased according to the incubation temperature and time.

Subsequent studies with CLSM, using mounted liposomes on a cover slip, resulted in a clear co-localization of the two fluorescent dyes. While the samples incubated at various temperatures (50°C to 80°C) were loaded with a self-quenching carboxyfluorescein solution, the second preparation of samples, incubated for different incubation periods (0 min to 60 min), contained a non-self-quenching fluorescent solution. Post-insertion at various temperatures resulted in a minimal increase in fluorescent signal, due to a reduced self-quenching effect, which derived from a decrease of the luminal CF concentration. The incubation of liposomes containing non-self-quenching concentrations of CF at 60°C resulted in a minimal loss of fluorescent signal, according to the incubation period. Studies using mounted liposomes on a cover slip with a CLSM revealed a clear co-localization of the two fluorescent dyes (Figure 15). Mean particle size did not change during the different incubation steps and the polydispersity index remained below 0.05, even at 80°C (data not shown).

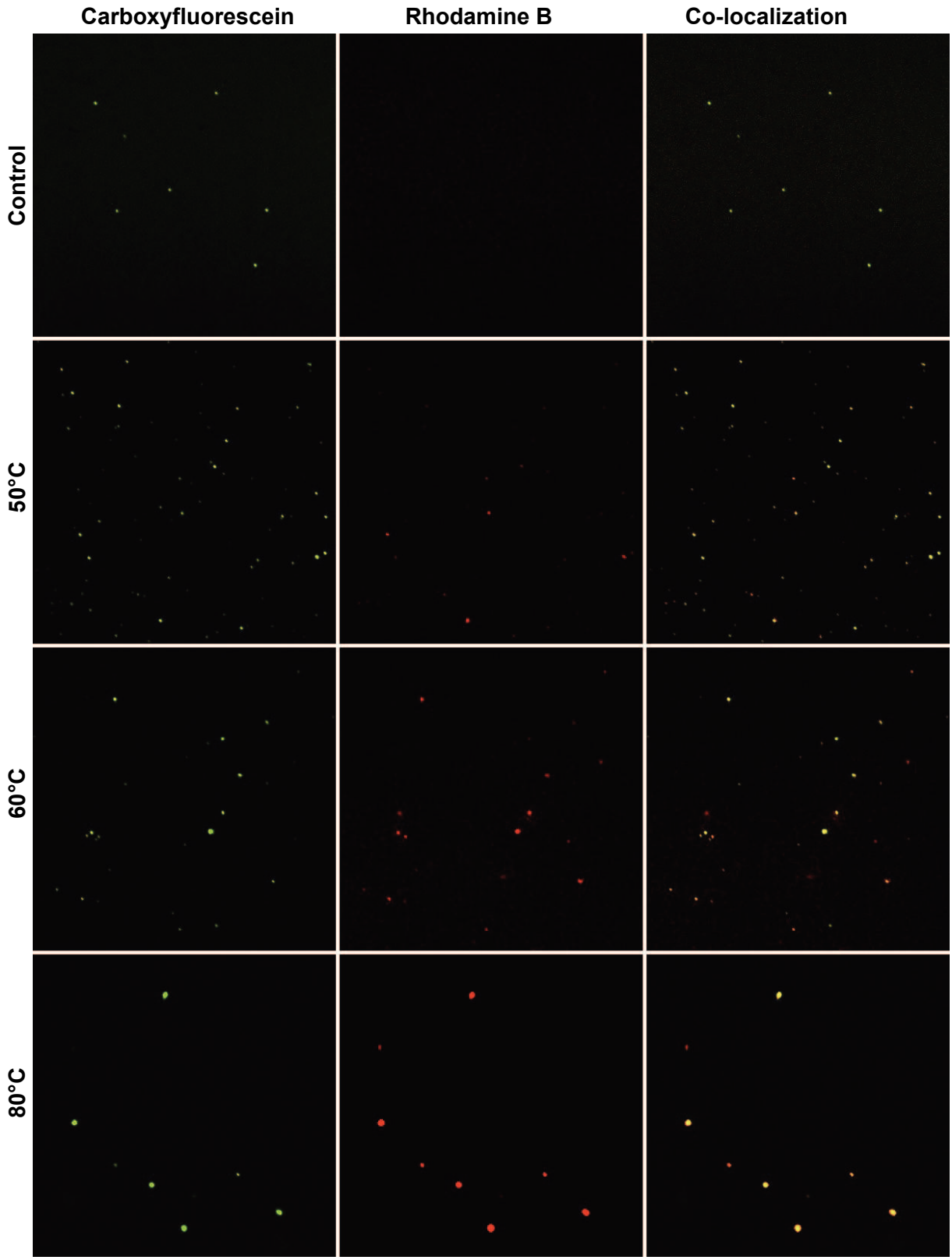

Figure 15: Visualization of the post-insertion method at various temperatures by CLSM. Liposomes were loaded with CF (green, first column) and incubated at various temperatures with Rho-labeled phospholipids (red, second column). Samples without incubation (control) and at 50°C rarely exhibit any spots of co-localization (third column, first and second picture). At 60°C and 80°C, most of the spots are co-localized (third column, third and fourth picture).

4.3. *In vitro* targeting of liposomes using asialofetuin as a vector

In vitro uptake of liposomes coupled to AF as a targeting vector was investigated with different fluorescent markers. Therefore, CF was attached either to the vector or was loaded inside the liposome. As an alternative, water soluble QDs were loaded into liposomes, which opens new possibilities in term of investigating uptake and distribution of liposomal cargo.

4.3.1. Uptake of pegylated liposomes coupled with carboxyfluorescein-labeled asialofetuin

To be able to investigate the route of the vector attached to the vesicles, CF-labeled AF was thiolated as described above and conjugated to maleimide-functionalized liposomes (Figure 16, panel D). After 30 min of incubation, a distinct uptake was observed, although a strong autofluorescence from the background of the cells was present (Figure 16, panel A). However, a clear contrast was visible when the signal was compared to the corresponding competition experiments. Therefore, cells were pre-incubated with an excess of free AF before incubating with AF-PEG-liposomes (Figure 16, panel B). The intensity of the autofluorescent signal from the background was visible in the control samples, which were incubated only with buffer (Figure 16, panel C).

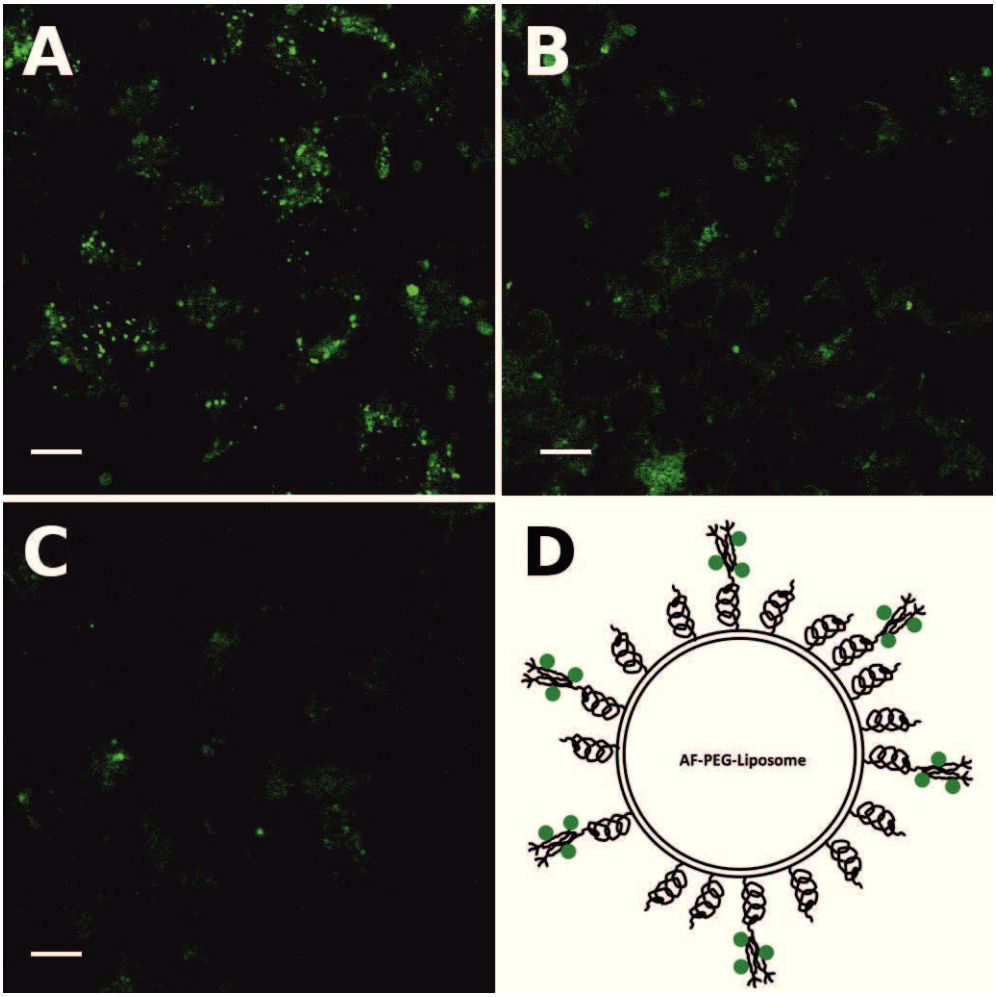

Figure 16: CLSM analysis of CF-labeled AF, attached on pegylated liposomes incubated with HepG2 cells. HepG2 cells were incubated 30 min with CF-labeled AF coupled to pegylated liposomes (panel A, corresponding to nominal 2.9 mM phospholipids). Control samples were treated identically after pre-incubation with 23 µM free AF (panel B). Cells showing only autofluorescence are presented in panel C. Panel D shows a schematic picture of the fluorescence-labeled AF attached to the liposomes. Scale bars represent 10 µm.

4.3.2. Uptake of asialofetuin-pegylated liposomes loaded with carboxyfluorescein

Additionally to the experiments with the CF-labeled AF attached on the liposomes, as described above, the fluorescent dye was incorporated inside of the liposomes by passive loading (Figure 17, panel D). In contrast to the delivery of only single fluorescent molecules, attached to the liposomal surface, the vesicles were loaded with a self-quenching solution of CF. After the uptake of the vesicles in the endosomal-lysosomal pathway and subsequent lyses of the liposomal membrane, the CF solution was diluted and the fluorescence liberated. The green fluorescent signal of the

vesicles was clearly visible (Figure 17, panel A), while giving a higher contrast to the background compared to the preparation described above (Figure 16, panel A). The competition experiment, with additional free AF, resulted in a substantial reduction in the signal (Figure 17, panel B). The background autofluorescence was again prominently visible as little green dots (Figure 17, panel C), but had a more blurred and a less intense signal than the CF-loaded liposomes. Therefore, the preparation with loading high amounts of CF inside the liposomes produced an increased signal, compared to the attachment of CF-labeled AF onto the surface of the vesicles.

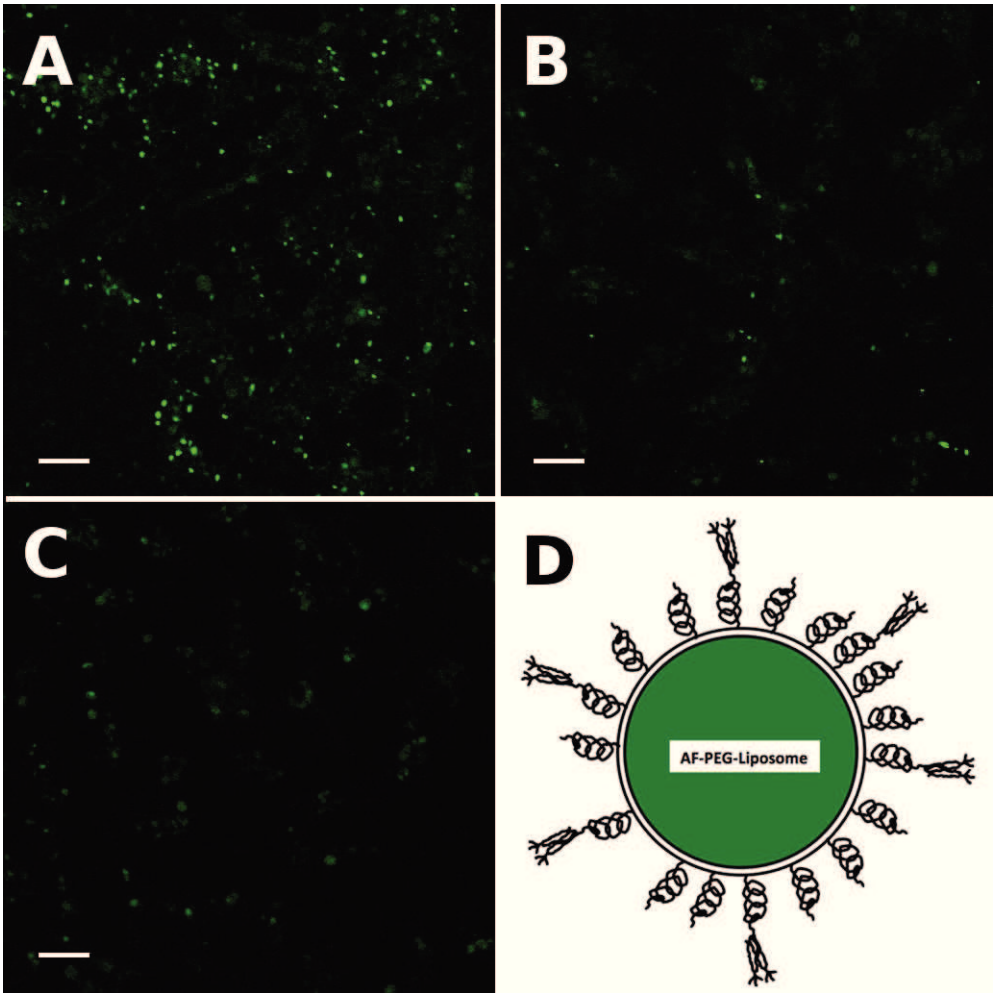

Figure 17: CLSM analysis of pegylated Liposomes coupled with AF and loaded with CF. AF-PEG-liposomes loaded with a CF solution of 60 mM were incubated 30 min with HepG2 cells (panel A, corresponding to nominal 2.9 mM phospholipids). Identically treated control samples were pre-incubated with 23 µM free AF (panel B). Panel C displays control cells. A schematic picture of the AF-PEG-liposomes loaded with CF is shown in panel D. Scale bars represent 10 µm.

4.3.3. Uptake of liposomes loaded with quantum dots

Quantum dots (QD) can be incorporated into liposomes as alternative fluorescent dyes. In our setting, the goal was to achieve an increased fluorescent signal-to-noise ratio by using QDs. An additional advantage is the resistance towards bleaching of these fluorescent materials.

4.3.3.1. Liberating fluorescent signal of quantum dots after *in vitro* uptake

Hardly any fluorescent signal was observed after incubation of QDs containing AF-PEG-liposomes (Figure 18, panel A). Further investigations revealed that photoactivation of the samples are needed to liberate the fluorescent signal. Visual examination resulted in the conclusion that best results were obtained after an exposure of the sample for 3 min at a wavelength of 490 nm (Figure 18, panel B). Additional periods of the exposure did not result in a remarkable increase in signal strength (Figure 18, panel C). The incubation of the sample at a lower and energy richer wavelength, already for a short period of time (15 s), resulted in a strong background signal from the cells, which made detection of QDs difficult (Figure 18, panel D).

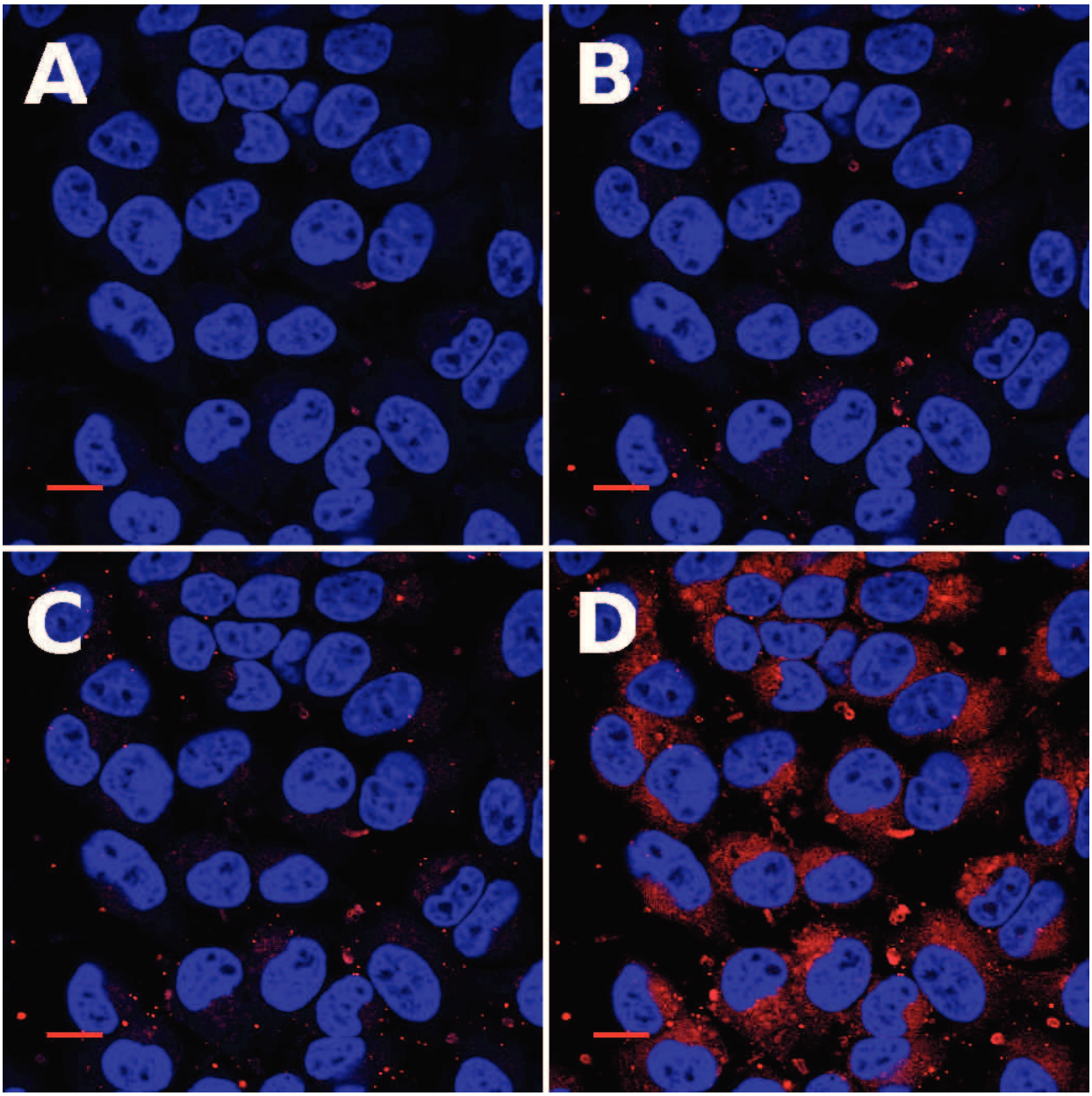

Figure 18: Photoactivation of liposomal QDs in HepG2 cells with irradiation. Panel A displays the cells without photoactivation. Panel B and C show the same sample after photoactivation at a wavelength of 490 nm for 3 min and 10 min, respectively. Panel D shows an unspecific arising of background signal after additional activation for 15 s at a wavelength of 400 nm. Scale bars represent 10 µm.

Next to liberating the fluorescent signal of QDs encapsulated in liposomes, the emission spectrum was investigated to validate the presence of QDs inside of the cells. Thus, a lambda scan of a HepG2 cell was performed and the spectra of fluorescing dots were compared (Figure 19). Bright spots showed a narrow emission peak around 610 nm, while spots from the background produced a broad emission spectra. The sharp emission peak demonstrated the presence of QDs. The

emission maximum of QDs (data not shown) shifted from 625 nm to 610 nm after liposomal incorporation and uptake by cells. This blue shift of the emission signal is an indication for a process resulting in a smaller QD-size. After liberating the fluorescent signal, no further emission shift could be observed even after a prolonged exposure or different wavelengths.

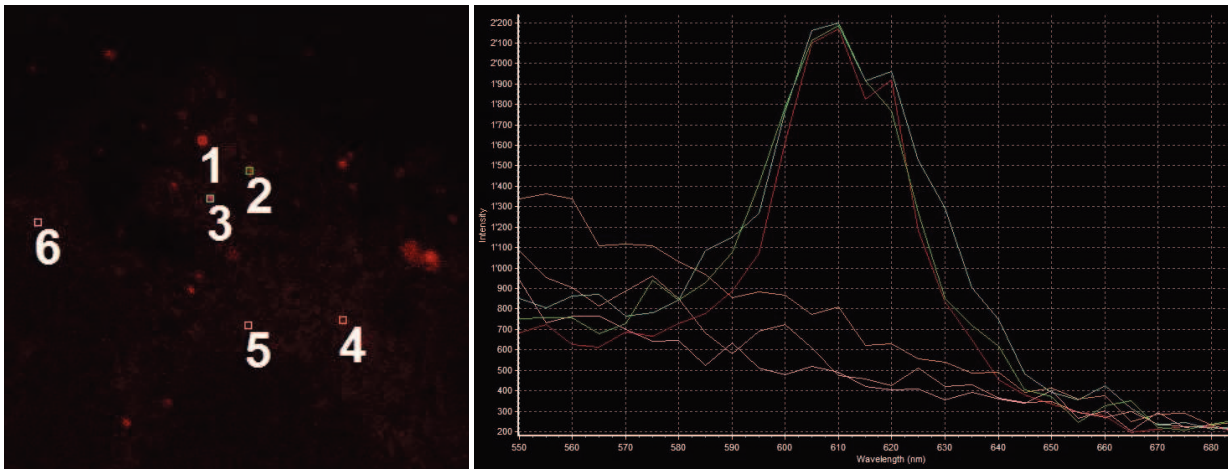

Figure 19: Determination of emission peaks of intracellular QDs. A lambda scan was performed from 550 to 700 nm with an excitation at 488 nm. The left picture shows HepG2 cells with three regions of interest (ROIs # 1 to 3) of fluorescent QDs compared with three identical ROIs of background signal (# 4 to 6). In the right picture, the intensity of these ROIs are displayed at various wavelengths. Green, blue and red lines indicate spectra of QDs.

4.3.3.2. *In vitro* uptake of quantum dot-liposomes coupled with asialofetuin

Despite the described optical limitations of QDs, a successful incorporation into AF-PEG-liposomes (Figure 20, panel E) and an uptake was achieved in HepG2 cells after 40 min of incubation. QDs were activated for 5 min at a wavelength of 490 nm with a light-emitting diode (LED) and small, well-defined spots became visible inside of the cells (Figure 20, panel A). Although the obtained signal was not as strong as comparable liposomal formulations with CF, a clear difference was observed when an excess of free AF was added to the sample (Figure 20, panel B). In further experiments, CF-labeled phospholipids were incorporated into AF-PEG-liposomes and loaded with QDs. Distribution and co-localization were investigated after the uptake or binding at 37°C and 4°C, respectively (Figure 20, panel C and D). While the QDs and the liposomal membrane accumulated in bigger spots at 37°C, indicating a cellular uptake and

accumulation within the endosomal or lysosomal compartments, a distinct distribution on the cell surface was visible at 4°C.

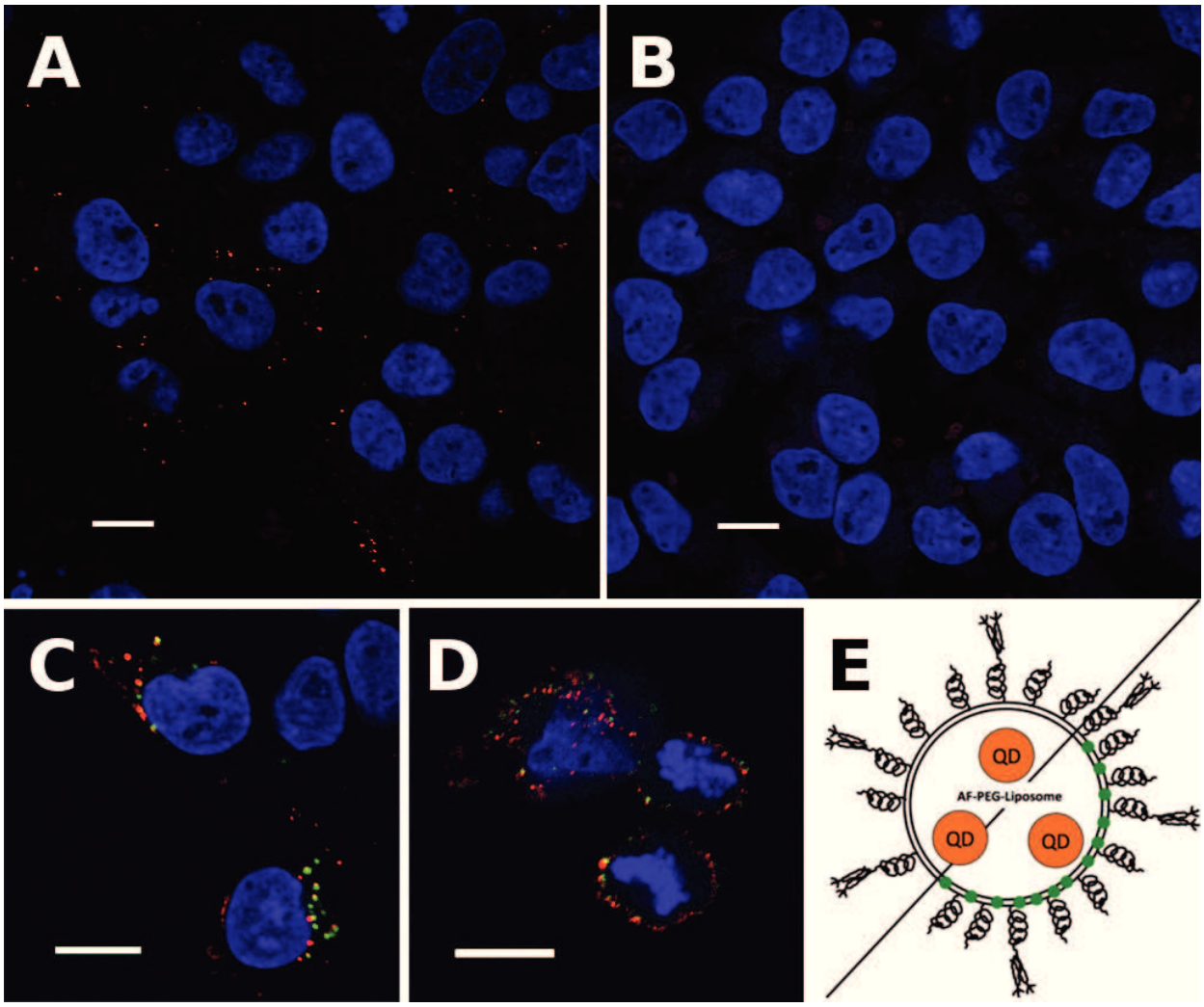

Figure 20: Cellular uptake of QDs encapsulated in AF-PEG-liposomes into HepG2 cells. Cells were incubated 40 min with AF-PEG-liposomes loaded with QDs (red spots, panel A, corresponding to nominal 0.13 mM phospholipids). Identically treated samples in presence of 23 µM free AF were compared (panel B). QDs were incorporated into AF-PEG-liposomes containing CF-phospholipids (green spots) and taken up for 40 min at 37°C (panel C) or bound to the cell surface at 4°C (panel D), respectively (corresponding to nominal 0.35 mM phospholipids). Nuclei are stained with Hoechst 33342 (blue signal). A schematic representation of loaded QDs inside AF-PEG-liposomes without and with additional CF-phospholipids is displayed in panel E. Scale bars represent 10 µm.

Further investigation of the uptake of AF-PEG-liposomes loaded with QDs revealed additional differences to conventional dyes, like CF. While the signal of CF became blurred when the vesicles were taken up and disrupted in the endosomes or lysosomes, the fluorescent signal of QDs remained as distinct spots inside of the cells (Figure 21). This observation could be attributed to

the crystal structure of QDs in the nm-range, permitting to trace the fluorochromes at a single-molecule level even after entering the endosomal or lysosomal pathway.

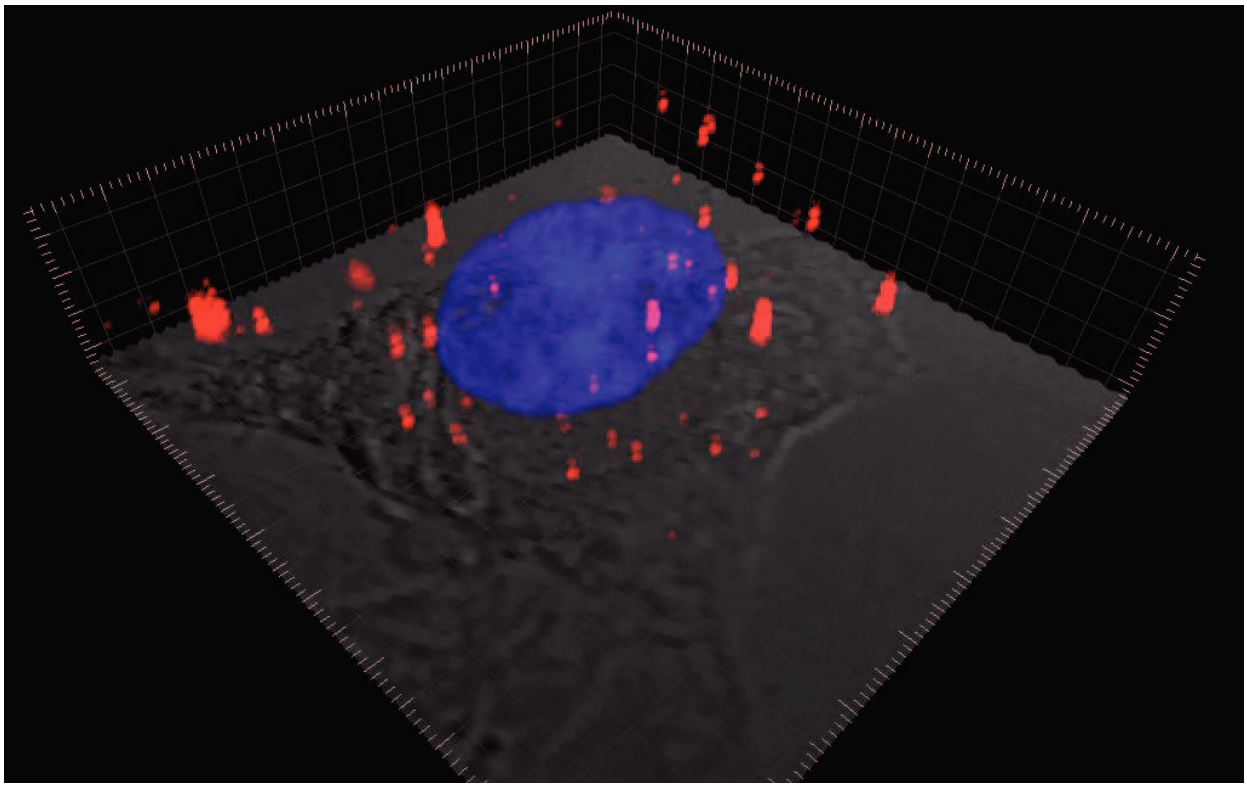

Figure 21: 3-D visualization of QDs after intracellular uptake of loaded AF-PEG-liposomes. A 3-dimensional scan of the nucleus (blue signal) of a HepG2 cell and uptake of distinct liposomal QDs (red signal) above a 2-dimensional differential interference contrast (DIC) image of the cell.

4.4. *In vivo* proof of concept

For investigating the liver distribution in rats, fluorescing phospholipids were incorporated in pegylated and non-pegylated liposomal formulations and intravenously administrated, together with carbon black, which is selectively taken up by Kupffer cells (Cowper et al. 1990). In the obtained liver sections, it was the goal to demonstrate a different distribution pattern of the varying liposomal preparations, which correspond to hepatocytes or Kupffer cells, respectively (Figure 22). Since dyes in the red spectra compete with a lower background signal, compared to dyes like CF with a green emission wavelength, rhodamine B was used as a fluorescent marker.

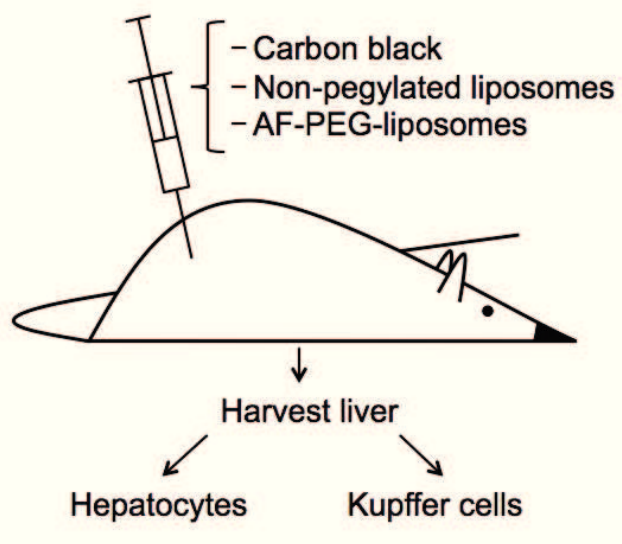

Figure 22: Schematic representation of *in vivo* animal experiments. Liver uptake and distribution patterns between hepatocytes and Kupffer cells were investigated in male rats after injection of AF-PEG-liposomes and compared with non-pegylated liposomes together with carbon black as Kupffer cell specific marker.

4.4.1. Uptake by hepatocytes and Kupffer cells

In general, liposomes accumulate in the liver in Kupffer cells, which belong to the RES. Therefore, pegylated formulations were used to increase the half-life and omit non-specific clearance from the circulation (Huwyler et al. 2008). To be able to distinguish the histological pattern of non-pegylated liposomes taken up by Kupffer cells from vesicles specifically targeting hepatocytes, control liposomes, labeled with rhodamine B-phospholipids, without PEG and AF were injected. In combination, colloidal carbon was administrated intravenously to stain Kupffer cells (Neyrinck et al. 2000). After an uptake period of 30 min, liver cryosections displayed well-defined single spots of accumulated fluorescent liposomes (Figure 23, panel A) together with the same pattern of carbon accumulation (Figure 23, panel B). An overlay of the two images demonstrated co-localization of the liposomal formulation and the colloidal carbon (Figure 23, panel C). The insert in panel C showed the cell density of the same image, which indicated that liposomal and carbon black-stained cells represented only a minority of total cells. This pattern was in accordance to a cell density of approximately 10%, which has been reported for Kupffer cells in the liver (Cowper et al. 1990).

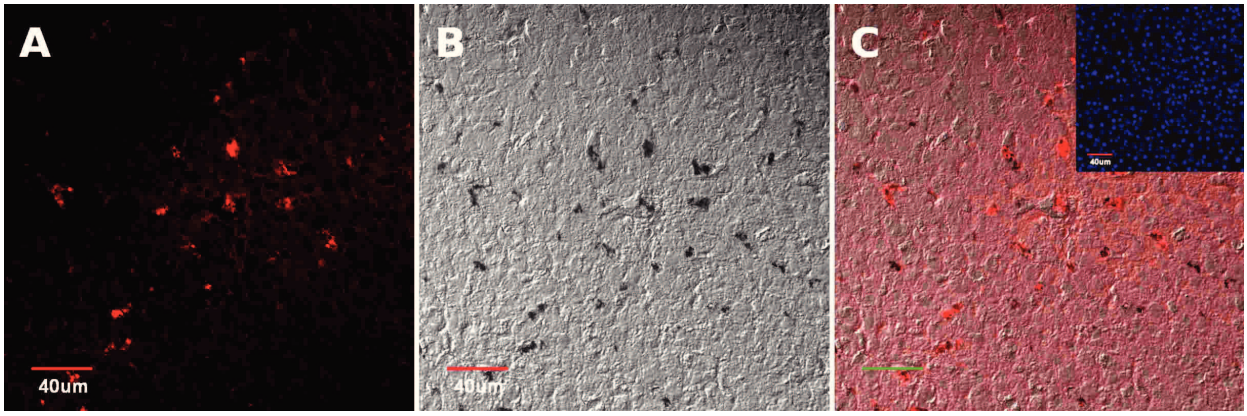

Figure 23: Accumulation of non-pegylated liposomes in Kupffer-cells. CLSM of cryosections after an *in vivo* uptake of 30 min. Non-pegylated liposomes (nominal 3 µmol phospholipids / animal) with membrane-labeled rhodamine B (red signal, panel A) were administrated by intravenous injection in combination with colloidal carbon, which accumulated in Kupffer cells (black signal, panel B). Overlay of the DIC images with the red fluorescent signal indicates a clear co-localization of liposomes and Kupffer cells (panel C). The insert in panel C shows nuclei stained with Hoechst 33352 (blue) of the same image. Scale bars represent 40 µm.

4.4.2. Uptake by hepatocytes and competition

In contrast to successful targeting of Kupffer cells with non-pegylated vesicles, AF-PEG-liposomes were used to specifically target hepatocytes. These rhodamine B-labeled liposomes were injected intravenously and the uptake was terminated after 30 min (Figure 24, panel A). A homogenous distribution of the fluorescent liposomes was observed in the liver sections, which corresponded to the ubiquitous presence of hepatocytes. This pattern showed a complete different appearance compared to the pattern detected with the non-targeted liposomes accumulated in the Kupffer cells above (Figure 23, panel A). In a second experiment, the same amount of rhodamine B-labeled AF-PEG-liposomes was intravenously injected in the presence of an excess of free AF (Figure 24, panel B). Cryosections between these two experiments were compared. While the uptake was not completely inhibited with the excess of free AF, and not all cryosections indicated the same appearance, a reduced accumulation was clearly visible in the latter experiment, indicating a specific uptake.

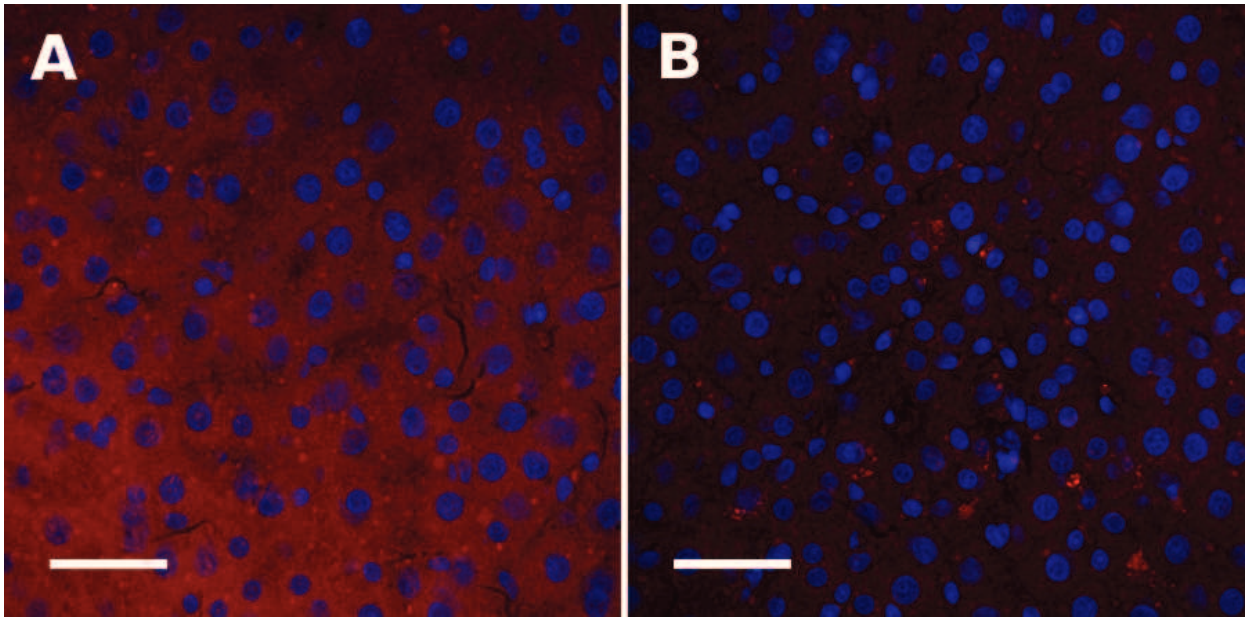

Figure 24: Uptake of AF-PEG-liposomes in the rat liver. Uptake of AF-PEG-liposomes nominal (3 µmol phospholipids / animal) with membrane-labeled rhodamine B (panel A) was compared to the same amount of liposomes in presence of 7 mg of free AF (panel B). Note the ubiquitous uptake of liposomes (panel A) compared with the reduced uptake in the control experiment. Nuclei were stained with Hoechst 33352 (blue). Scale bars represent 40 µm.

In both experiments using AF-PEG-liposomes, single spots with a higher accumulation were visible, resembling the pattern of Kupffer cells from the experiment above. The intensity and pattern did also not change in the presence of additional AF. Therefore, it must be assumed that AF-PEG-liposomes were taken up by Kupffer cells as well, although the majority of fluorescent-labeled vesicles were accumulated by hepatocytes. Nevertheless, it can be stated that the used AF-PEG-liposomes showed *in vitro* and *in vivo* a clear uptake by hepatocytes. This uptake was strongly reduced by the addition of free AF, which indicated specific endocytosis via the ASGPR.

5. Discussion

The following chapter discusses the analysis of the asialoglycoprotein receptor (ASGPR) expression by HepG2 cells, the evaluation of different ligands used for an ASGPR targeting, and the preparation of asialofetuin (AF)-coupled and pegylated liposomes. Such AF-PEG-liposomes were used for *in vitro* and *in vivo* uptake experiments. Special emphasis will be given to the use of fluorescent liposomal markers, such as organic dyes and quantum dots (QD).

5.1. Evaluation of different vectors targeting asialoglycoprotein receptor

The ASGPR is predominantly and abundantly expressed on the surface of liver parenchymal cells, and is capable to trigger a clathrin-mediated endocytosis (Schwartz 1995; Poelstra et al. 2012). To initiate a specific binding and uptake of vesicles, it is conceivable to use either ASGPR-specific antibodies or mimicking endogen ligands, which are bound to the liposomal surface.

In the present study, an extracellular binding monoclonal antibody against the ASGPR was used as a reference ligand to characterize the receptor. A strong expression of the receptor was validated in the used *in vitro* cell culture model HepG2. ASGPR is composed of the two ASGPR-1 and ASGPR-2 subunits. Although the used antibody was raised against ASGPR-1, it binds to ASGPR-2 as well, due to a similar protein sequence. Therefore, the lower two bands of the western blot (Figure 4) can be assigned to ASGPR-1/2 subunits, with an expected molecular weight of 33 kDa and 35 kDa, respectively (Uniprot.org 2012a; Uniprot.org 2012b). The third and upper band at 41 kDa is in agreement with the reported molecular weight of glycosylated human ASGPR subunits (J. Wu et al. 2002). Thus, the original purpose of validating the abundant expression of ASGPR was provided and is in accordance to earlier publications (Schwartz et al. 1981). In addition, ample expression of the receptor was confirmed by a signal shift of two orders in magnitude in flow cytometry (Figure 5) and a clear homogenous distribution of the signal on the

plasma membrane (Figure 6). The strong signal in flow cytometry and CLSM stem from the high amount of expressed ASGPR and the use of a polyclonal secondary antibody.

Monoclonal antibodies have been used at various occasions as a vector in immunoliposomes, like targeting cells of skeletal muscle (Schnyder et al. 2004), mesangial cells in the kidney (Tuffin et al. 2005), or the brain by bypassing the BBB (Huwyler et al. 1996). Antibodies can bind with a high affinity to the corresponding antigen and coupling them on to liposomes is a well-established procedure using covalent maleimide or non-covalent biotin-streptavidin conjugation techniques. Just recently, two groups published the development and characterization of a human anti-ASGPR antibody, which could be utilized for a drug-targeting strategy (Trahtenherts & Benhar 2009; X. Zhao et al. 2011). Therefore, a monoclonal antibody, binding to the extracellular moiety of the receptor, could likewise be used to target liver parenchymal cells. However, such an approach would face intrinsic difficulties. First, species selectivity of monoclonal antibodies makes extrapolation between different species difficult. Second, antibodies binding to extracellular domains are not necessary internalized and can therefore not always be used to promote cellular uptake (Mastrobattista et al. 1999). Third, monoclonal antibodies against ASGPR are commercially available only in limited quantities (i.e. a few µg), which impede the production of immunoliposomes even at small scale. Fourth, large scale production of monoclonal antibodies, as well as the industrial production of antibody-conjugate, remains a challenge.

As an alternative to monoclonal antibodies, cell specific receptors can be targeted with artificial or natural occurring ligands. Regarding the ASGPR, Gal or GalNAc is binding towards the receptor (Connolly et al. 1982), which can be used as a robust, cheap and good available vector. Therefore, various nanoparticles have been linked in the past to Gal to deliver various cargos to hepatocytes with variable success and specificity (Managit et al. 2005b; Pathak et al. 2008). In the present evaluation of different vectors, Gal was attached as a monosaccharide to a fluorochrome and cellular uptake was investigated. Although a dose depending accumulation in HepG2 cells was observed, it was not possible to inhibit this effect by adding an excess of unlabeled Gal or the

glycoprotein AF, which binds to the ASGPR with a high affinity (Figure 8 and 9). These results indicate that the uptake was non-specific and the ASGPR played no major role. This conclusion is comprehensible, since Gal is mainly taken up by cells through various glucose transporters (Uldry et al. 2002). Especially the glucose transporters (GLUT1), which transports next to galactose also glucose and mannose, is often upregulated in various types of cancer and especially in the HepG2 carcinoma cell line (F.-Q. Zhao & Keating 2007; Takanaga et al. 2008).

Naturally occurring ligands of the ASGPR contain multi-antennary glycan residues, which result in an increased affinity. Compared to inhibition constants (k_i) of β-galactose, mono-antennary and tri-antennary oligosaccharides have a 4 and 200 times higher affinity, respectively (Baenziger & Maynard 1980). It can be argued that multiple galactose residues attached to a liposome would mimic a multi-antennary glycan, but it must be kept in mind that an excess of surface bound terminal galactose results in an increased Kupffer cell uptake, since the protective properties of PEG are masked. This effect was observed in studies by Shimada et al., where they used up to 20% (mol) galactosylated lipids on the surface of liposomes, which resulted in a preferential uptake by Kupffer cells (K. Shimada et al. 1997). If we take in consideration that the optimal distance for a tri-antennary binding of the galactose lies between 1.5 nm and 2.5 nm (Stockert 1995), and the Gal residues are evenly distributed on the liposomal surface, we would need an average of 5 000 to 14 000 terminal Gal residues per 100 nm liposome, which equals approximately 6% to 17% of the 80 000 molecules of phospholipids in a 100 nm liposome (Hansen et al. 1995). Compared to immunoliposomes, these amounts of surface coupled vectors are several orders of magnitude above the reported optimal surface density of 30 mAb per vesicle (Maruyama et al. 1995; Huwyler et al. 1996). A significant increased number of attached vectors on the surface of liposomes might lead to an elevated uptake by Kupffer cells or other macrophages *in vivo*. It should be noted that the alternative use of lactose as a starting material and opening the glucose unit for attaching to a pegylated phospholid was successful (Morille et al. 2009), but it remains questionable if this mono-antennary strategy results *in vivo* in an increased hepatocyte delivery.

Desialated glycoproteins with multi-antennary Gal-terminated residues are possible alternatives for targeting the ASGPR. A prominent example is AF, with its bi- and tri-antennary N-linked glycans, which is specifically taken up in the liver by hepatocytes through the ASGPR (Tolleshaug et al. 1977; Rice et al. 1990). Because bovine AF can be obtained commercially in reasonable quantities, it was chosen for further studies. After successfully validating specific vector properties of bovine AF towards hepatocytes, it can be easily modified to be non-immunogenic for the usage in humans, by utilizing the isolated tri-antennary glycan residues from AF, or by replacing the whole protein with the human analogue α-2-HS-glycoprotein.

In analogy to Gal, AF was coupled to the fluorescent marker CF and cellular uptake was demonstrated in HepG2 cells. In contrast to the previous experiments with Gal, binding of labeled AF could be inhibited with an excess of free AF (Figure 11 and 12). Since AF is specifically taken up by hepatocytes through the ASGPR, and competition experiments resulted in a negligible uptake of the labeled glycoprotein, the intracellular accumulation of the fluorescent signal can be explained by an ASGPR specific uptake (Cawley et al. 1981). The described approach of using commercially obtained AF did not contain an additional characterization of the binding properties towards the ASGPR. It should be noted that significant differences in the characteristics of binding and uptake in hepatocytes were observed between different batches. Therefore, all experiments were carried out with the same batch of AF. In contrast to mAb, where the protein folding is essential for a specific antigen binding, AF is very robust to denaturing conditions, since only the glycan residue determines the affinity towards the receptor. Further, a modification of the protein backbone for a subsequent coupling on to a nanoparticle is not critical, since the oligosaccharides are not affected. Altogether, considering the commercial availability, binding affinity, lack of species specificity, and chemical robustness, AF is an optimal vector for delivering various cargos to hepatocytes.

5.2. Liposomal preparations

Liposome composition and preparation were based on previously successful targeting strategies to the brain and skeletal muscle (Huwyler et al. 1996; Schnyder et al. 2004). The lipid composition is important, since uptake of high phosphatidylcholine containing galactosylated liposomes by hepatocytes is limited to vesicles below 90 nm (Rensen et al. 2001). These results are in contrast to galactosylated liposomes containing a mixture of 50:45 to 70:25 (mol%) DSPC/Chol, which result in a specific uptake in the liver through the ASGPR (Murao et al. 2002). Therefore, a mixture of 53:44 (mol%) DSPC/Chol is in the range for an optimal uptake by hepatocytes. The access to the space of Disse (perisinusoidal space) is granted, since the particle sizes of the liposomal formulations were all below 150 nm (Pathak et al. 2008). Especially the AF-conjugated and pegylated liposomes without QDs were in the range of 90 nm. Particles with a similar size have been shown to be efficiently taken up by the ASGPR (Murao et al. 2002).

Binding of AF to the liposomal surface with maleimide functionalized lipids resulted in a high variability from 30 to 270 molecules of glycoprotein per vesicle. Similar ranges between 3 and 197 molecules of OX26 mAb per liposome were reported previously (Huwyler et al. 1996). In contrast to the described binding of OX26 mAb, 60 nmol maleimide functionalized DSPE were used, instead of 15 nmol, which resulted in a slightly higher number of bound AF and a doubled coupling efficiency of 20%, with respect to the thiolated protein. The total amount of bound ligand was calculated based on the AUC from the corresponding samples of the size exclusion chromatography.

An alternative to better control the amount of attached AF on the liposomal surface might be the post-insertion method, which was originally demonstrated by Ishida et al. with antibodies coupled to pegylated DSPE (Ishida et al. 1999). In the present work, incorporation of fluorescent-labeled phospholipids by the post-insertion method was used as a proof of concept. Incorporation of rhodamine B was successfully achieved, while the loss of luminal cargo was minimal (Figure 14). It

was expected that incubating the liposomes above the transition temperature of the main lipid component (approximately 55°C for DSPC) would result in substantial dilution of loaded CF, which was not observed. Neither did the particle size or size distribution change. Co-localization studies by CLSM of the loaded and latter inserted fluorescent markers revealed an overlay of the signals, especially at a temperature of 60°C and above (Figure 15). It must be noted that due to a limited optical resolution of visible light (~ 180 nm in xy axis and ~ 700 nm in z axis at a wavelength of 488 nm), a missing co-localization can rather disprove a homogenous incorporation into the vesicles than prove the inverse, since the signal could emerge from different agglomerated particles, which cannot be optically distinguished. The time and temperature depending increase of the fluorescent signal of the incorporated lipid indicates that the post-insertion method might be a better technique to control the amount of attached proteins to the liposomal surface. The co-localization experiments with the CLSM are supporting these conclusions.

5.3. *In vitro* targeting of hepatocytes using asialofetuin-conjugated liposomes

After a covalent binding of AF to the liposomal surface, different fluorescent markers were investigated to analyze a specific binding and uptake by hepatocytes. First, the fluorochrome CF with its high quantum yield (ratio of photons emitted to photons absorbed) was used, which allowed a sensitive detection (Resch-Genger et al. 2008). Therefore, AF was labeled with CF before it was attached to the vesicles. These particles were taken up by HepG2 cells, but a strong background signal was visible, while CF bleached after a short time of observation. The following experiments were conducted with liposomes filled with a high concentrated solution of CF. Calculated for a 100 nm vesicle, these can transport around 10 to 100 times more CF molecules, compared to fluorescent molecules attached to AF and coupled to liposomes. Therefore, a higher signal can be expected, especially when the liposomes filled with high concentrated CF are released in the endosomes and CF is diluted to non-self-quenching concentrations (Weinstein et al. 1977). Although a slight improvement in signal to background ratio was visible, compared to the experiment with CF-labeled AF, bound to the liposomes, the high background signal remained a

significant hurdle in tracing these particles inside of the cells (Figure 16 & 17, panel C). While the qualitative studies with the CLSM revealed a proof of concept with AF-PEG-liposomes labeled with CF, quantitative analyses were not successful with the green dye. Various metabolites and structural components in cell culture exhibit an autofluorescent signal in the green spectral area, which is the same wavelength where also CF is expected to fluoresce (Billinton & Knight 2001). Especially quantitative measurements in HepG2 cells with fluorescein derivates have been a challenge in the past (Tycko et al. 1983).

An alternative is the usage of a dye in the red spectra, such as rhodamine B, which is coupled to a phospholipid and incorporated into the liposomal membrane. Due to a special excitation wavelength around 559 nm, quantitative uptake analysis of these vesicles were hampered because of technical reasons. Because rhodamine B cannot be excited with lasers commonly present in flow cytometry apparatuses, these vesicles were only used for subsequent qualitative studies *in vivo*.

Although red fluorescent dyes generally emit in an area of the spectrum with a reduced background, it should be noted that they appear to our eye much darker, compared to an equally strong shining dye in the green spectrum (Thews et al. 1999). This effect is caused by different relative spectral responsiveness of cone cells in the retina of the human eye (Bowmaker & Dartnall 1980) and can make visual detection more difficult. Coincidentally, similar effects are known for photomultipliers in CLSM, due to lower quantum efficiencies of the detectors at larger wavelengths, but can be electronically compensated with an increased voltage applied to the detector (Olympus 2009). Although these effects can lead to a wrong first impression of a weak signal when analyzing samples with these dyes, they do not represent a relevant disadvantage compared to dyes emitting in other areas of the spectrum.

In addition to fluorescent dyes, doxorubicin was loaded inside of liposomes by the pH gradient method, and pharmacological effects were investigated (data not shown). Preliminary data indicate

a higher toxicity of AF-conjugated liposomes compared to control samples, which were only pegylated. But further studies are required to validate and quantify these results.

5.3.1. *In vitro* targeting using liposomes loaded with quantum dots

QDs, inorganic nanocrystals composed of specific semiconductors, such as CdSe, can be incorporated inside of liposomes and serve as alternatives to organic fluorochromes to track cellular uptake and distribution. Compared to organic dyes emitting in the same area of the spectra, the quantum yield of these QDs is in general lower, but the high absorption rate and the increased photo stability finally result in a brighter fluorescent signal, which opens up new possibilities to track the delivery of nano particles *in vitro* and *in vivo*. In addition, the large Stockes shift and the narrow emission spectra make a differentiation of the fluorochrome from the background easier, at least in fixed cells (X. Wu et al. 2003). Various applications of QDs as bioconjugates and the usage in live cell imaging were extensively reviewed (Medintz et al. 2005; Michalet et al. 2005). A recent example is the usage of two different colors of hydrophilic QDs, one was loaded inside of immunoliposomes and the second type of QDs was attached to the conjugated antibody to analyze an *in vitro* uptake and intracellular distribution (Sigot et al. 2010). Hydrophobic QDs can also be incorporated into the lipid bilayer of the liposomal membrane, but this approach can result in an altered membrane stability and an increased leakage of loaded substances (Tian et al. 2011).

Since most QDs contain toxic elements, such as cadmium, they are coated with a layer of ZnS to protect the surface from oxidation and leeching of Cd^{2+} ions into the environment. While the ZnS shell itself prevents QDs from being cytotoxic, the thickness of the shell is responsible for the photo stability of the nanoparticles (Derfus et al. 2004b; Ziegler et al. 2007). Various preparations of QDs exhibit different properties, such as shell thickness, outer coating, charge, oxidative, photolytic, and mechanical stability, which can result in distinct toxic effects (Hardman 2006). Because of these variable properties, it is difficult to make general assumptions about these particles. Nevertheless,

as long as the surface of the QDs is enclosed by a shell, no toxicity of most QDs preparations are present in *in vitro* and *in vivo* experiments (Lewinski et al. 2008).

Intravenous injection of QDs, coupled on to tumor specific antibodies, results in an extensive uptake by the RES in the liver and the spleen. In contrast, the same antibody, conjugated to a small organic fluorochrome such as Alexa 680, shows a specific tumor accumulation in mice (H. Zhang et al. 2009). Incorporation of QDs inside pegylated liposomes without an attached vector can be used to circumvent a non-specific uptake by the RES, which may result in a passive tumor accumulation (W. T. Al-Jamal et al. 2009). Compared to non-targeted vesicles loaded with QDs, a specific tumor uptake is achievable with immunoliposomes, at least *in vitro*. *In vivo,* a tumor accumulation is also accomplished, but the superiority of the targeted liposomes is variable, which can be attributed to different liposomal formulations, as well as different characteristics of the used *in vivo* tumor models (Weng et al. 2008; Mukthavaram et al. 2011).

The possibility to follow QDs at a single-molecule level, and the narrow emission spectra, permits the concurrent utilization of different types of QDs, each emitting at a specific wavelength, in *in vitro* and *in vivo* systems. For example, five different colors of QDs were injected subcutaneously into mice at five different sites and accumulation could be observed in real-time in separate lymphatic nodes up to 7 days (Kosaka et al. 2009). In theory, loading separate QDs inside different vesicles, such as liposomes or polymersomes, which differ in density or identity of an attached vector, particle size, charge, lipid mixture, additional loading, or other properties, allows simultaneous analysis and quantification of the optimal formulation, not only *in vitro* but also *in vivo*. The feasibility of concurrently distinguishing different colors permits a direct comparison and evaluation of a successful vesicle delivery to specific cells or organs in the same organism. Hence, various different preparations could be examined in the same animal at the same time, which would additionally exclude intra-individual variances when comparing different formulations. For example, conventional liposomes and AF-PEG-liposomes could be injected simultaneously, after loading with two different types of QDs, and the distribution in hepatocytes and Kupffer cells

could be compared in the same liver section. All these assumptions imply that the combined injection of two or more types of different vesicles do not interact with each other, which has to be validated at least in some scenarios. Altogether, this approach would not only simplify the development of an optimal drug delivery strategy, but could also contribute to the 3 R development (reduction, refinement, and replacement of animal experiments), by drastically reducing the number of needed animals for *in vivo* experiments.

The formulation of liposomes loaded with QDs, and cellular uptake, revealed several unexpected hurdles, which limit the direct application of these vesicles in biological systems. Most important and in contrast to organic dyes, the fluorescent properties of QDs have to be activated by irradiation after endosomal uptake into cells (Figure 18). This limitation hinders a direct qualitative and quantitative analysis of the fluorescent signal. These results are in agreement with recently published data from Generalov et al. that QDs need photoactivation inside of cells before they reveal their fluorescent properties. The decreased fluorescence, which can be partially reactivated by irradiation, is attributed to a large extent to protein adsorption on the surface of QDs as well as to surrounding phospholipids, a drop in pH in the endosomal compartment, and the presence of a high-ionic strength environment (Generalov et al. 2011).

After an endosomal uptake, the process of activation of QDs is accompanied by a blue shift of the fluorescent signal of approximately 15 nm (Figure 19), which is an indication of a decreased nanocrystal diameter, since the emitting wavelength is depending on the dot size (Chan et al. 2002). Although the activation process is not completely understood, a prominent part plays the process of photo-oxidation, triggered by irradiation with light of a short wavelength, and leading to a corrosion of QDs (Carrillo-Carrión et al. 2009). Together with photoactivation, surrounding areas of endocytosed QDs were bleached inside of cells, predominantly by illuminating at a shorter wavelength of 400 nm, which resulted in a substantial appearance of background signal (Figure 18). Photo-oxidation at the surface of QDs is described, including the production of radicals such as superoxides (Dembski et al. 2008) that conjugate further with surrounding water to peroxides.

These radicals cannot only bleach the surrounding structure, but might also contribute to the desorption of proteins from the surface of QDs. Hence, the corrosion of the outer layer of QDs by photo-oxidation can explain the increasing fluorescent signal after irradiation, which occurs accompanied by a blue shift of the fluorescent signal. But further studies are needed to uncover the exact molecular mechanism by which the fluorescent signal of QDs is quenched inside of cells, and how it is again reactivated, to be able to reveal the full potential of these new fluorochromes in biological settings.

Further limitations of incorporating QDs into liposomes were observed during the process of vesicle preparation. Although the diameter of the used QDs, including the ZnS shell and the polymer coating, is stated to be around 10 nm (Invitrogen 2012), it was not possible to produce liposomes of a size below 100 nm by filter extrusion, in contrast to liposomes containing organic dyes (Table 1). With an average particle size of approximately 130 nm, these vesicles may be substantially less endocytosed by hepatocytes through the ASGPR, compared to smaller vesicles (Popielarski et al. 2005). Incorporation of QDs of the same kind, by using different liposomal preparation techniques, are reported to result in similar or larger particle sizes, in combination with an unfavorable increased polydispersity index (Sigot et al. 2010; Muthu et al. 2012; C.-J. Wen et al. 2012).

The described properties of a decreased and reactivated fluorescent signal, as well as the behavior in the liposomal formulation, is depending on the combination of various components of the QDs, such as the elements of used semiconductor nanocrystal, the core-shell, the coating, and the liposomal lipid mixture. Especially the shell surrounding the core of the nanocrystal, and the overlaying coating, determine not only the solubility and the suitability for further conjugations, but influence also the chemical and physical stability, which are responsible for the resulting optical properties (Ziegler et al. 2007). Hence, for an improved tracing of liposomal QDs in *in vitro* and *in vivo* systems, further studies are needed with dots containing an improved shell and coating.

Altogether, QDs are promising tools to follow cellular uptake and intracellular localization of liposomal cargos (Figure 20 and 21), but the extensively quenching of the fluorescent signal inside of the cells limits their use as a direct replacement for conventional dyes. Further, the non-linear fluorescent properties and an intermittent on and off behavior (blinking) hinder quantitative analyses. Although the intracellular quenching can partly be overcome by photo-activation with irradiation, the use of organic dyes in these biological applications is still more straightforward.

5.4. *In vivo* proof of concept using asialofetuin-conjugated liposomes

When targeting the liver parenchymal cells with liposomes, it is crucial to investigate also the uptake by Kupffer cells, which are known for their unspecific engulfment of vesicles. Together with the macrophages in the spleen, they are mainly responsible for clearing non-pegylated liposomes from the blood circulation (Dave & Patel 1986). In rodents, the presence of the Kupffer cell receptor on the liver macrophages is a further complicating factor, since it is also known for its affinity towards glycoproteins bearing oligosaccharides that end with Gal and GalNAc (Fadden et al. 2003). Managit et al. demonstrated in mice that varying the amount of Gal attached to the liposomal surface is influencing the uptake ratio between liver parenchymal to non-parenchymal cells (Managit et al. 2005a). Additionally, experiments in rats showed that many desialated glycoproteins, including AF, are taken up specifically by hepatocytes and not by Kupffer cells (Morell et al. 1971). Therefore, AF can be used as a vector to investigate specific drug delivery to hepatocytes in rats.

In the present *in vivo* studies, Rho-labeled AF-PEG-liposomes were used and compared with non-targeted unpegylated liposomes, together with colloidal carbon. While the allocation pattern in the liver sections of colloidal carbon and non-targeted liposomes matched to the occurrence of isolated Kupffer cells (Neyrinck et al. 2000), AF-PEG-liposomes were homogenously distributed in the liver tissue (Figure 23 and 24). Since the non-pegylated liposomes perfectly co-localized with the colloidal carbon, it is reasonable to assume that these particles accumulated mostly in the Kupffer

cells, while the targeted vesicles were taken up by the liver parenchymal cells. Additional competition experiments, with an excess of free AF, revealed a substantial reduced uptake, which indicates that the process of endocytosis takes place through the ASGPR.

It has been demonstrated that the density of antibodies conjugated to pegylated liposomes is critical for an efficient targeting *in vivo* and lies in the range of 30 immunoglobulines per liposome. These values have been observed for immunoliposomes taken up by pulmonary endothelial cells (Maruyama et al. 1995), and by cells of the blood brain barrier, triggering a receptor mediated transcytosis of the bound vesicles (Huwyler et al. 1996). Therefore, it is reasonable to assume that the density of attached AF to the liposomal surface is also critical for an optimal cellular targeting of liver parenchymal cells. Additionally, the uptake through the ASGPR in hepatocytes and transcytosis in the blood brain barrier are both triggered through clathrin-mediated endocytosis and show therefore some functional similarities (Stockert 1995; Pang et al. 2011). In the present study, the amount of surface-conjugated AF on liposomes is varying approximately by a factor of 10, covering a range between 30 to 270 molecules of glycoprotein per liposome. Based on our *in vitro* experimentations, the density of receptor ligands on the surface of liposomes had no impact on the obtained results. Batch-to-batch variability, however, of AF was a critical factor. For this reason, all *in vivo* experiments were carried with AF-PEG-liposomes tested *in vitro* prior to *in vivo* experimentations. It should be noted that using post-insertion techniques (see chapter 5.2) may improve and allow a standardized coupling procedure.

In comparison to experiments from Hara et al., using non-pegylated AF-liposomes, the same amount of liposomes per animal were used in the present study, while for the competition experiments less than half of free AF were sufficient to observe a clear reduced uptake in hepatocytes (Hara et al. 1987). These results indicate a successful proof of concept for targeting hepatocytes by using pegylated liposomes with AF coupled to the distal end of PEG residues. To be able to optimize and compare the uptake *in vivo*, further experiments are needed to quantify the total amount of accumulated liposomes in different organs, liver parenchymal and non-

parenchymal cells. These results will allow to estimate the improvement of this approach compared to non-pegylated AF-liposomes or coupled Gal residues to liposomes (Hara et al. 1987; Murao et al. 2002; Managit et al. 2003; Popielarski et al. 2005). However, analysis of the liver sections is indicating that the main fraction of AF-PEG-liposomes is taken up by hepatocytes.

5.5. Conclusion

In a first step, various vectors were evaluated for the targeting of hepatocytes through the ASGPR. While Gal as a monosaccharide was neither efficiently nor specifically taken up in the *in vitro* cell culture model HepG2, the glycoprotein AF with tri-antennary glycans, each terminating with a Gal residue, was further investigated. This natural ligand resulted in a strong and specific uptake in the used liver carcinoma cell line. Therefore, considering the commercial availability, binding affinity, lack of species specificity, and chemical robustness, AF was chosen as an optimal vector for further development of a drug targeting strategy to hepatocytes.

While the concept of utilizing AF in combination with liposomal formulations was already described in 1975 from Gregoriadis et al. (Gregoriadis & Neerunjun 1975), the present work is the first to explore AF covalently coupled on to the surface of pegylated liposomes. Thereby, AF was conjugated to the distal end of maleimide-functionalized phospholipids after preparation and extrusion of the vesicles. Subsequently, a proof of principle for the targeting of hepatocytes with AF-PEG-liposomes was provided *in vitro* by a specific uptake and accumulation of these vesicles inside of HepG2 cells. The uptake was inhibited in the presence of free AF, indicating receptor-mediated endocytosis through the ASGPR.

The process of coupling the glycoprotein to the surface of liposomes was highly variable, resulting in a range between 30 to 270 molecules AF per vesicle. Although this is of no concern, a post-insertion technique might be a better manageable approach to control the final amount of surface-coupled vectors per liposome.

To trace endocytosis of liposomes and intracellular routing of transported molecules, the use of fluorescent QDs was analyzed and compared to organic dyes. While the bright fluorescence, combined with a narrow emission peak and the resistance to photobleaching, resulted in a distinct and strong signal from the QDs, their altered optical properties in a biological matrix limit their universal and straightforward usage in a liposomal targeting strategy. Nevertheless, QDs were successfully loaded into AF-PEG-liposomes and intracellular localization was observed after a specific activation of the fluorescence signal. Especially the possibility of combining multiple colors of QDs in different liposomal formulations and simultaneous analysis is a promising approach, although their blinking behavior and the need for photoactivation is particularly hindering quantitative measurements.

A successful proof of concept of targeting hepatocytes *in vivo* with AF-PEG-liposomes was provided. In contrast to conventional liposomes, which were uniquely accumulated in Kupffer cells, AF-PEG-liposomes were taken up by liver parenchymal cells. Further, endocytosis could be inhibited by administrating an excess of free AF, indicating a specific uptake through the ASGPR of the hepatocytes. Conclusively, the combination of pegylated liposomes with coupled AF as a vector is a prerequisite for further developments of a specific and species independent drug delivery system to hepatocytes.

5.6. Outlook

The described AF-PEG-liposomes promote a successful and specific vesicular uptake by hepatocytes *in vitro* and *in vivo.* Quantitative measurements are needed to be able to compare different formulations and to support semi-quantitative results presented in this study. Therefore, liposomes will be loaded with a radioactive marker, such as the metastable nuclear isomer of technetium-99 (^{99m}TC), and different organ or cell accumulations will be studied (Oyen et al. 1996; Underwood et al. 2012). Further, 3-D images can be obtained from living animals after injecting ^{99m}TC-labeled liposomes, by using single photon emission computed tomography (SPECT), showing an enrichment in selected organs which can be followed over time. Controlling of the vector density on the liposomal surface by the post-insertion method will additionally be an option to facilitate the preparation of AF-PEG-liposomes.

The used vector AF is isolated from fetal bovine serum and thus immunogenic in humans (J. Wu et al. 2002). To preserve the concept of targeting hepatocytes by glycans exhibiting a high affinity towards the ASGPR, several alternatives to bovine AF are possible. The protein can be replaced with the desialated derivatives of the human homologous protein α-2-HS-glycoprotein or the human α-1-acid glycoprotein (also known as orosomucoid), which carry tri- and tetra-antennary glycan residues, respectively. Another possibility is to isolate the tri-antennary glycan residue from bovine AF by specifically cleaving the N-linked glycosylations or by fragmenting the protein backbone with proteases, leaving only the oligosaccharides linked to a short non-immunogenic peptide. The isolated glycans can be coupled to the distal end of pegylated liposomes (glycanoliposomes) and might be an alternative to the usage of the whole glycoprotein. Another more conventional approach is the usage of monoclonal antibodies directed against the human ASGPR and covalently attaching them on to pegylated liposomes. But this approach includes the known limitations of immunoliposomes, such as species specificity of the vector, a difficult production and characterization at an industrial scale.

Besides optimizing the vector for the targeting of hepatocytes, liposomes might be loaded with variable cargos. QDs can be utilized to study a specific intracellular delivery in combination with nuclear or mitochondrial targeting peptides (Derfus et al. 2004a). Combining hepatocyte-specific liposomes with pH sensitive lipids and specific organelle targeting peptides will extend the drug targeting strategy to an intracellular specific delivery in liver parenchymal cells. Furthermore, transporting DNA to hepatocytes resulting in stable and efficient transcriptions could dramatically advance treatments in various genetic diseases, such as hemophilia A and B or α1-antitrypsin deficiency. For viral hepatitis, siRNA or γ-interferon might represent promising candidates to improve therapy options. Finally, the delivery of various cargos uniquely to hepatocytes will open up a plethora of additional applications in a variety of diseases related to liver parenchymal cells, which can be readily transferred to clinical applications.

6. References

Abuchowski, A. et al., 1977. Effect of covalent attachment of polyethylene glycol on immunogenicity and circulating life of bovine liver catalase. *The Journal of biological chemistry*, 252(11), pp.3582–3586.

Adler-Moore, J. & Proffitt, R.T., 2002. AmBisome: liposomal formulation, structure, mechanism of action and pre-clinical experience. *The Journal of antimicrobial chemotherapy*, 49 Suppl 1, pp.21–30.

Akinc, A. et al., 2010. Targeted delivery of RNAi therapeutics with endogenous and exogenous ligand-based mechanisms. *Molecular therapy: the journal of the American Society of Gene Therapy*, 18(7), pp.1357–1364.

Al-Jamal, W.T. et al., 2009. Tumor targeting of functionalized quantum dot-liposome hybrids by intravenous administration. *Molecular Pharmaceutics*, 6(2), pp.520–530.

Al-Jamal, W.T. & Kostarelos, K., 2011. Liposomes: from a clinically established drug delivery system to a nanoparticle platform for theranostic nanomedicine. *Accounts of Chemical Research*, 44(10), pp.1094–1104.

Allen, T.M. & Hansen, C.B., 1991. Pharmacokinetics of stealth versus conventional liposomes: effect of dose. *Biochimica et biophysica acta*, 1068(2), pp.133–141.

Arangoa, M.A., Düzgüneş, N. & Tros de Ilarduya, C., 2003. Increased receptor-mediated gene delivery to the liver by protamine-enhanced-asialofetuin-lipoplexes. *Gene Therapy*, 10(1), pp.5–14.

Aravalli, R.N., Cressman, E.N.K. & Steer, C.J., 2012. Cellular and molecular mechanisms of hepatocellular carcinoma: an update. *Archives of toxicology*. Available at: http://www.ncbi.nlm.nih.gov/pubmed/23007558 [Accessed October 1, 2012].

Aronsohn, A.I. & Hughes, J.A., 1998. Nuclear localization signal peptides enhance cationic liposome-mediated gene therapy. *Journal of drug targeting*, 5(3), pp.163–169.

Ashley, C.E. et al., 2011. The targeted delivery of multicomponent cargos to cancer cells by nanoporous particle-supported lipid bilayers. *Nature Materials*, 10(5), pp.389–397.

Ashok, B. et al., 2004. In vitro characterization of PEGylated phospholipid micelles for improved drug solubilization: effects of PEG chain length and PC incorporation. *Journal of pharmaceutical sciences*, 93(10), pp.2476–2487.

Baenziger, J.U. & Maynard, Y., 1980. Human hepatic lectin. Physiochemical properties and specificity. *The Journal of biological chemistry*, 255(10), pp.4607–4613.

Ballou, B. et al., 2004. Noninvasive imaging of quantum dots in mice. *Bioconjugate chemistry*, 15(1), pp.79–86.

Banno, Y., Ohki, K. & Nozawa, Y., 1983. Targeting of asialofetuin sugar chain-bearing liposomes to liver lysosomes. *Biochemistry International*, 7(4), pp.455–461.

Barenholz, Y., 2012. Doxil®--the first FDA-approved nano-drug: lessons learned. *Journal of controlled release: official journal of the Controlled Release Society*, 160(2), pp.117–134.

Barrera, P. et al., 2000. Synovial macrophage depletion with clodronate-containing liposomes in rheumatoid arthritis. *Arthritis and rheumatism*, 43(9), pp.1951–1959.

Becker, S., Spiess, M. & Klenk, H.D., 1995. The asialoglycoprotein receptor is a potential liver-specific receptor for Marburg virus. *The Journal of general virology*, 76 (Pt 2), pp.393–399.

Bernardes, G.J.L. et al., 2010. Design, synthesis and biological evaluation of carbohydrate-functionalized cyclodextrins and liposomes for hepatocyte-specific targeting. *Organic & Biomolecular Chemistry*. Available at: http://www.ncbi.nlm.nih.gov/pubmed/20820666 [Accessed September 30, 2010].

Bertrand, N. & Leroux, J.-C., 2012. The journey of a drug-carrier in the body: an anatomo-physiological perspective. *Journal of controlled release: official journal of the Controlled Release Society*, 161(2), pp.152–163.

Bider, M.D. et al., 1996. The oligomerization domain of the asialoglycoprotein receptor preferentially forms 2:2 heterotetramers in vitro. *The Journal of Biological Chemistry*, 271(50), pp.31996–32001.

Billinton, N. & Knight, A.W., 2001. Seeing the wood through the trees: a review of techniques for distinguishing green fluorescent protein from endogenous autofluorescence. *Analytical Biochemistry*, 291(2), pp.175–197.

Bowmaker, J.K. & Dartnall, H.J., 1980. Visual pigments of rods and cones in a human retina. *The Journal of physiology*, 298, pp.501–511.

Cai, P., Kaphalia, B.S. & Ansari, G.A.S., 2005. Methyl palmitate: inhibitor of phagocytosis in primary rat Kupffer cells. *Toxicology*, 210(2-3), pp.197–204.

Campos, S.K. & Barry, M.A., 2007. Current advances and future challenges in Adenoviral vector biology and targeting. *Current gene therapy*, 7(3), pp.189–204.

Carrillo-Carrión, C. et al., 2009. Quantum dots luminescence enhancement due to illumination with UV/Vis light. *Chemical communications (Cambridge, England)*, (35), pp.5214–5226.

Casey, L.C. & Lee, W.M., 2012. Hepatitis C therapy update. *Current opinion in gastroenterology*, 28(3), pp.188–192.

Cawley, D.B., Simpson, D.L. & Herschman, H.R., 1981. Asialoglycoprotein receptor mediates the toxic effects of an asialofetuin-diphtheria toxin fragment A conjugate on cultured rat hepatocytes. *Proceedings of the National Academy of Sciences of the United States of America*, 78(6), pp.3383–3387.

Chan, W.C.W. et al., 2002. Luminescent quantum dots for multiplexed biological detection and imaging. *Current opinion in biotechnology*, 13(1), pp.40–46.

Chan, W.C.W. & Nie, S., 1998. Quantum dot bioconjugates for ultrasensitive nonisotopic detection. *Science (New York, N.Y.)*, 281(5385), pp.2016–2018.

Chen, C. et al., 2010. An overview of liposome lyophilization and its future potential. *Journal of controlled release: official journal of the Controlled Release Society*, 142(3), pp.299–311.

Clarenburg, R., 1983. Asialoglycoprotein receptor is uninvolved in clearing intact glycoproteins from rat blood. *The American Journal of Physiology*, 244(3), pp.G247–253.

Connolly, D.T. et al., 1982. Binding and endocytosis of cluster glycosides by rabbit hepatocytes.

Evidence for a short-circuit pathway that does not lead to degradation. *The Journal of Biological Chemistry*, 257(2), pp.939–945.

Connor, J. & Huang, L., 1986. pH-sensitive immunoliposomes as an efficient and target-specific carrier for antitumor drugs. *Cancer research*, 46(7), pp.3431–3435.

CoolLED, 2012. LED Intensity - CoolLED. Available at: http://www.coolled.com/content/main.asp?pid=164 [Accessed October 17, 2012].

Cowper, K.B. et al., 1990. A new method to monitor Kupffer-cell function continuously in the perfused rat liver. Dissociation of glycogenolysis from particle phagocytosis. *The Biochemical journal*, 266(1), pp.141–147.

Dabbousi, B.O. et al., 1997. (CdSe)ZnS Core−Shell Quantum Dots: Synthesis and Characterization of a Size Series of Highly Luminescent Nanocrystallites. *The Journal of Physical Chemistry B*, 101(46), pp.9463–9475.

Dasí, F. et al., 2001. Asialofetuin liposome-mediated human alpha1-antitrypsin gene transfer in vivo results in stationary long-term gene expression. *Journal of molecular medicine (Berlin, Germany)*, 79(4), pp.205–212.

Dave, J. & Patel, H.M., 1986. Differentiation in hepatic and splenic phagocytic activity during reticuloendothelial blockade with cholesterol-free and cholesterol-rich liposomes. *Biochimica et biophysica acta*, 888(2), pp.184–190.

Dembski, S. et al., 2008. Photoactivation of CdSe/ZnS quantum dots embedded in silica colloids. *Small (Weinheim an der Bergstrasse, Germany)*, 4(9), pp.1516–1526.

Derfus, A.M., Chan, W.C.W. & Bhatia, S.N., 2004a. Intracellular Delivery of Quantum Dots for Live Cell Labeling and Organelle Tracking. *Advanced Materials*, 16(12), pp.961–966.

Derfus, A.M., Chan, W.C.W. & Bhatia, S.N., 2004b. Probing the Cytotoxicity of Semiconductor Quantum Dots. *Nano Letters*, 4(1), pp.11–18.

Drummond, D., Zignani, M. & Leroux, J.-C., 2000. Current status of pH-sensitive liposomes in drug delivery. *Progress in lipid research*, 39(5), pp.409–460.

Fadden, A.J., Holt, O.J. & Drickamer, K., 2003. Molecular characterization of the rat Kupffer cell glycoprotein receptor. *Glycobiology*, 13(7), pp.529–537.

Fuhrer, C. et al., 1994. The two subunits of the asialoglycoprotein receptor contain different sorting information. *The Journal of biological chemistry*, 269(5), pp.3277–3282.

Gabizon, A., Barenholz, Y. & Bialer, M., 1993. Prolongation of the circulation time of doxorubicin encapsulated in liposomes containing a polyethylene glycol-derivatized phospholipid: pharmacokinetic studies in rodents and dogs. *Pharmaceutical research*, 10(5), pp.703–708.

Gabizon, A., Shmeeda, H. & Barenholz, Y., 2003. Pharmacokinetics of pegylated liposomal Doxorubicin: review of animal and human studies. *Clinical pharmacokinetics*, 42(5), pp.419–436.

Generalov, R. et al., 2011. Entrapment in phospholipid vesicles quenches photoactivity of quantum dots. *International Journal of Nanomedicine*, 6, pp.1875–1888.

Gottesman, M.M., 2002. Mechanisms of cancer drug resistance. *Annual review of medicine*, 53, pp.615–627.

Gregoriadis, G. & Neerunjun, E.D., 1975. Homing of liposomes to target cells. *Biochemical and biophysical research communications*, 65(2), pp.537–544.

Guhagarkar, S.A. et al., 2010. Polyethylene sebacate-doxorubicin nanoparticles for hepatic targeting. *International Journal of Pharmaceutics*. Available at: http://www.ncbi.nlm.nih.gov/pubmed/20854883 [Accessed September 30, 2010].

Hacein-Bey-Abina, S. et al., 2003. LMO2-associated clonal T cell proliferation in two patients after gene therapy for SCID-X1. *Science (New York, N.Y.)*, 302(5644), pp.415–419.

Haisma, H.J. & Bellu, A.R., 2011. Pharmacological interventions for improving adenovirus usage in gene therapy. *Molecular pharmaceutics*, 8(1), pp.50–55.

Halm, U. et al., 2000. A phase II study of pegylated liposomal doxorubicin for treatment of advanced hepatocellular carcinoma. *Annals of oncology: official journal of the European Society for Medical Oncology / ESMO*, 11(1), pp.113–114.

Hansen, C.B. et al., 1995. Attachment of antibodies to sterically stabilized liposomes: evaluation, comparison and optimization of coupling procedures. *Biochimica Et Biophysica Acta*, 1239(2), pp.133–144.

Hara, T. et al., 1996. Effects of fusogenic and DNA-binding amphiphilic compounds on the receptor-mediated gene transfer into hepatic cells by asialofetuin-labeled liposomes. *Biochimica Et Biophysica Acta*, 1278(1), pp.51–58.

Hara, T. et al., 1995a. Receptor-mediated transfer of pSV2CAT DNA to a human hepatoblastoma cell line HepG2 using asialofetuin-labeled cationic liposomes. *Gene*, 159(2), pp.167–174.

Hara, T. et al., 1995b. Receptor-mediated transfer of pSV2CAT DNA to mouse liver cells using asialofetuin-labeled liposomes. *Gene Therapy*, 2(10), pp.784–788.

Hara, T. et al., 1987. Specific incorporation of asialofetuin-labeled liposomes into hepatocytes through the action of galactose-binding protein. *Biopharmaceutics & Drug Disposition*, 8(4), pp.327–339.

Hara, T. et al., 1988. Specific uptake of asialofetuin-labeled liposomes by isolated hepatocytes. *International Journal of Pharmaceutics*, 42(1–3), pp.69–75.

Haran, G. et al., 1993. Transmembrane ammonium sulfate gradients in liposomes produce efficient and stable entrapment of amphipathic weak bases. *Biochimica et biophysica acta*, 1151(2), pp.201–215.

Hardman, R., 2006. A toxicologic review of quantum dots: toxicity depends on physicochemical and environmental factors. *Environmental Health Perspectives*, 114(2), pp.165–172.

Harvey, H.A. et al., 2000. Gonococcal lipooligosaccharide is a ligand for the asialoglycoprotein receptor on human sperm. *Molecular microbiology*, 36(5), pp.1059–1070.

Henriksen-Lacey, M. et al., 2011. Liposomal vaccine delivery systems. *Expert opinion on drug delivery*, 8(4), pp.505–519.

Hermanson, G.T., 2008. *Bioconjugate Techniques* 2nd Revised edition (REV)., Academic Press.

Herzer, K., Sprinzl, M.F. & Galle, P.R., 2007. Hepatitis viruses: live and let die. *Liver international: official journal of the International Association for the Study of the Liver*, 27(3), pp.293–301.

Herzog, R.W. & Dobrzynski, E., 2004. Immune implications of gene therapy for hemophilia. *Seminars in thrombosis and hemostasis*, 30(2), pp.215–226.

Hosokawa, S. et al., 2004. Establishment and evaluation of cancer-specific human monoclonal antibody GAH for targeting chemotherapy using immunoliposomes. *Hybridoma and hybridomics*, 23(2), pp.109–120.

Hülsermann, U. et al., 2009. Uptake of apolipoprotein E fragment coupled liposomes by cultured brain microvessel endothelial cells and intact brain capillaries. *Journal of drug targeting*, 17(8), pp.610–618.

Huwyler, J. et al., 2002. By-passing of P-glycoprotein using immunoliposomes. *Journal of Drug Targeting*, 10(1), pp.73–79.

Huwyler, J., Drewe, J. & Krähenbuhl, S., 2008. Tumor targeting using liposomal antineoplastic drugs. *International Journal of Nanomedicine*, 3(1), pp.21–9.

Huwyler, J., Wu, D. & Pardridge, W.M., 1996. Brain drug delivery of small molecules using immunoliposomes. *Proceedings of the National Academy of Sciences of the United States of America*, 93(24), pp.14164–14169.

Imai, K. & Takaoka, A., 2006. Comparing antibody and small-molecule therapies for cancer. *Nature reviews. Cancer*, 6(9), pp.714–727.

Invitrogen, 2012. Qdot® 625 ITK™ Carboxyl Quantum Dots - Life Technologies. Available at: http://products.invitrogen.com/ivgn/product/A10200 [Accessed November 7, 2012].

Ishida, T. et al., 2006. Accelerated blood clearance of PEGylated liposomes upon repeated injections: effect of doxorubicin-encapsulation and high-dose first injection. *Journal of controlled release: official journal of the Controlled Release Society*, 115(3), pp.251–258.

Ishida, T. et al., 2003. Accelerated clearance of PEGylated liposomes in rats after repeated injections. *Journal of controlled release: official journal of the Controlled Release Society*, 88(1), pp.35–42.

Ishida, T., Iden, D.L. & Allen, T.M., 1999. A combinatorial approach to producing sterically stabilized (Stealth) immunoliposomal drugs. *FEBS letters*, 460(1), pp.129–133.

Ishihara, H. et al., 1991. Specific uptake of asialofetuin-tacked liposomes encapsulating interferon-gamma by human hepatoma cells and its inhibitory effect on hepatitis B virus replication. *Biochemical and Biophysical Research Communications*, 174(2), pp.839–845.

Kallinteri, P., Liao, W.Y., et al., 2001. Characterization, stability and in-vivo distribution of asialofetuin glycopeptide incorporating DSPC/CHOL liposomes prepared by mild cholate incubation. *Journal of Drug Targeting*, 9(2), pp.155–168.

Kallinteri, P., Papadimitriou, E. & Antimisiaris, S.G., 2001. UPTAKE OF LIPOSOMES WHICH INCORPORATE A GLYCOPEPTIDE FRACTION OF ASIALOFETUIN BY HepG(2) CELLS. *Journal of Liposome Research*, 11(2-3), pp.175–193.

Khorev, O. et al., 2008. Trivalent, Gal/GalNAc-containing ligands designed for the asialoglycoprotein receptor. *Bioorganic & Medicinal Chemistry*, 16(9), pp.5216–5231.

Kirby, C., Clarke, J. & Gregoriadis, G., 1980. Effect of the cholesterol content of small unilamellar liposomes on their stability in vivo and in vitro. *Biochemical Journal*, 186(2), pp.591–598.

Kosaka, N. et al., 2009. In vivo real-time, multicolor, quantum dot lymphatic imaging. *The Journal of Investigative Dermatology*, 129(12), pp.2818–2822.

Kreitman, R.J. et al., 2012. Phase I trial of anti-CD22 recombinant immunotoxin moxetumomab pasudotox (CAT-8015 or HA22) in patients with hairy cell leukemia. *Journal of clinical oncology: official journal of the American Society of Clinical Oncology*, 30(15), pp.1822–1828.

Lampertico, P. & Liaw, Y.F., 2012. New perspectives in the therapy of chronic hepatitis B. *Gut*, 61 Suppl 1, pp.i18–24.

Lewinski, N., Colvin, V. & Drezek, R., 2008. Cytotoxicity of nanoparticles. *Small (Weinheim an der Bergstrasse, Germany)*, 4(1), pp.26–49.

Ma, Y. et al., 2012. Repeated injections of PEGylated liposomal topotecan induces accelerated blood clearance phenomenon in rats. *European journal of pharmaceutical sciences: official journal of the European Federation for Pharmaceutical Sciences*, 45(5), pp.539–545.

Malam, Y., Loizidou, M. & Seifalian, A.M., 2009. Liposomes and nanoparticles: nanosized vehicles for drug delivery in cancer. *Trends in pharmacological sciences*, 30(11), pp.592–599.

Mamot, C. et al., 2012. Immunoliposomal delivery of doxorubicin can overcome multidrug resistance mechanisms in EGFR-overexpressing tumor cells. *Journal of drug targeting*, 20(5), pp.422–432.

Managit, C. et al., 2005a. Effect of galactose density on asialoglycoprotein receptor-mediated uptake of galactosylated liposomes. *Journal of Pharmaceutical Sciences*, 94(10), pp.2266–2275.

Managit, C. et al., 2003. Targeted and sustained drug delivery using PEGylated galactosylated liposomes. *International Journal of Pharmaceutics*, 266(1-2), pp.77–84.

Managit, C. et al., 2005b. Uptake characteristics of galactosylated emulsion by HepG2 hepatoma cells. *International Journal of Pharmaceutics*, 301(1-2), pp.255–261.

Mannucci, P.M. & Tuddenham, E.G.D., 2001. The hemophilias--from royal genes to gene therapy. *The New England journal of medicine*, 344(23), pp.1773–1779.

Marinò, M. & McCluskey, R.T., 2000. Role of thyroglobulin endocytic pathways in the control of thyroid hormone release. *American journal of physiology. Cell physiology*, 279(5), pp.C1295–1306.

Maruyama, K. et al., 1995. Targetability of novel immunoliposomes modified with amphipathic poly(ethylene glycol)s conjugated at their distal terminals to monoclonal antibodies. *Biochimica et biophysica acta*, 1234(1), pp.74–80.

Mastrobattista, Koning & Storm, 1999. Immunoliposomes for the targeted delivery of antitumor drugs. *Advanced drug delivery reviews*, 40(1-2), pp.103–127.

Matsumura, Y. et al., 2004. Phase I and pharmacokinetic study of MCC-465, a doxorubicin (DXR) encapsulated in PEG immunoliposome, in patients with metastatic stomach cancer. *Annals of oncology: official journal of the European Society for Medical Oncology / ESMO*, 15(3), pp.517–525.

Matsumura, Y. & Maeda, H., 1986. A new concept for macromolecular therapeutics in cancer

chemotherapy: mechanism of tumoritropic accumulation of proteins and the antitumor agent smancs. *Cancer research*, 46(12 Pt 1), pp.6387–6392.

Mayer, L.D., Bally, M.B. & Cullis, P.R., 1986. Uptake of adriamycin into large unilamellar vesicles in response to a pH gradient. *Biochimica Et Biophysica Acta*, 857(1), pp.123–126.

McVicker, B.L., Tuma, D.J. & Casey, C.A., 2000. Hyperphosphorylation of the asialoglycoprotein receptor in isolated rat hepatocytes following ethanol administration. *Biochemical pharmacology*, 60(3), pp.343–351.

Medintz, I.L. et al., 2005. Quantum dot bioconjugates for imaging, labelling and sensing. *Nature Materials*, 4(6), pp.435–446.

De Meyer, S. et al., 1997. Organ and species specificity of hepatitis B virus (HBV) infection: a review of literature with a special reference to preferential attachment of HBV to human hepatocytes. *Journal of viral hepatitis*, 4(3), pp.145–153.

Michalet, X. et al., 2005. Quantum dots for live cells, in vivo imaging, and diagnostics. *Science (New York, N.Y.)*, 307(5709), pp.538–544.

Midoux, P. et al., 1998. Membrane permeabilization and efficient gene transfer by a peptide containing several histidines. *Bioconjugate chemistry*, 9(2), pp.260–267.

Moghimi, S.M. & Hunter, A.C., 2001. Recognition by macrophages and liver cells of opsonized phospholipid vesicles and phospholipid headgroups. *Pharmaceutical research*, 18(1), pp.1–8.

Morell, A.G. et al., 1971. The role of sialic acid in determining the survival of glycoproteins in the circulation. *The Journal of biological chemistry*, 246(5), pp.1461–1467.

Morille, M. et al., 2009. Galactosylated DNA lipid nanocapsules for efficient hepatocyte targeting. *International Journal of Pharmaceutics*, 379(2), pp.293–300.

Motoyama, K. et al., 2011. In Vitro Gene Delivery Mediated by Asialofetuin-Appended Cationic Liposomes Associated with γ-Cyclodextrin into Hepatocytes. *Journal of drug delivery*, 2011, p.476137.

Mozafari, M.R., 2010. Nanoliposomes: preparation and analysis. *Methods in molecular biology (Clifton, N.J.)*, 605, pp.29–50.

Mukthavaram, R. et al., 2011. Assembly and Targeting of Liposomal Nanoparticles Encapsulating Quantum Dots. *Bioconjugate Chemistry*. Available at: http://www.ncbi.nlm.nih.gov/pubmed/21786821 [Accessed August 8, 2011].

Murao, A. et al., 2002. Targeting efficiency of galactosylated liposomes to hepatocytes in vivo: effect of lipid composition. *Pharmaceutical Research*, 19(12), pp.1808–1814.

Muthu, M.S. et al., 2012. Theranostic liposomes of TPGS coating for targeted co-delivery of docetaxel and quantum dots. *Biomaterials*, 33(12), pp.3494–3501.

Nathwani, A.C. et al., 2011. Adenovirus-associated virus vector-mediated gene transfer in hemophilia B. *The New England journal of medicine*, 365(25), pp.2357–2365.

Neue, K. et al., 2011. Elucidation of glycoprotein structures by unspecific proteolysis and direct nanoESI mass spectrometric analysis of ZIC-HILIC-enriched glycopeptides. *Journal of proteome research*, 10(5), pp.2248–2260.

Neyrinck, A.M. et al., 2000. Are Kupffer cells involved in the metabolic adaptation of the liver to dietary carbohydrates given after fasting? *Biochimica et biophysica acta*, 1475(3), pp.238–244.

Olympus, 2009. Olympus FluoView Resource Center: Electronic Light Detectors: Photomultipliers. Available at: http://www.olympusconfocal.com/theory/pmtintro.html [Accessed September 22, 2012].

Oyen, W.J. et al., 1996. Detecting infection and inflammation with technetium-99m-labeled Stealth liposomes. *Journal of nuclear medicine: official publication, Society of Nuclear Medicine*, 37(8), pp.1392–1397.

Pang, Z. et al., 2011. Brain delivery and cellular internalization mechanisms for transferrin conjugated biodegradable polymersomes. *International journal of pharmaceutics*, 415(1-2), pp.284–292.

Park, J.-H., Kim, K.L. & Cho, E.-W., 2006. Detection of surface asialoglycoprotein receptor expression in hepatic and extra-hepatic cells using a novel monoclonal antibody. *Biotechnology letters*, 28(14), pp.1061–1069.

Pasquetto, M.V. et al., 2011. Targeted drug delivery using immunoconjugates: principles and applications. *Journal of immunotherapy (Hagerstown, Md.: 1997)*, 34(9), pp.611–628.

Pasut, G. & Veronese, F.M., 2012. State of the art in PEGylation: the great versatility achieved after forty years of research. *Journal of controlled release: official journal of the Controlled Release Society*, 161(2), pp.461–472.

Pathak, A., Vyas, S.P. & Gupta, K.C., 2008. Nano-vectors for efficient liver specific gene transfer. *International Journal of Nanomedicine*, 3(1), pp.31–49.

Pérez-López, M.E. et al., 2007. Role of pegylated liposomal doxorubicin (Caelyx) in the treatment of relapsing ovarian cancer. *Anti-cancer drugs*, 18(5), pp.611–617.

Petrus, I., Chuah, M. & VandenDriessche, T., 2010. Gene therapy strategies for hemophilia: benefits versus risks. *The journal of gene medicine*, 12(10), pp.797–809.

Poelstra, K., Prakash, J. & Beljaars, L., 2012. Drug targeting to the diseased liver. *Journal of controlled release: official journal of the Controlled Release Society*, 161(2), pp.188–197.

Popielarski, S.R. et al., 2005. A nanoparticle-based model delivery system to guide the rational design of gene delivery to the liver. 2. In vitro and in vivo uptake results. *Bioconjugate Chemistry*, 16(5), pp.1071–1080.

Popov, Y. & Schuppan, D., 2009. Targeting liver fibrosis: strategies for development and validation of antifibrotic therapies. *Hepatology (Baltimore, Md.)*, 50(4), pp.1294–1306.

Rensen, P.C. et al., 2001. Determination of the upper size limit for uptake and processing of ligands by the asialoglycoprotein receptor on hepatocytes in vitro and in vivo. *The Journal of Biological Chemistry*, 276(40), pp.37577–37584.

Resch-Genger, U. et al., 2008. Quantum dots versus organic dyes as fluorescent labels. *Nature methods*, 5(9), pp.763–775.

Rice, K.G., Rao, N.B. & Lee, Y.C., 1990. Large-scale preparation and characterization of N-linked glycopeptides from bovine fetuin. *Analytical Biochemistry*, 184(2), pp.249–258.

Riddles, P.W., Blakeley, R.L. & Zerner, B., 1979. Ellman's reagent: 5,5′-dithiobis(2-nitrobenzoic acid)—a reexamination. *Analytical Biochemistry*, 94(1), pp.75–81.

Van Rooijen, N. et al., 1990. Depletion and repopulation of macrophages in spleen and liver of rat after intravenous treatment with liposome-encapsulated dichloromethylene diphosphonate. *Cell and tissue research*, 260(2), pp.215–222.

Van Rooijen, N. & Sanders, A., 1996. Kupffer cell depletion by liposome-delivered drugs: comparative activity of intracellular clodronate, propamidine, and ethylenediaminetetraacetic acid. *Hepatology (Baltimore, Md.)*, 23(5), pp.1239–1243.

Rotundo, R.F. et al., 1998. Circulating cellular fibronectin may be a natural ligand for the hepatic asialoglycoprotein receptor: possible pathway for fibronectin deposition and turnover in the rat liver. *Hepatology (Baltimore, Md.)*, 28(2), pp.475–485.

Sambrano, G.R. & Steinberg, D., 1995. Recognition of oxidatively damaged and apoptotic cells by an oxidized low density lipoprotein receptor on mouse peritoneal macrophages: role of membrane phosphatidylserine. *Proceedings of the National Academy of Sciences of the United States of America*, 92(5), pp.1396–1400.

Schnell, R. et al., 2002. Current strategies of antibody-based treatment in Hodgkin's disease. *Annals of oncology: official journal of the European Society for Medical Oncology / ESMO*, 13 Suppl 1, pp.57–66.

Schnyder, A. et al., 2005. Targeting of daunomycin using biotinylated immunoliposomes: pharmacokinetics, tissue distribution and in vitro pharmacological effects. *Journal of drug targeting*, 13(5), pp.325–335.

Schnyder, A. et al., 2004. Targeting of skeletal muscle in vitro using biotinylated immunoliposomes. *The Biochemical Journal*, 377(Pt 1), pp.61–67.

Schwartz, A.L. et al., 1981. Characterization of the asialoglycoprotein receptor in a continuous hepatoma line. *The Journal of Biological Chemistry*, 256(17), pp.8878–8881.

Schwartz, A.L., 1995. Receptor Cell Biology: Receptor-Mediated Endocytosis. *Pediatric Research*, 38(6). Available at: http://journals.lww.com/pedresearch/Fulltext/1995/12000/Receptor_Cell_Biology__Receptor_Mediated.3.aspx.

Schwartz, A.L., 1984. The hepatic asialoglycoprotein receptor. *CRC Critical Reviews in Biochemistry*, 16(3), pp.207–233.

Seow, Y.T., Tan, M.G.K. & Woo, K.T., 2002. Expression of a functional asialoglycoprotein receptor in human renal proximal tubular epithelial cells. *Nephron*, 91(3), pp.431–438.

Sharma, A. & Sharma, U.S., 1997. Liposomes in drug delivery: Progress and limitations. *International Journal of Pharmaceutics*, 154(2), pp.123–140.

Shimada, K. et al., 1997. Biodistribution of liposomes containing synthetic galactose-terminated diacylglyceryl-poly(ethyleneglycol)s. *Biochimica Et Biophysica Acta*, 1326(2), pp.329–341.

Shimizu, K. et al., 1996. Evaluation of dipalmitoylphosphatidylcholine liposomes containing a soybean-derived sterylglucoside mixture for liver targeting. *Journal of Drug Targeting*, 4(4), pp.245–253.

Siebler, J. & Galle, P.R., 2006. Treatment of nonalcoholic fatty liver disease. *World journal of gastroenterology: WJG*, 12(14), pp.2161–2167.

Sigot, V., Arndt-Jovin, D.J. & Jovin, T.M., 2010. Targeted cellular delivery of quantum dots loaded on and in biotinylated liposomes. *Bioconjugate Chemistry*, 21(8), pp.1465–1472.

Singh, A. et al., 2010. Biotin-directed assembly of targeted modular lipoplexes and their transfection of human hepatoma cells in vitro. *Drug Delivery*. Available at: http://www.ncbi.nlm.nih.gov/pubmed/20469969 [Accessed June 2, 2010].

Stewart, J.C., 1980. Colorimetric determination of phospholipids with ammonium ferrothiocyanate. *Analytical Biochemistry*, 104(1), pp.10–14.

Stockert, R.J., 1995. The asialoglycoprotein receptor: relationships between structure, function, and expression. *Physiological Reviews*, 75(3), pp.591–609.

Stokmaier, D. et al., 2009. Design, synthesis and evaluation of monovalent ligands for the asialoglycoprotein receptor (ASGP-R). *Bioorganic & Medicinal Chemistry*. Available at: http://www.ncbi.nlm.nih.gov/pubmed/19762243 [Accessed October 1, 2009].

Subramanian, A., Ranganathan, P. & Diamond, S.L., 1999. Nuclear targeting peptide scaffolds for lipofection of nondividing mammalian cells. *Nature biotechnology*, 17(9), pp.873–877.

Szoka, F.C., Jr, Milholland, D. & Barza, M., 1987. Effect of lipid composition and liposome size on toxicity and in vitro fungicidal activity of liposome-intercalated amphotericin B. *Antimicrobial agents and chemotherapy*, 31(3), pp.421–429.

Takanaga, H., Chaudhuri, B. & Frommer, W.B., 2008. GLUT1 and GLUT9 as major contributors to glucose influx in HepG2 cells identified by a high sensitivity intramolecular FRET glucose sensor. *Biochimica et biophysica acta*, 1778(4), pp.1091–1099.

Tanaka, M. et al., 2011. Liver stem/progenitor cells: their characteristics and regulatory mechanisms. *Journal of biochemistry*, 149(3), pp.231–239.

Tanaka, T. et al., 2004. Cellular disposition of arabinogalactan in primary cultured rat hepatocytes. *European Journal of Pharmaceutical Sciences: Official Journal of the European Federation for Pharmaceutical Sciences*, 22(5), pp.435–444.

Testa, B. & Krämer, S.D., 2006. The biochemistry of drug metabolism--an introduction: part 1. Principles and overview. *Chemistry & biodiversity*, 3(10), pp.1053–1101.

Thermo Scientific, 2009. Technical Tip #31. Available at: http://www.piercenet.com/Objects/View.cfm?type=File&ID=F0DF0BDC-8D74-4B6F-8AD7-77CF31C0F305 [Accessed August 10, 2010].

Thews, G., Mutschler, E. & Vaupel, P., 1999. *Anatomie, Physiologie, Pathologie des Menschen* 5. ed., Stuttgart: Wissenschaftliche Verlagsgesellschaft mbH.

Tian, B. et al., 2011. Doxorubicin-loaded lipid-quantum dot hybrids: Surface topography and release properties. *International Journal of Pharmaceutics*. Available at: http://www.ncbi.nlm.nih.gov/pubmed/21315141 [Accessed May 27, 2011].

Tiphine, M., Letscher-Bru, V. & Herbrecht, R., 1999. Amphotericin B and its new formulations: pharmacologic characteristics, clinical efficacy, and tolerability. *Transplant infectious disease: an official journal of the Transplantation Society*, 1(4), pp.273–283.

Tolleshaug, H. et al., 1977. Uptake and degradation of 125I-labelled asialo-fetuin by isolated rat hepatocytes. *Biochimica et biophysica acta*, 499(1), pp.73–84.

Trahtenherts, A. & Benhar, I., 2009. An internalizing antibody specific for the human asialoglycoprotein receptor. *Hybridoma (2005)*, 28(4), pp.225–233.

Trerè, D. et al., 1999. The asialoglycoprotein receptor in human hepatocellular carcinomas: its expression on proliferating cells. *British journal of cancer*, 81(3), pp.404–408.

Tros de Ilarduya, C., 2010. Serum-resistant lipoplexes in the presence of asialofetuin. *Methods in Molecular Biology (Clifton, N.J.)*, 605, pp.425–434.

Tsuchiya, S. et al., 1986. Preparation and disposition of asialofetuin-labelled liposome. *Biopharmaceutics & drug disposition*, 7(6), pp.549–558.

Tuffin, G. et al., 2005. Immunoliposome targeting to mesangial cells: a promising strategy for specific drug delivery to the kidney. *Journal of the American Society of Nephrology: JASN*, 16(11), pp.3295–3305.

Tycko, B., Keith, C.H. & Maxfield, F.R., 1983. Rapid acidification of endocytic vesicles containing asialoglycoprotein in cells of a human hepatoma line. *The Journal of Cell Biology*, 97(6), pp.1762–1776.

Uldry, M. et al., 2002. GLUT2 is a high affinity glucosamine transporter. *FEBS letters*, 524(1-3), pp.199–203.

Underwood, C. et al., 2012. Intravenous technetium-99m labelled PEG-liposomes in horses: a safety and biodistribution study. *Equine veterinary journal*, 44(2), pp.196–202.

Uniprot.org, 2012a. Asialoglycoprotein receptor 1 - Homo sapiens (Human). Available at: http://www.uniprot.org/uniprot/P07306 [Accessed October 3, 2012].

Uniprot.org, 2012b. Asialoglycoprotein receptor 2 - Homo sapiens (Human). Available at: http://www.uniprot.org/uniprot/P07307 [Accessed October 3, 2012].

Uniprot.org, 2012c. Sequence Alignment UniProt Database. Available at: http://www.uniprot.org/align/ [Accessed September 16, 2012].

University Hospital Basel, Switzerland, 2012. Departement Biomedizin: Research. Available at: http://biomedizin.unibas.ch/research/research-group-details/research/researchgroup/medical-oncology/ [Accessed October 7, 2012].

Wang, S. et al., 2010. Sustained Liver Targeting and Improved Antiproliferative Effect of Doxorubicin Liposomes Modified with Galactosylated Lipid and PEG-Lipid. *AAPS PharmSciTech*. Available at: http://www.ncbi.nlm.nih.gov/pubmed/20490957 [Accessed May 28, 2010].

Warren, G.S. & Fowler, M.W., 1982. Transference of the high molecular weight carbohydrate sequences of fetuin to the surface of carrot embryo protoplasts. *Biochimica et Biophysica Acta (BBA) - Biomembranes*, 691(1), pp.125–132.

Weinstein, J.N. et al., 1977. Liposome-cell interaction: transfer and intracellular release of a trapped fluorescent marker. *Science (New York, N.Y.)*, 195(4277), pp.489–492.

Weissig, V., 2012. Mitochondria-specific nanocarriers for improving the proapoptotic activity of small molecules. *Methods in enzymology*, 508, pp.131–155.

Wen, C.-J. et al., 2012. Theranostic liposomes loaded with quantum dots and apomorphine for brain targeting and bioimaging. *International journal of nanomedicine*, 7, pp.1599–1611.

Weng, K.C. et al., 2008. Targeted tumor cell internalization and imaging of multifunctional quantum dot-conjugated immunoliposomes in vitro and in vivo. *Nano Letters*, 8(9), pp.2851–2857.

Wu, J. et al., 1998. Increased liver uptake of liposomes and improved targeting efficacy by labeling with asialofetuin in rodents. *Hepatology (Baltimore, Md.)*, 27(3), pp.772–778.

Wu, J., Nantz, M.H. & Zern, M.A., 2002. Targeting hepatocytes for drug and gene delivery: emerging novel approaches and applications. *Frontiers in Bioscience: A Journal and Virtual Library*, 7, pp.d717–725.

Wu, J. & Zern, M.A., 2000. Hepatic stellate cells: a target for the treatment of liver fibrosis. *Journal of gastroenterology*, 35(9), pp.665–672.

Wu, X. et al., 2003. Immunofluorescent labeling of cancer marker Her2 and other cellular targets with semiconductor quantum dots. *Nature biotechnology*, 21(1), pp.41–46.

Yan, X. et al., 2005. The role of apolipoprotein E in the elimination of liposomes from blood by hepatocytes in the mouse. *Biochemical and biophysical research communications*, 328(1), pp.57–62.

Zhang, H. et al., 2009. Fluorescent tumour imaging of type I IGF receptor in vivo: comparison of antibody-conjugated quantum dots and small-molecule fluorophore. *British Journal of Cancer*, 101(1), pp.71–79.

Zhao, F.-Q. & Keating, A.F., 2007. Functional properties and genomics of glucose transporters. *Current genomics*, 8(2), pp.113–128.

Zhao, X. et al., 2011. Construction and characterization of an anti-asialoglycoprotein receptor single-chain variable-fragment-targeted melittin. *Biotechnology and applied biochemistry*, 58(6), pp.405–411.

Ziegler, J. et al., 2007. High-quality ZnS shells for CdSe nanoparticles: rapid microwave synthesis. *Langmuir: the ACS journal of surfaces and colloids*, 23(14), pp.7751–7759.

7. Appendix - Published pharmacokinetic investigations

7.1. In vitro assessment of the formation of ceftriaxone-calcium precipitates in human plasma

Schmutz HR, Detampel P, Bühler T, Büttler A, Gygax B, Huwyler J.

J Pharm Sci. (2011) Jun;100(6):2300-10

In Vitro Assessment of the Formation of Ceftriaxone–Calcium Precipitates in Human Plasma

HANS-RUDOLF SCHMUTZ,[1] PASCAL DETAMPEL,[2,3] THEO BÜHLER,[1] ANDRÉ BÜTTLER,[1] BENJAMIN GYGAX,[1] JÖRG HUWYLER[3]

[1]Institute of Chemistry and Bioanalytics, University of Applied Sciences-FHNW, Muttenz, Switzerland

[2]Institute of Pharmaceutical Technology, University of Applied Sciences-FHNW, Muttenz, Switzerland

[3]Division of Pharmaceutical Technology, Department of Pharmaceutical Sciences, University of Basel, Basel, Switzerland

Received 15 October 2010; revised 23 November 2010; accepted 7 December 2010

Published online 19 January 2011 in Wiley Online Library (wileyonlinelibrary.com). DOI 10.1002/jps.22466

ABSTRACT: Ceftriaxone is a third-generation cephalosporin antibiotic, which has a broad spectrum of bactericidal activity. Ceftriaxone is highly soluble as a sodium salt, but far less soluble as a calcium salt. Incompatibility of ceftriaxone with calcium and the possible formation of precipitates have been stated in the product label from early on. It was the objective of the present *in vitro* study to further assess the risk of precipitation of calcium-ceftriaxone in human plasma. Analytical methods were developed (high-performance liquid chromatography and flame atomic absorption spectroscopy) to quantitate calcium and ceftriaxone in human plasma supernatants and human plasma precipitates. Using high concentrations of ceftriaxone (10 mmol/L) and calcium (4.2 mmol/L) did not result in any precipitation after 2 h incubation in human plasma at 37°C. Under conditions of forced precipitation only, formation of precipitation was observed. The identity of the precipitated material was confirmed by energy-dispersive X-ray analysis and Fourier transform infrared spectroscopy. We conclude that calcium-ceftriaxone in human plasma has an apparent kinetic solubility product constant of greater than 0.42×10^{-4} $(mol/L)^2$, which exceeds the normal thermodynamic solubility product in water by a factor of 26. Under these conditions, the formation of plasma precipitates is unlikely. © 2011 Wiley-Liss, Inc. and the American Pharmacists Association J Pharm Sci 100:2300–2310, 2011

Keywords: ceftriaxone; calcium; precipitation; *in vitro*; plasma; FTIR; HPLC; Solubility; Spectroscopy

INTRODUCTION

Ceftriaxone (Fig. 1) is a well-known third-generation cephalosporin antibiotic,[1,2] which was introduced worldwide in the early 1980s. It is commercially available as a highly soluble sodium salt.[3] However, in combination with calcium ions, it can form a poorly soluble ceftriaxone–calcium salt.[4] Although the solubility product constant for calcium-ceftriaxone is around 1.62×10^{-6} $(mol/L)^2$, 10-fold supersaturation of the salt is described for solutions in water and bile by Shiffman et al.[4] This effect appears to be long lasting because such solutions do not show precipitation even after 24 h.[4] Pharmacokinetics of the drug differs between age groups, mainly due to different renal function and protein binding.[1,5–13] Infusion of a single intravenous (i.v.) dose of ceftriaxone (2 g) for 30 min results in a maximum plasma concentration (C_{max}) of approximately 0.47 mmol/L in healthy adults,[5,6] whereas an accumulated C_{max} up to 0.624 mmol/L has been reported after administering 2 g every 12 h for 4 days.[6] The question arises whether i.v. infusions or bolus injections of high concentrations of ceftriaxone can be combined with i.v. calcium-containing fluids. In such a situation, the formation of precipitates under *in vivo* conditions might occur.

The current clinical interest for this potential adverse drug reaction stems from several fatal-case

Abbreviations used: C_{max}, maximum plasma concentration; EDTA, ethylenediaminetetraacetic acid; EDX, energy-dispersive X-ray analysis; F-AAS, flame atomic absorption spectroscopy; FTIR, Fourier transform infrared spectroscopy; HPLC, high-performance liquid chromatography; i.v., intravenous; LOD, limit of detection; LOQ, limit of quantification; SEM, scanning electron microscopy.

Correspondence to: Jörg Huwyler (Telephone: +41-61-267-15-00/13; Fax: +41-61-267-15-16; E-mail: joerg.huwyler@unibas.ch)

Journal of Pharmaceutical Sciences, Vol. 100, 2300–2310 (2011)
© 2011 Wiley-Liss, Inc. and the American Pharmacists Association

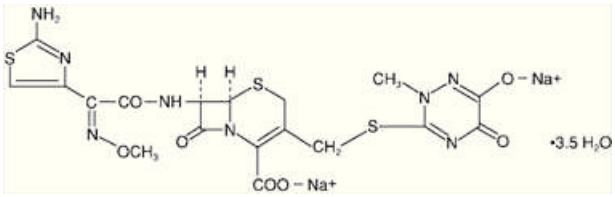

Figure 1. Structure of ceftriaxone.

reports of calcium–ceftriaxone precipitation in neonates during the past 2 decades.[14,15] Of the reported incidents, three showed the presence of a crystalline material or white precipitate in the vascular beds, mostly in the lungs and kidneys. However, many of these infants received several other medications, such as amikacin, which are known to be physically incompatible when mixed with ceftriaxone, and in some reports, the incident was not immediately related to the last ceftriaxone administration. In addition, although the material found was most likely a precipitate of ceftriaxone, none of the cases established the identity of the material.[14] Thus, in these clinical cases, it is not possible to confirm the presence of calcium–ceftriaxone precipitates, and other contributing factors cannot be ruled out. In addition, the concentrations of calcium and ceftriaxone required for precipitates to be formed *in vivo* are not known.

The formation of calcium–ceftriaxone precipitates has been addressed previously in another context. Various analyses concerning the formation of biliary sludge[4,16,17] and nephrolithiasis[18] have been published. The situation concerning the solubility in plasma is not comparable with urine, nor to bile. This is in part due to the extensive albumin binding of ceftriaxone and calcium,[19,20] which affects the apparent solubility. The amount of dissolved ceftriaxone in various physiological fluids was quantified previously by high-performance liquid chromatography (HPLC) or by an agar-diffusion bioassay.[7,21,22] However, to our knowledge, there is still no method available for chemical analysis of ceftriaxone precipitates in human plasma.

With the objective of further evaluating the interaction of ceftriaxone with calcium-containing products and in view of ongoing discussions around these issues,[14,15,23–29] we therefore decided to assess the risk of precipitations using an alternative strategy to quantitatively analyze the formation of calcium–ceftriaxone precipitates in plasma from adults. For these experiments, we used fresh human plasma from adults, supplemented with exogenous calcium and ceftriaxone, using upper clinically relevant concentrations, while respecting a reasonable safety margin. By using fresh, uncentrifuged human plasma, potential nuclei of crystallization are not eliminated. Furthermore, plasma proteins, such as albumin, are preserved from denaturation and precipitation. Potential precipitates of calcium and ceftriaxone were analyzed quantitatively by flame atomic absorption spectroscopy (F-AAS) to measure calcium and by HPLC to determine ceftriaxone concentrations. The identity of calcium–ceftriaxone precipitates in human plasma was confirmed by electron microscopy, combined with energy-dispersive X-ray (EDX) and Fourier transform infrared (FTIR) spectroscopy.

All data presented are discussed in the context of known properties of ceftriaxone, combined with the clinical relevance of the findings.

MATERIALS AND METHODS

Reagents and Pretreatments

Ceftriaxone disodium salt (sterile) bulk Ca^{2+}–ceftriaxone (amorphous powder) and fresh pooled heparinized adult human plasma (i.e., neither frozen nor centrifuged) were provided by F. Hoffmann-La Roche Ltd., Basel, Switzerland Methanol and acetonitrile for chromatography and nitric acid (69.0%-70.0%; "instra-analyzed" quality) were from Baker Ltd. (Mallinckrodt Baker, Phillipsburg, New Jersey). Hydrogen peroxide solution ("trace select ultra for trace analysis" quality) and atomic spectroscopy Ca^{2+} standard solution were from Fluka (Buchs, Switzerland). Water (nanopure) was prepared inhouse using a Barnstead (Thermo Fisher Scientific, Waltham, Massachusetts). Nanopure diamond system (electrical resistance: 18.2 $M\Omega\ cm^{-1}$). All other chemicals and reagents were of analytical grade and were obtained from commercial suppliers. Volumetric flasks, microwave tubes, and Teflon inserts were pretreated with 10% HNO_3 for at least 12 h and rinsed three times with nanopure water before use. Autosampler tubes were rinsed once with sample solution.

METHOD DEVELOPMENT AND VALIDATION

Calcium Analysis

Ca^{2+}–ceftriaxone supernatants (0.2 mL) were mixed with 2.0 mL of HNO_3 (70.0%) and 2.0 mL of H_2O_2 in a Teflon digestion tube followed by microwave radiation (5 min in at 250 W output power, 5 min at 400 W output power, and 5 min at 500 W output power) using a Milestone mls1200 mega microwave digester (Shelton, Connecticut) equipped with a MDR-300/S rotor and microwave resistant Teflon inserts. Samples were allowed to cool down to ambient temperature for 10 min and were transferred to a volumetric flask. The digestion vessels and the Teflon tubes were rinsed three times with 0.2% HNO_3. Wash solutions

were also transferred to the volumetric flask, and the final volume was adjusted to 25 mL with 0.2% HNO_3.

Ca^{2+}–ceftriaxone plasma precipitates (pellets) were washed in 0.5 mL of cold water (6°C), vortexed for 1 min, centrifuged, and resuspended in 5 mL of buffer solution (pH 7; 50 mmol/L potassium dihydrogen phosphate, 19 mmol/L sodium hydroxide). They were then spiked with 10 mg ethylenediaminetetraacetic acid (EDTA) and incubated for 2 h at 37°C on an orbital shaker with 180 rpm. Two milliliters of the suspension was mixed with 2.0 mL of HNO_3 (70.0%) and 2.0 mL of H_2O_2. They were digested as described above for plasma pellets. Digested samples were transferred to a volumetric flask and the volume adjusted to 10 mL using 0.2% HNO_3. Aliquotes of each sample (10 mL) solution were analyzed by a AA800 F-AAS instrument with a flame interface (acetylene/air) and equipped with a AS-93plus autosampler (PerkinElmer, Waltham, Massachusetts). Data collection and analysis were performed using PerkinElmer WinLab32 software. Air flow was 17 L/min, and acetylene flow was 2.5 L/min. Element calcium was monitored at a wavelength of 422.7 nm using a slit of 0.7 nm and a time average of 3 s for the atomic absorption signal. Data represent means of n equals to three independent measurements. The F-AAS method was monitored in each series by inclusion of quality control samples, using mineralized, digested Ca^{2+}-spiked plasma samples, and diluted standard samples in the same concentration range. Before each series of measurements, a calibration curve was established using six distinct calibration standard solutions covering a range from 0.125 to 5 mg/L. Aliquots of each standard solution (10 mL) were analyzed by F-AAS. Recovery was calculated by comparing peak areas of calibration solutions prepared in water with peak areas of spiked plasma samples.

Ceftriaxone Analysis

Plasma (100 μL) containing ceftriaxone was mixed with 900 μL water/methanol (4:9, v/v), vortexed, and incubated on ice for at least 30 min. After centrifugation (10 min at 20,000 × g), 50 μL aliquots of supernatants were transferred to HPLC sample vials and diluted to a final volume of 1 mL using H_2O. This solution was analyzed by HPLC. Samples containing Ca^{2+}–ceftriaxone or plasma precipitates containing Ca^{2+}–ceftriaxone were washed in 0.5 mL of cold water (6°C), vortexed for 1 min, centrifuged, and resuspended in 5 mL buffer solution (pH 7; 50 mmol/L potassium dihydrogen phosphate, 19 mmol/L sodium hydroxide). Washed samples were spiked with 10 mg EDTA and incubated for 2 h at 37°C. Prior to HPLC analysis, insoluble particles were removed by centrifugation and filtration through a 0.45-μm filter (Titan-2 HPLC Filters with PVDF membrane, 17-mm diameter, 0.45-μm pore size; Thermo Fisher Scientific). HPLC analysis was performed on a quaternary Agilent HPLC 1200 chromatography system (Agilent Technologies, Santa Clara, California) operated at a flow rate of 0.5 mL/min. The stationary phase was a Waters C_{18} XBridge™ column (3.5 μm, 150 × 3.0 mm I.D., Waters Ltd., Milford, Pennsylvania) kept at 30°C during analysis. Injection volume was 10 μL. The separation of analytes was achieved using an isocratic separation lasting 7 min in solvent A [1.0% formic acid/methanol (80:20, v/v)], followed by a linear gradient of 2 min to 70% of solvent B (1.0% formic acid in methanol) followed by an isocratic step of 3 min under the same conditions. Before the next sample was injected, the solvent composition was changed to the initial conditions of 100% solvent A, and the system was equilibrated for 8 min. Analytes were detected by ultraviolet (UV) absorbance at 261 nm, using an Agilent DAD 1200 UV detector (Agilent Technologies). Samples were kept in a cooled sample tray at 10°C before injection. All ceftriaxone standards were prepared from stock solutions of ceftriaxone (45 mmol/L ceftriaxone disodium salt in H_2O) covering a range from 0.4 to 438 μM. Calibration solutions and quality standards were stored at −20°C. The HPLC method in each series was monitored by inclusion of quality control standards prepared in water as well as human plasma. Recovery was calculated by comparison of peak areas of calibration solutions prepared in water, with peak areas of spiked plasma samples. Data evaluation was perfomed using Agilent Chemstation for LC 3D System software (Agilent Technologies).

Quantitative Analysis of Calcium and Ceftriaxone in Human Plasma

Serial dilutions of ceftriaxone in 0.5 mL plasma were prepared and added to test tubes containing either 0.5 mL of plasma (control) or plasma spiked with calcium (final concentration 4.2 mmol/L Ca^{2+}), and were incubated at 37°C on a rotary platform (60 rpm) for 2 h. The concentration of ceftriaxone was between 0.63 to 10.05 mmol/L. Plasma supernatants were separated from plasma precipitates by centrifugation (20,000 × g for 10 min at room temperature). The analysis of calcium and ceftriaxone in precipitates, as well as in supernatants, was carried out as described above in the validated concentration range.

Qualitative Analysis of Calcium and Ceftriaxone in Human Plasma

Preparation of Plasma Precipitates by Forced Precipitation of Ceftriaxone

For the forced precipitation of calcium-ceftriaxone, two equal amounts of fresh human plasma samples were spiked with either Na^+–ceftriaxone or exogenously added $CaCl_2$ and mixed, resulting in a

concentration of 20 mmol/L ceftriaxone and 20 mmol/L calcium. Samples were incubated for 1 h at 37°C, followed by centrifugation. The analysis of plasma precipitates was performed by light microscopy and scanning electron microscopy (SEM) combined with EDX analysis.

Light Microscopy

Plasma precipitates were analyzed by visual inspection, using an inverted Olympus IX-71 microscope or a direct transmission Olympus BX-51 microscope (Olympus Ltd., Tokyo, Japan). Both microscopes were equipped with a digital camera. Phase-contrast images were obtained under 400 × magnifications.

SEM and EDX Analysis

For SEM combined with EDX analysis of plasma precipitates, a Zeiss Gemini supra 40VP field emission scanning electron microscope was used (Carl Zeiss, Jena, Germany). The instrument was operated under secondary electron, back-scattered detection, and EDX mode. The accelerating voltage was 20 keV.

FTIR Spectroscopy

Fourier transform infrared spectra were acquired using a Digilab FTS 7000 Series FTIR spectrophotometer equipped with a Germanium-ATR MCT detector (Varian Medical Systems Inc., Palo Alto, California). FTIR spectra represent the mean of 32 scans obtained with a resolution of 4 cm^{-1}.

RESULTS

Method Development and Validation

Flame atomic absorption spectroscopy gave a linear range of the calcium response (Table 1), and the limit of detection (LOD) and limit of quantification (LOQ) were determined according to guidelines of the International Conference on Harmonisation (ICH) [30]: LOD = 0.025 mg/L, LOQ = 0.075 mg/L. These values were associated with a relative standard deviation of 30% and 10%, respectively (data not shown). It is important to note that the intrinsic concentrations of calcium in the human plasma preparations were measured and were in the expected physiological range of 2.74 mmol/L ± 1.8% (mean ± rel. SD, n = 5). Here, measured calcium concentrations always refer to the total amount of calcium present in a given sample. They are thus representative of the sum of exogenously added calcium and the endogenous plasma calcium concentration of 2.74 mmol/L.

Recovery of Ca^{2+} was determined in human plasma by adding calcium to a final concentration of 3.2 mmol/L (addition of 0.5 mmol/L Ca^{2+}) and 4.2 mmol/L (addition of 1.5 mmol/L Ca^{2+}) (Table 1).

Recovery was calculated by comparing peak areas of calibration solutions prepared in 0.2% HNO_3 with peak areas of spiked plasma samples. It should be noted that identical results were obtained irrespective of the origin of the measured calcium (i.e., either Ca^{2+} standard or Ca^{2+}–ceftriaxone) because all procedures for the determination of Ca^{2+} were based on the complete digestion of any organic matter, before the solutions were analyzed with F-AAS. For the quantitative determination of ceftriaxone in human plasma, an HPLC-based method was utilized, wherein ceftriaxone showed a retention time of approximately 6 min. Calibration samples were prepared in water, and unknown plasma samples were diluted with water into the linear range. The assay was linear over a concentration range of three orders of magnitude (Table 1). The corresponding LOD represents a signal-to-noise ratio of 3, whereas the LOQ represents a signal-to-noise ratio of 9. Overall, accuracy and precision of ceftriaxone determination in human plasma were measured at ceftriaxone concentration levels of 10, 5, 2.5, 1.26, and 0.62 mmol/L (Table 1). Recovery of ceftriaxone in human plasma was determined at ceftriaxone concentration levels of 10, 2.5, and 0.6 mmol/L. Highest recovery of ceftriaxone from precipitates was achieved at pH 7 in presence of EDTA (Table 1).

Table 1. Validation of the Method to Analyze the Amount of Calcium and Ceftriaxone in Human Plasma

Analyte	Matrix	% Recovery (Concentration, mmol/L)	Precision (Concentration, mmol/L)	Accuracy (Concentration, mmol/L)	Linear Range (μmol/L) [R^2]	Limit of Quantification (μmol/L)
Ca^{2+}	Supernatant	102.6 ± 5.2, n = 4 (3.2) 100.8 ± 4.4, n = 4 (4.2)	±1.2%, n = 4 (2.7)	–	3.1–125 [0.999]	1.87
Ca^{2+}	Pellet	102.6 ± 5.2, n = 4 (3.2) 100.8 ± 4.4, n = 4 (4.2)	±1.2%, n = 4 (2.7)	–	3.1–125 [0.999]	1.87
Ceftriaxone	Supernatant	95 ± 1.0, n = 3 (0.6) 98.9 ± 1.4, n = 3 (2.5) 103 ± 1.0, n = 3 (10)	±3.2%, n = 20 (0.62–10)	102% (0.62–10)	0.44–440 [0.999]	0.49
Ceftriaxone	Pellet	93.4	± 3.2%, n = 20 (0.62-10)	102% (0.62–10)	0.44–440 [0.999]	0.49

Calibration samples were prepared in water. Unknown plasma samples were diluted with water into the linear range. Ceftriaxone is stable over 22 h at 10°C. Different experiments are summarized, which were performed using the indicated concentration of analytes. Values are means ± RSD. Used concentrations are given in parenthesis.

Table 2. Analysis of Supernatants and Plasma Precipitates

		Supernatant		Pellet	
Ceftriaxone (mmol/L)	Calcium (mmol/L)	% Recovery Ceftriaxone	% Recovery Calcium	% Recovery Ceftriaxone	% Recovery Calcium
0.63	4.2	97.6 ± 0.2	108.6 ± 0.0	0.24 ± 0.08	3.76 ± 0.38
1.26	4.2	99.1 ± 1.9	104.7 ± 3.4	0.30 ± 0.09	2.55 ± 0.95
2.51	4.2	99.5 ± 0.1	106.2 ± 1.1	0.25 ± 0.00	2.42 ± 0.38
5.03	4.2	100.9 ± 0.8	107.0 ± 0.0	0.18 ± 0.04	2.29 ± 0.57
10.05	4.2	100.3 ± 3.0	101.5 ± 1.1	0.26 ± 0.13	2.55 ± 0.57
Recovery mean		99.5	105.6	0.25	2.72
SD		1.8	2.6	0.08	0.56
N		20	10	20	10

Recovery of calcium (4.2 mmol/L total concentration) and ceftriaxone (0.63–10.05 mmol/L) in fresh human plasma. Values are means ± RSD.

Quantitative Analysis of Calcium and Ceftriaxone in Human Plasma

The serial dilutions of ceftriaxone in human plasma were mixed with plasma-containing $CaCl_2$ and incubated. Note that the fresh human plasma used for these experiments was not frozen and was not precentrifuged. The results are presented in Table 2.

Total recovery of calcium from plasma pellets was consistently low and did not depend on the added ceftriaxone concentrations. For ceftriaxone, a trend toward a lower recovery from plasma supernatants was observed with decreasing ceftriaxone concentrations.

Within the uncertainty of measurement, the content of ceftriaxone and calcium in the pellets was in the range of 0.25% to 2.72% of the amounts initially added. Within the uncertainty of measurement, a nominal 100% of added ceftriaxone, as well as added calcium, was recovered from human plasma supernatants. There was no apparent loss due to precipitation (Table 2).

It should be noted that our methods cannot be used to analyze the formation of cefriaxone precipitates in full blood. Precipitates are separated from the incubation mix by centrifugation. The hematocrit or packed cell volume of human blood would make it very difficult to detect small amounts of drug precipitates.

Qualitative Analysis of Calcium and Ceftriaxone in Human Plasma

Inspection of Plasma Precipitates Using Light Microscopy and EDX Analysis of Calcium for Qualitative Analysis

Fresh human plasma had a clear appearance and did not contain any crystalline material (Fig. 2, panel a). This situation was very similar to the situation in which fresh human plasma spiked with 1.5 mmol/L of $CaCl_2$ (4.2 mmol/L total calcium) and ceftriaxone (10 mmol/L) after incubation for 1 h at 37°C (Fig. 2, panel B). Furthermore, incubation for 2, 4, and 24 h did not yield any precipitation (data not shown). Small particles found in these negative-control experiments presumably represent cell debris or precipitated plasma proteins (Fig. 2, panel a). In order to prepare plasma precipitates of calcium-ceftriaxone needed for visual inspection, a "forced precipitation" protocol was used in which nonphysiological concentrations of calcium (20 mmol/L) and ceftriaxone (20 mmol/L) were added to fresh human plasma. Under these forced conditions, precipitates were formed, with a large number of small crystals observed within 1 h (Fig. 2, panel c), followed by a phase of crystal growth during a second hour of incubation (data not shown). From these experiments, plasma precipitates were recovered (Fig. 3) and the identity of Ca^{2+}–ceftriaxone was further analyzed by EDX analysis and FTIR spectroscopy. Very similar elemental X-ray dispersive spectra were obtained, using precipitates from water as well as precipitates isolated from human plasma that had been spiked with 20 mmol/L

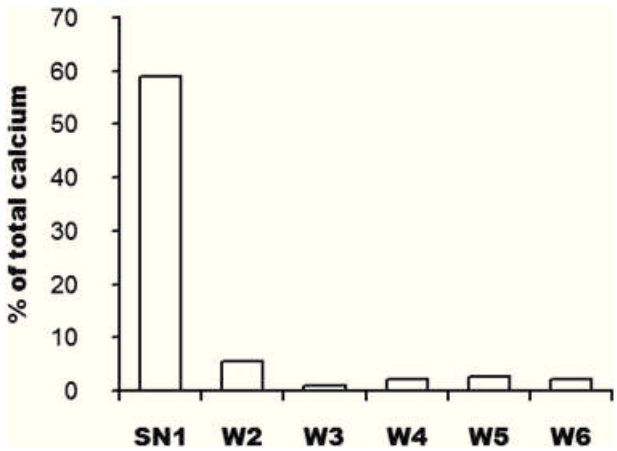

Figure 2. Efficiency of wash steps during sample preparation of plasma pellets. Human plasma (0.5 mL) was spiked with about 2.7 μmol of calcium-ceftriaxone. Plasma pellets containing insoluble calcium-ceftriaxone were collected after repeated centrifugation and wash steps. SN1, plasma supernatant recovered after the first centrifugation step. Measured Ca^{2+} represents endogenous calcium and calcium derived from dissolved calcium-ceftriaxone. W2 to W6, analysis of wash solutions recovered after the indicated centrifugation step.

 DOI 10.1002/jps

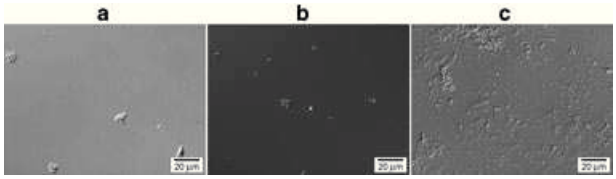

Figure 3. Visual inspection of plasma precipitates from fresh human plasma. Negative controls (panel a) or plasma spiked with 1.5 mmol/L $CaCl_2$ and 10 mmol/L ceftriaxone (panel b) or plasma spiked with 20 mmol/L $CaCl_2$ and 20 mmol/L ceftriaxone (representing conditions of forced precipitation, panel c). Samples were incubated for 1 h at 37°C. Small particles found in these negative control experiments represent presumably cell debris or precipitated plasma proteins.

$CaCl_2$ and 20 mmol/L ceftriaxone (representing conditions of forced precipitation) (Fig. 4). The spectra of FTIR spectroscopy of dried plasma precipitates were similar to the ceftriaxone reference spectra provided by Roche (Fig. 5).

DISCUSSION

Several analytical procedures were evaluated in order to identify a robust and reliable method for the quantitative analysis of Ca^{2+}, both in plasma supernatants and plasma precipitates. Inductively coupled–plasma mass spectrometry was initially tested, but without success: ^{40}Ar, which is used as plasma gas, has the same molecular weight as ^{40}Ca. Therefore, less abundant isotopes such as ^{43}Ca have to be used for the quantitative determination of calcium, with a very low sensitivity of this method. Tests with graphite furnace atomic absorption spectroscopy (GF-AAS) resulted in a linear response of the instrument with respect to calcium in a range of 0.4–8 μg/L, with a detection limit in the range of 0.1–0.5 μg/L. A problem associated with this very high sensitivity is interference of contaminating Ca^{2+}. Because calcium is ubiquitous, this effect can hardly be controlled, and would interfere with the analysis of samples that have to be diluted by a factor of approximately 1000 to 10,000 to obtain calcium concentrations in the expected range of the experiments. As a consequence, a less sensitive method for the detection of calcium was evaluated (F-AAS). Tests resulted in a 100 times less sensitive method than GF-AAS, and in a suitable range of quantification for total calcium in plasma supernatants and precipitates.

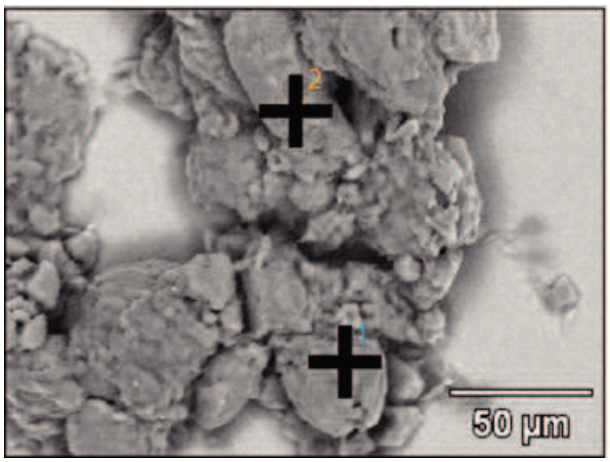

Figure 4. Inspection by scanning electron microscopy of plasma precipitates. Samples were obtained from fresh human plasma spiked with 20 mmol/L $CaCl_2$ and 20 mmol/L ceftriaxone (representing conditions of forced precipitation). Positions used for energy-dispersive X-ray analysis (Fig. 5) are labeled by a black cross. Accelerating voltage: 20.0 kV; magnification, 1480×.

Analytical procedures for quantitative analysis of Ca^{2+} in plasma precipitates were evaluated. After centrifugation of plasma samples, the supernatant was separated by decanting from the pellet. The pellets remained contaminated with adherent supernatant. Therefore, recovered plasma pellets were washed with a small volume of 0.5 mL H_2O (ice-cold water) to remove residual supernatant without dissolving Ca^{2+}–ceftriaxone. After one washing step, the content of contaminating calcium was reduced to a minimum. Further washing is not recommended because with every additional wash cycle, an amount of approximately 0.2 mmol/L Ca^{2+}–ceftriaxone is dissolved and lost (Fig. 6).

On the basis of these results, it can be stated that a validated analytical procedure could be established. This method was used subsequently for the quantitative determination of ceftriaxone and Ca^{2+} in human plasma and human plasma precipitates.

Using a HPLC-based analytical method, ceftriaxone-containing plasma supernatants and pellets were analyzed. Validation of the method demonstrated a high recovery and a linear response covering a concentration range from 0.5 to 500 μmol/L.

Formation of calcium–ceftriaxone precipitates was studied in human plasma, with a total concentration of 4.2 mmol/L calcium, which is well above physiological limits.[31,32] Ceftriaxone concentrations tested started at 0.63 mmol/L, which reflects the maximum amount that has been measured in a clinical study,[6] and increased to a level of 10.05 mmol/L.

To simulate *in vivo* conditions, we used fresh, pooled, and noncentrifuged human plasma. Without precentrifugation, we expected to preserve crystal nuclei needed to initiate possible plasma precipitation. As a consequence, a small amount of particulate materials (i.e., cell debris and protein aggregates) was recovered in plasma in all experiments, including negative controls (Fig. 2a).

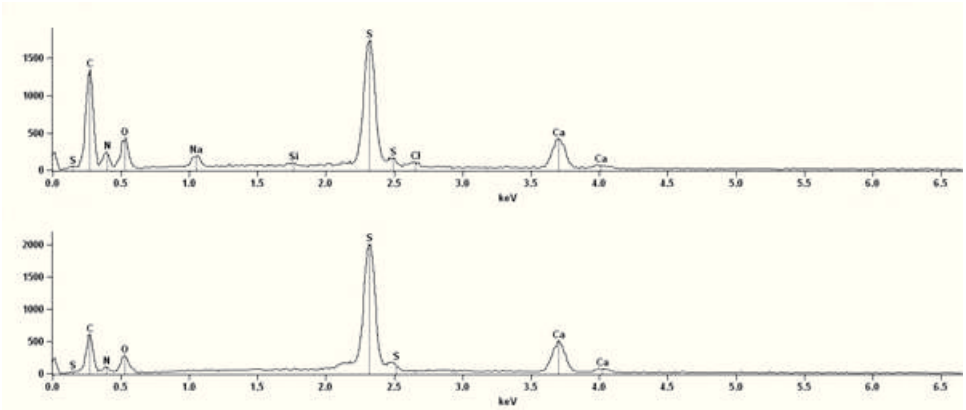

Figure 5. Determination of elemental composition of Ca^{2+}–ceftriaxone. Samples were obtained by precipitation in water (upper panel) and plasma precipitates of Ca^{2+}–ceftriaxone (lower panel) by energy-dispersive X-ray analysis. The used plasma precipitate (Fig. 4) was obtained from fresh human plasma spiked with 20 mmol/L $CaCl_2$ and 20 mmol/L ceftriaxone (representing conditions of forced precipitation).

In experiments in which plasma was spiked with 4.2 mmol/L calcium and varying concentrations of ceftriaxone, a mean of 2.72% calcium and 0.25% ceftriaxone was recovered in the plasma pellet after centrifugation. This is considered to represent a small amount of adherent supernatant solution that was not fully removed by the washing procedures. This percentage was independent from the ceftriaxone concentrations tested and therefore did not reflect calcium–ceftriaxone precipitates. Consequently, approximately 100% of the analytes were recovered from the supernatants. It should be noted that for ceftriaxone, a trend toward a higher recovery from plasma supernatants was observed with increasing ceftriaxone concentrations (Tables 1 and 2). An analytical artifact (e.g., degradation during storage of samples in the HPLC autosampler prior to analytics) can be excluded because the effect was also visible if the order of experiments was reversed. A likely explanation for the effect could be protein binding. It has been described by Brodersen and Robertson[33] that a second molecule of ceftriaxone is bound weakly to albumin. Thus, a disproportionately low amount of ceftriaxone would be bound to plasma proteins at higher concentrations.

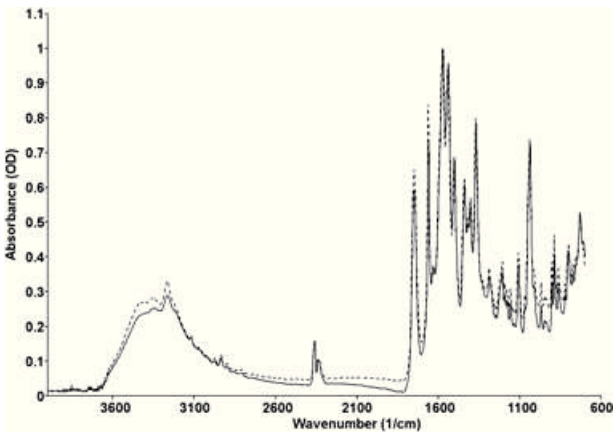

Figure 6. Fourier transform infrared spectroscopy spectra of dried human plasma precipitates (dashed line) obtained by forced precipitation of Ca^{2+}–ceftriaxone in plasma. For comparison, a reference spectrum of Ca^{2+}–ceftriaxone in water is superimposed (continuous line).

In addition to the quantitative assays, we confirmed the absence of calcium–ceftriaxone precipitates under the maximum tested concentrations of 10 mmol/L ceftriaxone and 4.2 mmol/L total calcium with a light microscope (1 h incubation at 37°C Fig. 2b). Small particles could be attributed to cell debris or precipitated plasma proteins, which were also seen in control samples containing only fresh human plasma (Fig. 2a). Even after 24 h, no precipitates were visible. These results confirm our observation that at the tested concentrations of ceftriaxone and calcium, no relevant precipitation occurs in fresh, pooled, and noncentrifuged human plasma.

In a set of additional control experiments, formation of calcium–ceftriaxone precipitates was induced using very high (nonphysiological) concentrations of both ceftriaxone and calcium (20 mmol/L each). However, the first signs of precipitations were apparent only after 1 h of incubation (Fig. 2c). The identity of the precipitated material was confirmed to be calcium-ceftriaxone using SEM (Fig. 3) and EDX analysis (Fig. 4). EDX analysis resulted in very similar elemental spectra compared with samples obtained from calcium–ceftriaxone precipitations in water and revealed the presence of elemental sulfur and calcium in both samples (Fig. 4). Thus, human plasma precipitates generated under conditions of forced precipitation were confirmed to contain Ca^{2+}–ceftriaxone. The

identity of Ca^{2+}–ceftriaxone recovered from plasma precipitates, under conditions of forced precipitation, was further confirmed by FTIR spectroscopy. Again, IR spectra of dried plasma precipitates were similar to the ceftriaxone reference spectra (Fig. 5).

Our results are in line with the following statements:

First, no calcium–ceftriaxone precipitates were detected in fresh human plasma at concentrations of calcium up to 4.2 mmol/L and ceftriaxone up to 10 mmol/L.

Second, formation of plasma precipitates could be induced under conditions of forced precipitation (20 mmol/L each).

Third, the identity of calcium–ceftriaxone precipitates, prepared under forced conditions, was confirmed qualitatively by microscopy and spectroscopy methods.

The question arises, how these results can be interpreted in the context of the clinical use of ceftriaxone.

On the basis of our results, the concentration of 10 mmol/L ceftriaxone in plasma from adults does not form precipitates in the presence of 4.2 mmol/L calcium. Thus, an apparent kinetic solubility product constant of greater than 0.42×10^{-4} $(mol/L)^2$ can be calculated. This value is around 26 times higher than the thermodynamic solubility product in water determined by Shiffman et al.[4]

This difference can be attributed to following factors:

First, the presence of a supersaturated solution, which exceeds the solubility product constant by a factor of 10, has also been described in water and bile by Shiffman et al.[4] This state was described as "metastable" by Shiffmann et al.[4] and showed no visible or microscopic precipitates, even after 24 h. Even when calcium–ceftriaxone precipitates in an aqueous solution, the formation is rather slow. Using a light obscuration particle counter, Nakai et al.[23] demonstrated that the formation of precipitates from a supersaturated solution is time dependent. Depending on the concentration and temperature, the formation of microparticles did not occur for several hours. Even after mixing 18 mmol/L ceftriaxone with 2.5 mmol/L calcium, no immediate precipitates were visible. On the basis of the clinical reports, supersaturation is apparently exceeded in the excreting organs, the liver and kidneys, where the nonmetabolized drug is excreted. Compared with blood plasma, up to 10-fold higher concentrations of ceftriaxone are obtained in urine,[20] whereas the concentration in bile even exceeds the urinary levels several fold.[34] Calcium concentrations in urine are also several fold augmented, compared with blood plasma, and depend on the calcium uptake.[19,35] The free Ca^{2+} concentration in bile is normally in the same range as in plasma, in contrast to total calcium concentration, which is increased.[36–38] However, as a result of the high ceftriaxone concentration in the bile, free calcium passively enters the canalicular bile and further increases the concentration of the supersaturated solution.[39] Formation of calcium–ceftriaxone precipitates is further favored through the concentrating function of the gallbladder,[16,40] especially during overnight fasting. Taking into account these higher concentrations of ceftriaxone and calcium, and the stasis in the urinary bladder as well as in the gallbladder, it is comprehensible why renal and biliary lithiasis emerges.[18,41–45] Therefore, biliary precipitation and nephrolithiasis limit the C_{max} that can be achieved *in vivo*.

Second, the process of precipitation can also be modified by interfering plasma proteins. Similar effects have been described for the formation of cholesterol gallstone in the gallbladder, where biliary proteins inhibit crystallization and stabilize a supersaturated state of cholesterol in bile, or induce precipitation.[46–48] For supersaturated drug delivery systems, Brouwers et al.[49] mentioned different mechanisms of precipitation inhibition, which can also be applied to our situation, especially when plasma proteins possibly influence the process of nucleation and crystal growth.

Third, differences in solubility between blood plasma, compared with water, were shown for several other drugs and were attributed to protein binding.[50,51] Ceftriaxone is reversibly bound to albumin in plasma, and only the free fraction can contribute to the process of initial salification. The fraction of free drug is dependent on several factors including ceftriaxone concentration that can vary between 5% and greater than 35%.[52,53] The free fraction of endogenous calcium in plasma is in the range of 1.1 to 1.4 mmol/L. This amount represents approximately 50% of the total calcium concentration in plasma, which is in the range of 2.65 mmol/L.[31,32] Our apparent kinetic solubility product constant in human plasma is a hypothetical value calculated using total (i.e., free and bound) plasma concentrations. One could argue that this constant should be calculated using free concentrations only. In the latter case, the apparent kinetic solubility product constant in plasma would decrease by approximately one order of magnitude.

Taking all the above-mentioned factors, such as supersaturation, crystal growth, and protein binding together, we have a good explanation why our apparent kinetic solubility product constant in plasma differs from the reported thermodynamic solubility product in water by Shiffman et al.[4]

The question arises, whether or not push injections of 0.5 and 1 g ceftriaxone, which are available in many countries in Europe for more than 20 years, can lead to precipitate formation before the drug has been distributed in the body. To define upper critical doses

of ceftriaxone, kinetic factors such as hydrodynamic parameters (e.g. blood flow rate at the injection site), injection rate, and *in situ* crystal growth rate have to be known.[54,55] Portmann and Simmons[50] showed for several other drugs that no crystals or oily droplets are formed in plasma at critical concentrations in an *in vitro* dynamic injection system due to a rapid dilution effect. Therefore, we expect to observe precipitation rather in more static environment than in a dynamic injection system.

Although we cannot make precise assumption on the basis of our data about the hydrodynamic behavior during push injections, there have been no fatal cases reported in adults in the context of intravascular precipitation. The lack of reports of such fatal incidents in adults, including widespread use of bolus injections, has been mentioned several times.[24] Taking all that is known of ceftriaxone from both nonclinical and clinical sources, combined with its favorable tolerability profile over the last 2.5 decades,[2] it is very unlikely that relevant calcium–ceftriaxone precipitation occurs in human adults, even after a push injection.

Because the combination of calcium and ceftriaxone is contraindicated in neonates, we used in the present study blood plasma from adults only. Care should be taken to extrapolate from our results to the situation in neonates: the affinity of ceftriaxone to albumin is remarkably lower in newborns than in adults.[33] Furthermore, bilirubin competes with ceftriaxone to the binding site of albumin and thereby influences the free fraction of the drug in neonates.[33]

Next to this theoretical point of view, the question remains why these fatal adverse drug events with the precipitation of ceftriaxone occurred only in neonates. If we take a closer look at the data, it turns out that one case was reported twice, and another lethal case was assigned to pneumonia and sepsis with disseminated intravascular coagulation in an autopsy.[14] In two cases, the causality of the calcium–ceftriaxone interaction was questionable because either no precipitates were found in the autopsy[14,15] or the patient responded well to adrenaline after a bradycardia,[56] which is unlikely to have an effect on potential calcium–ceftriaxone precipitates. Of the remaining five cases, four used either a Y-set or the same line to coadminister calcium-containing fluids. In the fifth case, the route of administration is unknown.[14] It should be noted that in these cases, ceftriaxone was not administered according to the product label, which states that ceftriaxone must not be administered simultaneously with calcium-containing i.v. solutions, including continuous calcium-containing infusions such as parenteral nutrition via a Y-site. Although ceftriaxone seems to be compatible with some parenteral nutrition for adults, even with higher calcium concentrations,[57] precipitates are formed in parenteral nutrition for neonates.[25,58] This observation can be explained by a higher amount of calcium in parenteral nutrition of neonates,[58] and may be related to the fact that no fatal cases of calcium–ceftriaxone interactions in adults have been reported. There may have been some administration errors in the past decades in adults as well, but in contrast to newborns, review of cumulative data did not suggest clinically relevant consequences. In either case, coadministration by mixing these two solutions must be prevented under all circumstances.[20] The lack of evidence of plasma precipitation between ceftriaxone and calcium in adults was recently supported by Steadman et al.,[24] by comparing adverse event reports of calcium combined with ceftriaxone or ceftazidime, another well-known third-generation cephalosporin. Furthermore, a recent cohort study by Dalton et al.[59] showed no difference in adverse outcomes and mortality in high-risk patients receiving high concentrations of calcium chloride.

The greatest risk in neonates is probably hyperbilirubinemia because of the competition between ceftriaxone and bilirubin for albumin.[33] Free bilirubin can pass the blood–brain barrier and can cause kernicterus, which is associated with neurological impairment or death. In addition to the age-dependent levels of bilirubin increased in neonates, there are also different opinions about the critical values of bilirubin in the blood.[15,60–62] Therefore, switching from ceftriaxone to safer alternatives in neonates is reasonable, especially because the risk of calcium–ceftriaxone precipitation in neonates is not clearly determined. This point of view supports information in the product label advising that the use of ceftriaxone with calcium-containing i.v. solutions in neonates must be avoided because of the risk of precipitation of ceftriaxone and calcium.[20]

CONCLUSION

With the presented data, we conclude that ceftriaxone concentration up to 10 mmol/L combined with 4.2 mmol/L total calcium in fresh adult plasma results in no precipitation. The lack of evidence for such precipitation supports our conclusion. Therefore, we can state that the use of ceftriaxone in adults is a low risk, even at higher i.v. calcium concentrations.

This conclusion cannot be applied to patients at extremes of age, and especially not to neonates because we used fresh human plasma from adults.

On the basis of our data, we cannot draw conclusions about the safety of ceftriaxone push injections. However, owing to the slow formation of precipitates, even at forced conditions, as well as the lack of evidence from nonclinical evaluations or clinical reports in adults over the past 2 decades, no incidents would be expected.

Our *in vitro* method to quantify the precipitates of ceftriaxone in human plasma can be used for further studies. With EDX analysis, and especially with FTIR spectroscopy, we provide two methods to verify the presence of calcium–ceftriaxone precipitates in human plasma samples. This technique can help in clinical incidents to verify the presence of calcium-ceftriaxone, in which precipitated material is found in an autopsy. In this way, other possible causes can be excluded, especially when multiple medications have been used, which are known to interact physically.

ACKNOWLEDGMENTS

The present study received financial support by F. Hoffmann-La Roche Ltd. Pascal Detampel was supported by the Senglet-Foundation. We thank Dr. G. Gross and Dr. R. Wyss from F. Hoffmann-La Roche Ltd. for helpful discussions and for proofreading of the manuscript.

REFERENCES

1. Perry TR, Schentag JJ. 2001. Clinical use of ceftriaxone: A pharmacokinetic–pharmacodynamic perspective on the impact of minimum inhibitory concentration and serum protein binding. Clin Pharmacokinet 40:685–694.
2. Lamb HM, Ormrod D, Scott LJ, Figgitt DP. 2002. Ceftriaxone: An update of its use in the management of community-acquired and nosocomial infections. Drugs 62:1041–1089.
3. The Merck Index. 2001. Merck index. 13th ed. Rahway, New Jersey: Merck Research Laboratories.
4. Shiffman ML, Keith FB, Moore EW. 1990. Pathogenesis of ceftriaxone-associated biliary sludge. In vitro studies of calcium–ceftriaxone binding and solubility. Gastroenterology 99:1772–1778.
5. Joynt GM, Lipman J, Gomersall CD, Young RJ, Wong EL, Gin T. 2001. The pharmacokinetics of once-daily dosing of ceftriaxone in critically ill patients. J Antimicrob Chemother 47:421–429.
6. Pollock AA, Tee PE, Patel IH, Spicehandler J, Simberkoff MS, Rahal JJ. 1982. Pharmacokinetic characteristics of intravenous ceftriaxone in normal adults. Antimicrob Agents Chemother 22:816–823.
7. Findlay CD, Brown RM, Allcock JE, Lowe PA, Wise R. 1982. A study of the relationship between dose and pharmacokinetics of ceftriaxone. J Antimicrob Chemother 9:57–62.
8. Hayton WL, Stoeckel K. 1986. Age-associated changes in ceftriaxone pharmacokinetics. Clin Pharmacokinet 11:76–86.
9. Martin E, Koup JR, Paravicini U, Stoeckel K. 1984. Pharmacokinetics of ceftriaxone in neonates and infants with meningitis. J Pediatr 105:475–481.
10. Patel IH, Kaplan SA. 1984. Pharmacokinetic profile of ceftriaxone in man. Am J Med 77:17–25.
11. McCracken GH, Siegel JD, Threlkeld N, Thomas M. 1983. Ceftriaxone pharmacokinetics in newborn infants. Antimicrob Agents Chemother 23:341–343.
12. Schaad UB, Hayton WL, Stoeckel K. 1985. Single-dose ceftriaxone kinetics in the newborn. Clin Pharmacol Ther 37:522–528.
13. Schaad UB, Stoeckel K. 1982. Single-dose pharmacokinetics of ceftriaxone in infants and young children. Antimicrob Agents Chemother 21:248–253.
14. Bradley JS, Wassel RT, Lee L, Nambiar S. 2009. Intravenous ceftriaxone and calcium in the neonate: Assessing the risk for cardiopulmonary adverse events. Pediatrics 123:e609–e613.
15. Monte SV, Prescott WA, Johnson KK, Kuhman L, Paladino JA. 2008. Safety of ceftriaxone sodium at extremes of age. Expert Opin Drug Saf 7:515–523.
16. Purdum PP, Shiffman ML, Moore EW. 1992. In vivo studies of biliary ceftriaxone excretion and solubility in guinea pig hepatic bile. J Lab Clin Med 120:604–613.
17. Park HZ, Lee SP, Schy AL. 1991. Ceftriaxone-associated gallbladder sludge. Identification of calcium–ceftriaxone salt as a major component of gallbladder precipitate. Gastroenterology 100:1665–1670.
18. Avci Z, Koktener A, Uras N, Catal F, Karadag A, Tekin O, Degirmencioglu H, Baskin E. 2004. Nephrolithiasis associated with ceftriaxone therapy: A prospective study in 51 children. Arch Dis Child 89:1069–1072.
19. Nordin BE. 1990. Calcium homeostasis. Clin Biochem 23:3–10.
20. Roche Pharmaceuticals. 2010. Rocephin [Package Insert]. Available from: http://www.gene.com/gene/products/information/rocephin/pdf/pi.pdf. Accessed Date: January 5, 2011.
21. Granich GG, Krogstad DJ. 1987. Ion pair high-performance liquid chromatographic assay for ceftriaxone. Antimicrob Agents Chemother 31:385–388.
22. Trautmann KH, Haefelfinger P. 1981. Determination of the cephalosporin Ro 13-9904 in plasma, urine, and bile by means of ion-pair reversed phase chromatography. J High Resolut Chromatogr 4:54–59.
23. Nakai Y, Tokuyama E, Yoshida M, Uchida T. 2009. Incompatibility of ceftriaxone sodium with calcium-containing products. Yakugaku Zasshi 129:1385–1392.
24. Steadman E, Raisch DW, Bennett CL, Esterly JS, Becker T, Postelnick M, McKoy JM, Trifilio S, Yarnold PR, Scheetz MH. 2010. Evaluation of a potential clinical interaction between ceftriaxone and calcium. Antimicrob Agents Chemother 54:1534–1540.
25. Puzovic M, Hardy G. 2008. Comment: Clinical pharmaceutics and calcium ceftriaxone. Ann Pharmacother 42:1914.
26. Nakai Y, Tokuyama E, Yoshida M, Uchida T. 2010. Prediction of incompatibility of ceftriaxone sodium with calcium ions using the ionic product. Yakugaku Zasshi 130:95–102.
27. Parker RI. 2010. Thrombosis in the pediatric population. Crit Care Med 38:S71–S75.
28. Rapp RP, Kuhn R. 2007. Clinical pharmaceutics and calcium ceftriaxone. Ann Pharmacother 41:2072.
29. Gin AS, Wheaton H, Dalton B. 2008. Clinical pharmaceutics and calcium-ceftriaxone. Ann Pharmacother 42:450–451.
30. ICH Expert Working Group. 2005. ICH harmonised tripartite guideline; Validation of analytical procedures: Text and methodology Q2(R1). Available from: http://www.ich.org/fileadmin/Public_Web_Site/ICH_Products/Guidelines/Quality/Q2_R1/Step4/Q2_R1__Guideline.pdf. Accessed Date: January 5, 2011.
31. Burritt MF, Slockbower JM, Forsman RW, Offord KP, Bergstralh EJ, Smithson WA. 1990. Pediatric reference intervals for 19 biologic variables in healthy children. Mayo Clin Proc 65:329–336.
32. Sitzmann FC. 1976. Normalwerte. München, Germany: Hans Marseille Verlag.
33. Brodersen R, Robertson A. 1989. Ceftriaxone binding to human serum albumin: Competition with bilirubin. Mol Pharmacol 36:478–483.
34. Owens NJ, Nightingale CH, Quintiliani R, Pyrtek LJ. 1987. Concentrations of ceftriaxone in gallbladder wall, bile, and

serum in patients undergoing cholecystectomy. Clin Pharm 6:967–968.
35. Thode J. 1985. The calcium ion activity and the standardized excretion rate of calcium in urine of healthy adults. Scand J Clin Lab Invest 45:327–334.
36. Shiffman ML, Sugerman HJ, Kellum JM, Moore EW. 1992. Calcium in human gallbladder bile. J Lab Clin Med 120:875–884.
37. Gleeson D, Hood KA, Murphy GM, Dowling RH. 1992. Calcium and carbonate ion concentrations in gallbladder and hepatic bile. Gastroenterology 102:1707–1716.
38. Sutor DJ, Wilkie LI, Jackson MJ. 1980. Ionised calcium in pathological human bile. J Clin Pathol 33:86–88.
39. Xia Y, Lambert KJ, Schteingart CD, GU JJ, Hofmann AF. 1990. Concentrative biliary secretion of ceftriaxone. Inhibition of lipid secretion and precipitation of calcium ceftriaxone in bile. Gastroenterology 99:454–465.
40. Wheeler HO. 1971. Concentrating function of the gallbladder. Am J Med 51:588–595.
41. Bonnet JP, Abid L, Dabhar A, Lévy A, Soulier Y, Blangy S. 2000. Early biliary pseudolithiasis during ceftriaxone therapy for acute pyelonephritis in children: A prospective study in 34 children. Eur J Pediatr Surg 10:368–371.
42. Prince JS, Senac MO. 2003. Ceftriaxone-associated nephrolithiasis and biliary pseudolithiasis in a child. Pediatr Radiol 33:648–651.
43. Schaad UB, Wedgwood-Krucko J, Tschaeppeler H. 1988. Reversible ceftriaxone-associated biliary pseudolithiasis in children. Lancet 2:1411–1413.
44. Araz N, Okan V, Demirci M, Araz M. 2007. Pseudolithiasis due to ceftriaxone treatment for meningitis in children: Report of 8 cases. Tohoku J Exp Med 211:285–290.
45. Becker CD, Fischer RA. 2009. Acute cholecystitis caused by ceftriaxone stones in an adult. Case Rep Med 2009:132452.
46. Ohya T, Schwarzendrube J, Busch N, Gresky S, Chandler K, Takabayashi A, Igimi H, Egami K, Holzbach RT. 1993. Isolation of a human biliary glycoprotein inhibitor of cholesterol crystallization. Gastroenterology 104:527–538.
47. Rege RV, Dawes LG, Moore EW. 1989. Canine common duct and gallbladder bile contain antinucleating factors that inhibit CaCO3 precipitation. J Lab Clin Med 113:642–650.
48. Moore EW. 1990. Biliary calcium and gallstone formation. Hepatology 12:206S–214S; discussion 214S–218S.
49. Brouwers J, Brewster ME, Augustijns P. 2009. Supersaturating drug delivery systems: The answer to solubility-limited oral bioavailability? J Pharm Sci 98:2549–2572.
50. Portmann GA, Simmons DM. 1995. Microscopic determination of drug solubility in plasma and calculation of injection rates with a plasma circulatory model to prevent precipitation on intravenous injection. J Pharm Biomed Anal 13:1189–1193.
51. Cox JW, Sage GP, Wynalda MA, Ulrich RG, Larson PG, Su CC. 1991. Plasma compatibility of injectables: Comparison of intravenous U-74006F, a 21-aminosteroid antioxidant, with Dilantin brand of parenteral phenytoin. J Pharm Sci 80:371–375.
52. Stoeckel K, McNamara PJ, Brandt R, Plozza-Nottebrock H, Ziegler WH. 1981. Effects of concentration-dependent plasma protein binding on ceftriaxone kinetics. Clin Pharmacol Ther 29:650–657.
53. Popick AC, Crouthamel WG, Bekersky I. 1987. Plasma protein binding of ceftriaxone. Xenobiotica 17:1139–1145.
54. Li P, Vishnuvajjala R, Tabibi SE, Yalkowsky SH. 1998. Evaluation of in vitro precipitation methods. J Pharm Sci 87:196–199.
55. Yalkowsky SH, Valvani SC, Johnson BW. 1983. In vitro method for detecting precipitation of parenteral formulations after injection. J Pharm Sci 72:1014–1017.
56. Belliard CR, Sibille G. 2007. Anaphylactoid shock or precipitation of calcium–ceftriaxone in a premature newborn. A case report. Arch Pediatr 14:199–200.
57. Trissel LA, Gilbert DL, Martinez JF, Baker MB, Walter WV, Mirtallo JM. 1997. Compatibility of parenteral nutrient solutions with selected drugs during simulated Y-site administration. Am J Health Syst Pharm 54:1295–1300.
58. Hardy G, Messing B. 2005. Beyond the bag horizon. Nutrition 21:1179–1180.
59. Dalton BR, Zuege DJ, Shahpori R, Laupland KB. 2010. Concomitant ceftriaxone and high-concentration intravenous calcium therapy in adult critical care patients: A matched cohort study. Ann Pharmacother 44:1158–1163.
60. Dennery PA, Seidman DS, Stevenson DK. 2001. Neonatal hyperbilirubinemia. N Engl J Med 344:581–590.
61. 1994. Practice parameter: Management of hyperbilirubinemia in the healthy term newborn. American Academy of Pediatrics. Provisional Committee for Quality Improvement and Subcommittee on Hyperbilirubinemia. Pediatrics 94:558–565.
62. Porter ML, Dennis BL. 2002. Hyperbilirubinemia in the term newborn. Am Fam Phys 65:599–606.

7.2. Drug interaction potential of resveratrol

Detampel P, Beck M, Krähenbühl S, Huwyler J.

Drug Metab Rev. (2012) Aug;44(3):253-65

Drug Metabolism Reviews, 2012; 44(3): 253–265
© 2012 Informa Healthcare USA, Inc.
ISSN 0360-2532 print/ISSN 1097-9883 online
DOI: 10.3109/03602532.2012.700715

informa
healthcare

REVIEW ARTICLE

Drug interaction potential of resveratrol

Pascal Detampel[1]*, Mareike Beck[2]*, Stephan Krähenbühl[3], and Jörg Huwyler[1]

[1]Division of Pharmaceutical Technology, Department of Pharmaceutical Sciences, University of Basel, Basel, Switzerland, [2]DSM Nutritional Products Ltd, NIC-RD/HN–Safety, Kaiseraugst, Switzerland, and [3]Division of Clinical Pharmacology and Toxicology, University Hospital, Basel, Switzerland

Drug Metabolism Reviews Downloaded from informahealthcare.com by 178.38.226.196 on 07/13/12
For personal use only.

Abstract

Resveratrol is a naturally occurring polyphenol that is often used as a food supplement. Many positive health effects, including cardio protection, tumor suppression, and immune modulation, are associated with the intake of resveratrol. Resveratrol is well tolerated in healthy subjects without any comedication. However, supplemental doses of resveratrol in the range of 1 g/day or above by far exceed the natural intake through food. Whether resveratrol-drug interactions can be harmful in patients taking additional medications remains unknown. Recent *in vivo* studies and clinical trials indicate a possible drug-drug interaction potential using high-dosage formulations. In this review, the known *in vitro* and *in vivo* effects of resveratrol on various cytochrome P450 (CYP) isoenzymes are summarized. They are discussed in relation to clinically relevant plasma concentrations in humans. We conclude that resveratrol may lead to interactions with various CYPs, especially when taken in high doses. Aside from systemic CYP inhibition, intestinal interactions must also be considered. They can potentially lead to reduced first-pass metabolism, resulting in higher systemic exposure to certain coadministrated CYP substrates. Therefore, patients who ingest high doses of this food supplement combined with additional medications may be at risk of experiencing clinically relevant drug-drug interactions.

Keywords: Resveratrol, drug-drug interactions, drug metabolism, cytochrome P450

Copyright © 2012 Informa Healthcare
Not for Sale or Commercial Distribution
Unauthorized reproduction prohibited. Authorized users may print a single copy for personal use only.

Introduction

Resveratrol (*trans*-3,4′,5-trihydroxystilbene) (Figure 1; Table 1) is a natural polyphenol found in grape skin and red wine. It is believed to contribute to the so-called "French paradox," which is based on the observation that the French population has a low incidence of cardiovascular diseases while consuming a diet that is relatively high in fat (Kopp, 1998). Next to its potential cardioprotective effects, additional health benefits have been ascribed to resveratrol (Jang et al., 1997). Most recently, for instance, it has been demonstrated that resveratrol mimics calorie-restriction effects in obese humans (Timmers et al., 2011). These positive effects are brought about by a variety of molecular mechanisms that have been reviewed elsewhere (Vang et al., 2011; Yu et al., 2011). With respect to the cancer-preventive activity of resveratrol, a reduction in the exposure of cells to carcinogens was proposed, resulting from its inhibition of various cytochrome P450 metabolic enzymes (CYPs). In addition, resveratrol was proposed to block the transcription of various CYPs through antagonism of the nuclear aryl hydrocarbon receptor (AHR). These mechanisms are expected to reduce the cellular load of chemically reactive—and therefore potentially toxic—drug metabolites.

On the other hand, inhibition of CYP activity by resveratrol could lead to safety problems by altering the pharmacokinetics (i.e., absorption and disposition) of coadministered drugs. Biotransformation of xenobiotics is catalyzed by a broad array of metabolizing enzymes. One of the most important metabolic enzyme systems involved in drug metabolism is the CYP superfamily of mixed function oxidases, which are responsible for phase I oxidative metabolism of many compounds (Table 2). These enzymes contain a common catalytic center, but a different three-dimensional structure at each active site, which conveys substrate specificity to individual enzymes. Among the

*These authors contributed equally to the present work.

Address for Correspondence: Prof. Dr. Jörg Huwyler, Division of Pharmaceutical Technology, Department of Pharmaceutical Sciences, University of Basel, Klingelbergstrasse 50, CH-4056 Basel, Switzerland; Fax: +41 61 267 15 16; E-mail: joerg.huwyler@unibas.ch

(Received 13 March 2012; revised 21 May 2012; accepted 04 June 2012)

various CYP isozymes identified to date, hepatic CYP1A2, 2C9, 2C19, 2D6, 2E1, and 3A4 are the most important isoforms in human drug metabolism. Drug-drug interactions (as well as food-drug or nutrient-drug interactions) with these CYP isoenzymes can have a strong effect on drug concentrations in plasma or tissue and may therefore result in serious toxic side effects. For example, coadministration of CYP3A4 inhibitors with terfenadine, cisapride, or astemizole can lead to QT prolongation and life-threatening ventricular tachycardia (Zhou et al., 2005). Consequently, studies on drug-drug interactions are a key aspect of drug development. By the same token, enzyme induction may lead to the accelerated elimination of a drug and therefore might reduce its efficacy.

Although resveratrol is only one of several polyphenols found in grapes, the topic of potential resveratrol-drug interactions is of great interest, because an increasing variety of resveratrol food supplements is commercially available to the public. Dosages used cover a range of 50 mg up to 2 g/day (Williams et al., 2009), which greatly exceeds the amounts of resveratrol taken up from natural sources. Though typical food-supplement servings contain 20–200 mg of resveratrol, higher doses (≥500 mg) are currently under investigation for pharmacological uses. Other possible drug interactions with polyphenols, such as catechines from green tea, have also been reviewed recently (Yang and Pan, 2012).

The aim of the present review is to summarize published information on resveratrol in consideration of potential interactions with different medications. Special emphasis is placed on the modulation of activity and the expression levels of drug-metabolizing enzymes, such as CYP enzymes.

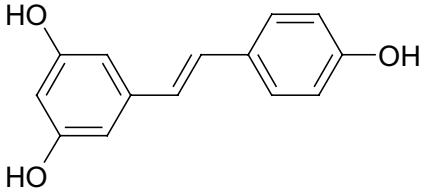

Figure 1. Chemical structure of resveratrol.

Table 1. Basic chemical data for resveratrol.

Name and synonyms	*trans*-Resveratrol
	5-[(1E)-2-(4-hydroxyphenyl) ethenyl]-1,3-benzenediol
	3,5,4′-trihydroxystilbene
	3,4′,5-stilbenetriol
	(E)-5-(p-hydroxystyryl)resorcinol
CAS Registry Number	501–36–0
Chemical formula	$C_{14}H_{12}O_3$
Molecular weight (g/mol)	228.24
logP (octanol/water)[a]	3.1
pKa[a]	9.14

[a]Calculated using Advanced Chemistry Development Software V11.02 (ACD/Labs, Toronto, Canada).

Interaction of wine, as a naturally occurring resveratrol source, with CYP

Resveratrol is synthesized in grape skin and seed in response to plant stress, injury, (fungal) infection, and ultraviolet radiation. Naturally occurring amounts of resveratrol found in grapes are in the range of 5–7 mg/kg of grape skin and 1 mg/kg of grape seeds. As the amount of resveratrol in grape products (e.g., juice, white wine, rosé, and red wine) depends on numerous factors, such as the vine cultivar, geographic origin, intensity of fungal infection, and enological practices (i.e., skin maceration time, storage, and so on), high variability is observed. Though the resveratrol content in white wine is usually below 0.1 mg/L, red wine contains an average of 1.9 ± 1.7 mg/L (8.3 ± 7.4 μM) *trans*-resveratrol, ranging from nondetectable levels to 14.3 mg/L (62.7 μM). *Cis*-resveratrol content in red wine is usually lower (1.0 ± 0.9 mg/L; range, 0.0–5.1 mg/L). The average level of *trans*-resveratrol-glucoside (*trans*-piceid) in red wine is 5.4 ± 4.8 mg/L and may be as much as 29.2 mg/L. The

Table 2. Summary of selected CYP enzymes.

CYP isoform	Species	Comment	Reference
CYP1A1	Human, mouse, rat	Extrahepatic	(Ingelman-Sundberg, 2004) (Mugford and Kedderis, 1998)
CYP1A2	Human, mouse, rat	Liver	(Ingelman-Sundberg, 2004) (Mugford and Kedderis, 1998)
CYP1B1	Human	Extrahepatic	(Ingelman-Sundberg, 2004)
CYP2B1/2	Mouse, rat	Liver, substrate specificity between species	(Ingelman-Sundberg, 2004) (Martignoni et al., 2006)
CYP2B6	Human	Human homolog to rodent CYP2B1/2	(Ingelman-Sundberg, 2004) (Martignoni et al., 2006)
CYP2C9	Human	Liver; polymorphic,10% of drugs metabolized	(Ingelman-Sundberg, 2004) (Zhou et al., 2009)
CYP2C19	Human	Liver; polymorphic	(Ingelman-Sundberg, 2004) (Zhou et al., 2009)
CYP2D6	Human	Liver; polymorphic, 30% of drugs metabolized	(Ingelman-Sundberg, 2004) (Zhou et al., 2009)
CYP2E1	Human, mouse, rat	Liver	(Ingelman-Sundberg, 2004) (Mugford and Kedderis, 1998)
CYP3A4	Human	Liver, intestine; 50% of drugs metabolized	(Ingelman-Sundberg, 2004) (Zhou et al., 2009)
CYP3A	Rat	Homolog to human CYP3A4, substrate similarity highest between male rat and human	(Ingelman-Sundberg, 2004) (Bogaards et al., 2000)

Drug Metabolism Reviews Downloaded from informahealthcare.com by 178.38.226.196 on 07/13/12
For personal use only.

respective *cis*-piceid content is 1.4 ± 2.4 mg/L (Stervbo et al., 2007).

CYP interactions with white and red wine have been addressed in several *in vitro* studies, mostly using reconstituted wine "solids" (i.e., nonvolatile compounds). These are prepared by evaporating a certain volume of wine to dryness, followed by a reconstitution with as many volumes of buffer as necessary to result in the desired "natural strength." In one study, red wine solids (RWS) were reported to potently inhibit CYP3A4 activity *in vitro* in a concentration-dependent manner. At 8% of natural strength, enzyme activity was inhibited by approximately 85%, whereas white wine solids (WWS) did not appreciably inhibit CYP3A4 activity (Chan et al., 1998). Inhibition by RWS was found to be primarily reversible in nature in this study. In contrast, RWS inhibition of CYP3A4 in human liver microsomes was categorized as irreversible in a later study (Piver et al., 2001). The observed inhibition was nicotinamide adenine dinucleotide phosphate (NADPH)-dependent and could not be reversed by dilution, suggesting an irreversible, mechanism-based inactivation. The half-maximal inhibitory concentration (IC_{50}) was reported to be at 8 and 9% of natural strength for human liver CYP3A4 and heterologously expressed CYP3A4, respectively. Further, RWS strongly inhibited CYP1A1/2 in human liver microsomes (IC_{50} at approximately 3% natural strength) and heterologously expressed CYP1A1 and 1A2, with IC_{50} values of 1 and 0.3% of natural strength, respectively (Piver et al., 2001). Inhibition of CYP2E1 in human liver microsomes by RWS was noncompetitive and reversible, with an IC_{50} of 3% natural strength (Piver et al., 2001).

It should be noted that studies carried out with RWS are often controversial. For example, red wine caused a 50% increase in apparent clearance after oral ingestion of the immunosuppressant, cyclosporine, a known CYP3A4 substrate. The significant decrease in cyclosporine exposure was the result of reduced absorption (Tsunoda et al., 2001). In this case, the mechanism of CYP-related resveratrol-cyclosporine interaction is doubtful, because cyclosporine requires a special drug formulation for optimal intestinal absorption. Moreover, the solubility of cyclosporine in red wine appears to be lower than in water, which could also explain a lower oral absorption. In other reports, the discrepancy between studies was attributed to the different origins of red wine, leading to different resveratrol content in RWS. It is assumed, without further analytical confirmation, that resveratrol amounts correspond to approximately 0.6–0.8 μM in RWS at 8% natural strength. An additional complicating factor is the complex chemical composition of RWS, containing various other polyphenols and secondary metabolites. Because resveratrol content does not correlate with CYP inhibition, several groups consider that resveratrol is not the main CYP inhibitor present in red wine (Chan and Delucchi, 2000; Piver et al., 2001, 2003).

In contrast to the monomer, the role of naturally occurring oligomers of resveratrol has hardly been explored because of their complex structure. With new approaches to the synthesis of these compounds (Snyder et al., 2011), we will probably hear more of their biological properties in the near future. Further, some resveratrol derivatives have shown higher activity with respect to several targets in *in vitro* test systems, as well as higher systemic bioavailability in rats (Kondratyuk et al., 2011).

Interaction of resveratrol with specific CYP isoenzymes

CYP3A4

Resveratrol has been reported to inhibit the activity of CYP3A4 *in vitro* and *in vivo*. High intakes of resveratrol could theoretically increase bioavailability and the risk of toxicity of drugs that undergo extensive first-pass metabolism by CYP3A4. Drugs known to be metabolized by CYP3A4 with a high intestinal and/or hepatic extraction include—but are not limited to—3-hydroxy-3-methylglutaryl-coenzyme A reductase inhibitors (e.g., atorvastatin, lovastatin, and simvastatin), calcium-channel antagonists (e.g., felodipine, nicardipine, nifedipin, nisoldipin, nitrendipin, nimodipine, and verampamil), antiarrhythmic agents (e.g., amiodarone), human immunodeficiency virus protease inhibitors (e.g., saquinivir), immunosuppressants (e.g., cyclosporine and tacrolimus), antihistamines (e.g., terfenadine), benzodiazepines (e.g., midazolam and triazolam), and drugs used to treat erectile dysfunction (e.g., sildenafil) (Delcò et al., 2005).

In a clinical trial performed by Chow et al., an increased area under the plasma-concentration versus time curve (AUC) by a factor of 1.33 was found for buspirone after administrating 1 g of resveratrol per day for 4 weeks (Chow et al., 2010). For the CYP3A4 substrate nicardipine, which has a low bioavailability, it was shown, in male rats, that resveratrol at 10 mg/kg body weight (b.w.) increased the AUC and maximum concentration (C_{max}) by a factor of 2.3 and 2.2, respectively (Choi et al., 2009). Less-dominant effects were observed in an analogous experiment using diltiazem as a CYP3A4 substrate, resulting in an AUC and C_{max} augmented by a factor of approximately 1.6 for both values (Hong et al., 2008). Interestingly, no significant changes in AUC or C_{max} were observed after intravenous administration of nicardipine, which indicates a prominent role of the intestinal CYP3A4 and/or P-glycoprotein (Pgp).

In vitro resveratrol showed inhibition of human CYP3A4-dependent transformation of cyclosporine with an IC_{50} value of 4.5 μM (approximately 1 μg/mL) and also inhibition of 6β-hydroxylation of testosterone by CYP3A4 with an IC_{50} value of 1.4 μM. The latter CYP3A4 enzyme activity of testosterone 6β-hydroxylation was also inhibited by resveratrol-related compounds, such as piceid (IC_{50} = 31 μM), resveratroloside (IC_{50} ≥40 μM), 5,4'-dihydroxy-3-O-methoxystilbene (IC_{50} = 0.47 μM), and 5,3-dihydroxy-4'-O-methoxystilbene (IC_{50} = 0.42 μM) (Regev-Shoshani et al., 2004). Both glucosyl stilbenes were found to be weak

Drug Metabolism Reviews Downloaded from informahealthcare.com by 178.38.226.196 on 07/13/12
For personal use only.

© 2012 Informa Healthcare USA, Inc.

Drug Metabolism Reviews Downloaded from informahealthcare.com by 178.38.226.196 on 07/13/12
For personal use only.

inhibitors of CYP3A4, whereas the methoxy stilbenes had lower IC_{50} values than resveratrol, suggesting that lipophilicity, rather than number or positions of free hydroxyls (3,5 or 5,4'), determines the CYP3A4 inhibition capacity of polyphenols. IC_{50} values of 1.1 μM of resveratrol for 6β-testosterone hydroxylation were reported using the complementary DNA (cDNA) recombinant expressed human isoenzyme (Yu et al., 2003). In other studies, an IC_{50} value of 10 and 4 μM were determined using heterologously expressed CYP3A4 (Piver et al., 2001) and human liver microsomes, respectively. Similar experiments using heterologous expression in *Escherichia coli* showed an IC_{50} value of 6.8 μM (McLaughlin et al., 2008). Human microsomes appear to be more sensitive to inhibition, because the IC_{50} value for CYP3A-mediated testosterone 6β-hydroxylation in rat microsomes was observed to be much higher (20 versus 4 μM) (Piver et al., 2001). In a different study using Sf9 insect microsomes containing baculovirus-derived human CYP3A4 and NADPH-cytochrome CYP reductase, resveratrol inactivated CYP3A4 in a time- and NADPH-dependent manner, with rate (k_{inact}) and affinity (equilibrium dissociation constant for enzyme-inhibitor complex; K_I) of 0.2 min^{-1} and 20 μM, respectively (Chan and Delucchi, 2000). These values are in the range of the inhibitory potency of bergamottin (present in grapefruit juice), which is known as a strong inhibitor of CYP3A4 activity and displays a k_{inact} and K_i of 0.3 min^{-1} and 7.7 μM, respectively (He et al., 1998). Using human recombinant enzyme, resveratrol inhibited CYP3A4-mediated 7-benzyloxy-4-trifluoromethylcoumarin O-dealkylation with a K_i of 10.2 μM (Chang and Yeung, 2001).

Resveratrol seems to be a low-affinity substrate of CYP3A4 [Michaelis constant (K_m) of ~58 μM] (Regev-Shoshani et al., 2004). However, a specific metabolite of resveratrol deriving from the reaction with CYP3A4 has never been identified. Besides a noncompetitive inactivation between resveratrol and CYP3A4 (Chang and Yeung, 2001), it was speculated that epoxidation might occur at the ethylene bridge between the phenolic rings of resveratrol. A reactive p-benzoquinone methide derivative might be subsequently generated, followed by covalent modification of CYP3A4. This would agree with a suggested, irreversible, mechanism-based inactivation of CYP3A4 (Chan and Delucchi, 2000; Piver et al., 2001).

In a reporter gene assay, using the human pregnane X receptor and promoter regions of CYP3A4 transiently transfected into HepG2 cells, resveratrol had no influence on CYP3A4 messenger RNA expression (Raucy, 2003). Thus, resveratrol seems to interact with CYP3A4 by direct inhibition of enzyme activity, rather than by modulation of gene expression.

With respect to the major metabolite in human plasma (resveratrol-3-sulfate), no inhibition of CYP3A4 was observed up to the highest concentration (50 μM) tested (Yu et al., 2003). Using recombinant enzyme preparations and an NADPH-regenerating system, a high IC_{50} value for resveratrol-3-sulfate in the range of 16 μM was confirmed (unpublished data by M. Beck).

CYP1A1 and CYP1A2

A weak induction of CYP1A2 was shown *in vivo* after 4 weeks of 1 g of resveratrol per day in healthy volunteers by measuring the ratio between caffeine and the metabolite, paraxanthine (Chow et al., 2010). The induction was measured by comparing the concentration ratio of parent to metabolite after 4 hours in plasma. Induction resulted in a decrease in the metabolic ratio by a factor of 0.84. A moderate increase of CYP1A2 in the rat was detected in liver samples after induction with resveratrol (100 mg/kg b.w.) (Trusov et al., 2010). Also, Sergent et al. showed an increase in CYP1A1 activity after 24 hours in Caco-2 cells *in vitro* (Sergent et al., 2009).

In vitro resveratrol seems to be a weak inhibitor of CYP1A1/2. The IC_{50} value of resveratrol exceeded 50 μM in CYP1A2-dependent ethoxyresorufin deethylation using cDNA recombinant expressed human isoenzyme (Yu et al., 2003). Using the same type of activity test (ethoxyresorufin-O-dealkylase; EROD), similar IC_{50} values of 150, 40, and 30 μM were found in another study, using human liver microsomes or cells containing recombinant CYP1A1 and 1A2, respectively (Piver et al., 2001). Ciolino and Yeh found EROD activity (CYP1A1/2 inhibition) in microsomes from human HepG2 cells and in intact cells with a resveratrol IC_{50} value of 1.1 μM (Ciolino and Yeh, 1999). The calculated binding affinity was 0.42 μM. Interestingly, resveratrol proved to be a stronger inhibitor of CYP1A activity in rat microsomes (IC_{50} = 5 μM). In a further study, using human liver microsomes, resveratrol inhibited EROD activity (CYP1A1/2) weakly with an IC_{50} value of 1.1 mM (Chun et al., 1999). Interestingly, the IC_{50} value was lower [23 and 11 μM for EROD and methoxyresorufin-O-dealkylase (MROD) activity, respectively] when recombinant CYP1A1 enzyme was used. Inhibition of recombinant CYP1A2 was weak (IC_{50} = 1.2 and 0.58 mM for EROD and MROD activity, respectively). Resveratrol inhibited human recombinant CYP1A1 and 1A2 with a K_i of 1.2 and 15.5 μM, respectively. In contrast to CYP1A1, CYP1A2 inhibition was mechanism based and therefore irreversible (Chang et al., 2001).

Although the clinical data showed a weak induction, the published *in vitro* results for human CYP1A1/2 often indicate a moderate-to-weak inhibition with a wide IC_{50} range. Resveratrol seems to antagonize the transactivation of genes. This process is mediated by AHR interactions and has been verified in different cell types with various polycyclic aromatic hydrocarbons (7,12-dimethylbenz(a)anthracene, tetrachloro-dibenzo-*p*-dioxin, and benzo[*a*]-pyrene) (e.g., Casper et al., 1999). However, the ability of resveratrol to bind to AHR and act as a competitive antagonist of this receptor is controversial. Some investigators demonstrated that resveratrol suppresses CYP1A1 transcription by preventing the conversion of the ligand-bound cytosolic AHR into its nuclear DNA-binding form. For example, resveratrol prevented the induction of CYP1A1 in the lungs of mice after administration of the potent inducer, benzo[*a*] pyrene (Revel et al., 2003). Others have shown that the inhibitory activity of resveratrol rather takes place during

the interaction between AHR and the transcriptional complex. The discrepancy in the available experimental results is likely to be the result of technical differences in methodology (Gusman et al., 2001).

In a study with human liver microsomes, resveratrol was suggested to be metabolized by CYP1A2, giving rise to its metabolites (piceatannol and tetrahydroxystilbene M1) (Piver et al., 2004). The P450 dependence of the reactions was evidenced by its need of NADPH as well as by its inhibition by classical P450 inhibitors. In this context, it is noteworthy that the stability of piceatannol is poor because of its fast photo-oxidation in aqueous medium or at low concentrations (Gill et al., 1987).

CYP2D6

Data in humans showed a decrease of CYP2D6 activity after 4 weeks of 1 g of resveratrol per day (Chow et al., 2010). The metabolic ratio between dextromethorphan and dextrorphan increased in this study by a factor of 1.70, measured in the urine after 8 hours.

In vitro, resveratrol did not inhibit cDNA recombinantly expressed human isoenzyme. The IC_{50} value of CYP2D6-dependent bufuralol hydroxylation exceeded 50 μM (Yu et al., 2003). An IC_{50} value of 9.8 μM was reported using heterologously expressed CYP2D6 in *E. coli* (McLaughlin et al., 2008).

CYP2C9

Resveratrol ingestion of 1 g per day for 4 weeks decreased human CYP2C9 activity. In this study, the metabolic ratio in urine between losartan and its metabolite (E3174) was increased after 8 hours by a factor of 2.71 (Chow et al., 2010).

In vitro, resveratrol IC_{50} values exceeded 50 μM in CYP2C9-dependent diclofenac hydroxylation using cDNA recombinantly expressed human isoenzyme (Yu et al., 2003). On the other hand, an IC_{50} value of 2.3 μM was recorded in CYP2C9 using *E. coli* as an expression system (McLaughlin et al., 2008).

No CYP2C9 enzyme inhibition was observed with resveratrol-3-sulfate by Yu et al. (2003). In contrast, resveratrol-3-sulfate moderately inhibited CYP2C9 (IC_{50} of 9 μM) in an assay using human recombinant enzyme preparations (unpublished data by M. Beck).

CYP2C19

Resveratrol showed an IC_{50} value of 11.6 μM on CYP2C19-dependent (S)mephenytoin hydroxylation using the cDNA recombinantly expressed human isoenzyme. Resveratrol was considered to be a weak inhibitor of CYP2C19 (Yu et al., 2003).

CYP2E1

Resveratrol was shown to be a very weak, noncompetitive, reversible inhibitor of CYP2E1, with IC_{50} values of 75 and 150 μM in microsomes from rat and human liver, respectively (Piver et al., 2001). In liver microsomes of acetone-induced mice, resveratrol inhibited p-nitrophenol hydroxylase, an enzymatic marker of CYP2E1, with an IC_{50} value of 18.5 μM (Mikstacka et al., 2002).

CYP1B1 and CYP2B1/2

CYP1B1 has gained a lot of interest lately because of its overexpression in a wide variety of human tumors. It is hardly- or non-detectable in liver microsomes and catalyzes aromatic hydroxylation reactions. It is speculated that it might act as a tumor suppressor or "rescue" enzyme and serve to activate nontoxic dietary components into growth-inhibitory substances. Using a microsomal preparation of the human recombinant CYP1B1, resveratrol was found to be metabolized to piceatannol and a second tetrahydroxystilbene, M1 (Potter et al., 2002; Piver et al., 2004).

A moderate increase of CYP2B1/2 was detected in liver samples of resveratrol-treated rats (100 mg/kg b.w.) (Trusov et al., 2010). This stands in contrast to the results of Canistro et al., who showed a moderate reduction of CYP2B1/2 in male CD1 mice (Canistro et al., 2009).

Additional considerations

In vivo, resveratrol is extensively metabolized by phase II enzymes, which results in much lower levels of the aglycone than the corresponding resveratrol conjugates. Rapid, efficient conjugation of resveratrol (i.e., intestinal and hepatic first pass in humans) does not result in the inhibition of metabolizing enzymes, such as glutathione *S*-transferase and uridine diphosphate glucuronosyl transferase (UGT) (Chow et al., 2010). The phase II conjugates of resveratrol show no binding to CYP isoenzymes at relevant concentrations. No inhibition of CYP1A2, 2C19, 2D6, and CYP3A4 has been found in *in vitro* tests for the main metabolite observed in human plasma, resveratrol-3-sulfate (Yu et al., 2003). Only CYP2C9 showed some moderate inhibition (IC_{50} of 9 μM, human recombinant enzyme preparations; unpublished data by M. Beck).

In the rat, resveratrol (100 mg/kg b.w.) has no effect on phase II metabolism (i.e., quinone reductase, hemoxygenase-1, glutathione transferase, and UGT) (Trusov et al., 2010). However, high doses of resveratrol (0.3, 1.0, and 3 g/kg b.w./day for 4 weeks) have an effect on phase I and II detoxifying enzymes in rat liver. A general trend toward downregulating genes encoding phase I drug-metabolizing enzymes and to upregulating phase II response was observed. Enzyme expression and stress responses were studied using cDNA stress arrays coupled with drug-metabolizing enzymatic assays (Hebbar et al., 2005).

In addition to the relatively low resveratrol plasma levels resulting from fast metabolic conjugation, it is noteworthy that protein binding of resveratrol is high and in the range of 97–98% in both human and rat plasma (unpublished data by M. Beck).

Discussion

The aim of this review is to summarize the known facts about the *in vitro* and *in vivo* involvement of resveratrol

Drug Metabolism Reviews Downloaded from informahealthcare.com by 178.38.226.196 on 07/13/12
For personal use only.

© 2012 Informa Healthcare USA, Inc.

in CYP inhibition. Possible clinical risks, which might emerge from a resveratrol-CYP inhibition, shall be discussed below.

Resveratrol inhibition of CYPs: mechanism of inhibition

A broad range of therapeutic drugs, as well as herbal and dietary constituents, have been reported to undergo metabolic activation by metabolizing enzymes. Such reactive metabolites may bind covalently to various target proteins, such as the reactive site of metabolizing enzymes. Drug-protein adducts may cause toxicity either through immune-mediated mechanisms or mechanism-based inhibition (i.e., irreversible inactivation) of CYPs (Zhou et al., 2005).

It has been proposed that metabolism of resveratrol may yield chemically reactive metabolites, although the overall rate of metabolism of resveratrol by phase I enzymes seems to be very low (Chan and Delucchi, 2000; Piver et al., 2001). Resveratrol has the potential to inactivate CYP3A4, and possibly CYP1A2, by acting as a mechanism-based inhibitor. Bioactivation of chemicals is a common phenomenon. However, there is no direct link between the formation of protein-drug adducts and organ toxicity, which limits our ability to predict whether a reactive metabolite will be toxic or not (Evans et al., 2004). It has therefore been proposed that threshold values be defined for *in vivo* covalent protein binding (Evans et al., 2004), based on the observation that drugs given at daily doses of 10 mg or less are rarely, if ever, associated with a significant degree of adverse drug reactions related to reactive metabolites. In view of the very low systemic exposure of free resveratrol observed after dietary intake, as well as the very low rate of CYP-mediated metabolism of resveratrol, the risk for adverse reactions associated with systemic exposure to resveratrol should be negligible in the lower dose range. But, also for higher doses, no reactive metabolites for resveratrol have been reported to date.

It should be noted that resveratrol is most likely not one of the main constituents of red wine that causes CYP3A4 inactivation. Fractions of red wine, which did not contain resveratrol, inhibited CYP3A4 significantly *in vitro*. In addition, the resveratrol content in red wine was too low to account for the degree of CYP3A4 inactivation observed after red wine treatment. These results were corroborated by inactivation studies using a variety of red wine types. They showed that CYP3A4 inactivation did not correlate with resveratrol content (Chan and Delucchi, 2000; Piver et al., 2001).

Resveratrol inhibition of CYPs: drug-drug interactions affecting drug absorption

The reported resveratrol IC_{50} values for CYP3A4 activity are lower than for the other CYP isoenzymes (1–5 μM). In addition to potential hepatic CYP3A4 inhibition, there is an additional aspect to be considered, because this enzyme is also the predominant CYP present in the small intestine. For certain drugs that are good substrates of CYP3A4, hepatic extraction is not the main mechanism determining their bioavailability, because the intestinal metabolism by CYP3A4 is the body's first defense in limiting drug entry into the systemic circulation. A prominent "food and diet" representative for this kind of (clinically significant) selective intestinal CYP3A4 interaction is grapefruit juice (Kupferschmidt et al., 1995; Bailey et al., 1998; Ozdemir et al., 1998). Grapefruit juice augments the AUC and the C_{max} of several CYP3A4 substrates, including cyclosporine, felodipine, midazolam, nicardipine, nifidipine, saquinavir, and verapramil (Kupferschmidt et al., 1995; Bailey et al., 1998). Bergamottin, one of several active inhibitors in grapefruit juice, caused an increase of felodipine in C_{max} of 40% and in the AUC of 37% after administrating 12 mg orally to healthy volunteers (Goosen et al., 2004).

One clinical study in humans addressed the drug-interaction potential of red wine, compared to that of grapefruit juice, using cisapride (Offman et al., 2001). Because resveratrol probably is not the only CYP inhibitor in red wine, it is not possible to extrapolate the results directly to resveratrol ingested as a food supplement. However, the results indicate a potential for drug-drug interactions, because the IC_{50} values of both beverage extracts are at the same order of magnitude (Piver et al., 2001), and the mechanism of inactivation of CYP3A4 by resveratrol and bergamottin, a mechanism-based CYP3A4 inhibitor in grapefruit juice, might share some similarities.

With respect to resveratrol, it should be kept in mind that the concentrations in red wine are variable and rather low. Resveratrol concentrations in red wine typically range from 0.3 to up to 15 mg/L. A concentration of approximately 3 mg/L or 10–15 μM is considered realistic, but on the somewhat high side (Stervbo et al., 2007). Although 250 mL of grapefruit juice significantly increased the bioavailability of cisapride by more than 50%, the same volume of red wine had a much smaller effect, with an increase of 15% in both the AUC and C_{max}. In addition, compared to control (water), the difference with red wine was not statistically significant (Offman et al., 2001). However, in some individuals with a preexisting high intestinal CYP3A4 content, red wine caused a marked interaction similar to that of grapefruit juice. When compared to wine consumption (approximately 1 mg of resveratrol intake by one serving of 250 mL), the dose of resveratrol ingested as a supplement is much higher. For example, if 500 mg of resveratrol are dissolved in a gastrointestinal (GI) fluid volume of 250 mL (Zhang et al., 2008; Galetin et al., 2010), the possible resveratrol concentration at the site of absorption can be as high as 8.8 mM. This value exceeds the observed IC_{50} values for CYP3A4 inhibition (*in vitro*) by an order of magnitude of 3–4.

Supplement doses of resveratrol might lead to significant clinical interactions with drugs that are predominantly metabolized by intestinal CYP3A4. For example, in the male rat, moderate resveratrol doses of 2.5 and 10 mg/kg b.w. lead to an increase in oral bioavailability

Drug Metabolism Reviews Downloaded from informahealthcare.com by 178.38.226.196 on 07/13/12
For personal use only.

of diltiazem and nicardipine. For diltiazem, the C_{max} and AUC rose between 46 and 60% with 2.5 and 10 mg/kg b.w. of resveratrol, respectively (Hong et al., 2008). The C_{max} and AUC more than doubled for nicardipine (Choi et al., 2009). In these experiments, the observed effects were attributed to a reduced intestinal metabolism and elevated absorption, because the metabolic ratio of diltiazem to desacetyldiltiazem, a major metabolite of diltiazem, did not change with various doses of resveratrol. Further, it was shown, by *in vitro* experiments, that resveratrol in higher concentrations (100 μM) inhibited the activity of the drug-efflux transporter Pgp, which may have contributed to the increased drug absorption (Hong et al., 2008).

In humans, possible intestinal CYP3A4 inhibition by resveratrol is supported by a controlled study, which observed inhibition of CYP3A4 in healthy volunteers (Chow et al., 2010). In this study, volunteers ingested 1 g of resveratrol daily for 4 weeks. Considering the high dose, a rather low, 1.33-fold increase in AUC was observed for the CYP3A4 substrate buspirone. It should be noted that buspirone has a bioavailability of only 5% as the result of an extensive first-pass metabolism (Lilja et al., 1998). Therefore, the observed effects are most likely the result of inhibition of intestinal CYP3A4.

Altogether, data from *in vitro* experiments and animal and clinical trials point to a potential metabolic interaction of resveratrol with intestinal CYP3A4. The question arises as to whether the effect on concomitant intake of intestinal CYP3A4 substrate drugs other than buspirone is similar or more pronounced and, ultimately, if such interactions might be of clinical relevance (e.g., for drugs with a steep dose-response relationship or a narrow therapeutic range). Current data are not sufficient to define a resveratrol dose below which a drug interaction with intestinal CYP3A4 can be ruled out. In addition, it is difficult to extrapolate from animals to humans. Adapting doses between species can be done by normalization to b.w. (mg/kg b.w.) or by normalizing to body-surface area (mg/m^2) (FDA, 2005). Taking a dose of 2.5 mg/kg b.w. in rats and transfering it to a 60-kg person results in a corresponding dose of 24 or 150 mg of resveratrol normalized to the surface area or to b.w., respectively. This amount is in the range of resveratrol as sold commercially as a food supplement (Williams et al., 2009). However, to date, no drug interactions have been reported in patients who ingest resveratrol supplements in combination with drugs. More clinical trials will be needed to clarify the question of whether the observed *in vivo* and *in vitro* interactions of resveratrol with intestinal CYP3A4 is of clinical significance, and whether the concomitant intake of resveratrol with drugs that are metabolized mainly by intestinal CYP3A4 should be avoided.

Resveratrol inhibition of CYPs: drug-drug interactions affecting drug clearance

Resveratrol is generally accepted to be a moderate-to-weak inhibitor of CYPs. Concentrations required for *in vitro* inhibition of CYPs are mostly in the range of 1–100 μM. Lowest *in vitro* IC_{50} values were reported consistently for CYP3A4 inhibition (1–5 μM), whereas reported IC_{50} results varied widely for CYP1A1/2 (1 μM–1.2 mM), CYP2C9 (2.3 and >50 μM), and CYP2D6 (9.8 and >50 μM). CYP2C19 displayed an IC_{50} value of 11.6 μM, and CYP2E1 showed a value above 50 μM. For an overview, see Tables 3 and 4.

The question arises as to whether this inhibitory potential of resveratrol could possibly lead to systemic drug-drug interactions. A quantitative assessment of interaction potentials is often carried out on the basis of the I/K_i ratio (Blanchard et al., 2004). In this formula,

Table 3. Reported IC_{50} values of CYP inhibition by resveratrol: isolated enzymes.

Isoform	Substrate	Species	IC_{50} (μM)	K_i (μM)	Reference
CYP3A4	Cyclosporine	Human	4.5		(Regev-Shoshani et al., 2004)
	Testosterone	Human	1.4		(Regev-Shoshani et al., 2004)
	(6β-OH formation)		10		(Piver et al., 2001)
			1.1		(Yu et al., 2003)
			<10	20	(Chan and Delucchi, 2000)
	BFC *O*-dealkylation	Human		10.2	(Chang and Yeung, 2001)
	DBF	Human	6.8		(McLaughlin et al., 2008)
CYP1A1	EROD	Human	40		(Piver et al., 2001)
				1.2	(Chang et al., 2001)
	EROD/MROD	Human	23/11		(Chun et al., 1999)
CYP1A2	EROD	Human	>50		(Yu et al., 2003)
			30		(Piver et al., 2001)
				15.5	(Chang et al., 2001)
	EROD/MROD	Human	1,200/580		(Chun et al., 1999)
CYP2D6	bufuralol hydroxylation	Human	>50		(Yu et al., 2003)
	AMMC		9.8		(McLaughlin et al., 2008)
CYP2C9	Diclofenac hydroxylation	Human	>50		(Yu et al., 2003)
	VIVID CYP2C9 Red	Human	2.3		(McLaughlin et al., 2008)
CYP2C19	(S)-mephenytoin hydroxylation	Human	11.6		(Yu et al., 2003)

DBF, dibenzyl fluorescein; AMMC, 3-[2-(N,N-diethyl-N-methylammonium)-ethyl]-7-methoxy-4-methylcoumarin.

© 2012 Informa Healthcare USA, Inc.

Drug Metabolism Reviews Downloaded from informahealthcare.com by 178.38.226.196 on 07/13/12
For personal use only.

"I" corresponds to the inhibitor concentrations at the site of metabolism, a value that can be approximated by the unbound concentrations in the systemic circulation. "K_i" represents the constant of inhibition, which is usually lower than the IC_{50} value, depending on the K_m and substrate concentration (Todesco et al., 2009). The substitution of K_i by the IC_{50} value at the ratio of I/K_i tends therefore to underestimate the risk of interactions. An I/K_i ratio >0.1 and <1 is considered to be indicative of a medium risk of *in vivo* drug-drug interactions, whereas an I/K_i ratio >1 is often associated with a high risk of clinically significant drug-drug interactions. In the case of resveratrol, K_i or IC_{50} values in the range between 1 and 10 μM are more than 10-fold higher than concentrations in systemic circulation after an intake of doses of resveratrol up to 500 mg. Very high levels of resveratrol (= aglycone) in plasma can only be reached with extremely high doses and/or special drug formulations, such as micronization, as outlined in Table 5. The maximum plasma concentration of resveratrol observed in humans was in the micromolar range of (8.5 μM = 1.942 μg/mL) after oral intake of 5 g of micronized resveratrol. Considering *in vitro* measured IC_{50} values, the risk of drug interactions is higher for CYP3A4 than for the other CYPs. Therefore, the potential for systemic drug-drug interaction must be considered at very high doses (e.g., >1 g) of resveratrol, especially for CYP3A4. However, these results should be discussed in the context of the high protein binding of resveratrol, which reduces the risk of an interaction.

In mice, resveratrol inhibits AHR-mediated transcriptional activation of CYP1A1 and thus may interfere with the induction and/or upregulation of CYP1A1 (Revel et al., 2003). In contrast, the clinical study by Chow et al. revealed an increase in CYP1A2 activity (Chow et al., 2010), which is also regulated by AHR (Nebert et al., 2000). Whether these differences are dose or species

Table 4. Reported IC_{50} values of CYP inhibition by resveratrol: liver microsomes.

Isoform	Substrate	Species	IC_{50} (μM)	Reference
CYP3A4	Testosterone (6β-OH)	Human	4	(Piver et al., 2001)
CYP3A		Rat	20	(Piver et al., 2001)
CYP1A2	EROD	Human	150	(Piver et al., 2001)
CYP1A1/2	EROD	Rat	5	(Piver et al., 2001)
		Human	1,100	(Chun et al., 1999)
		Human HepG2	1.1[a]	(Ciolino and Yeh, 1999)
CYP2E1	Chlorozoxazone 6-OH	Human	150	(Piver et al., 2001)
		Rat	75	(Piver et al., 2001)

[a]K_i (calc): 0.42 μM; also inhibition of CYP1A1 transcription.

Table 5. Maximal plasma concentration of resveratrol aglycone.

Species	Dose	Dosing	Route	C_{max} (μg/mL)	C_{max} (μM)	Reference
Rabbit	20 mg/kg	Single	Oral	0.25	1.1	(Asensi et al., 2002)
Rat	50 mg/kg	Single	Oral	1.5	6.57	(Marier et al., 2002)
Mouse	20 mg/kg	Single	Oral	0.6	2.6	(Piver et al., 2003)
	230 mg/kg	Single	i.g.	7.3	32	(Sale et al., 2004)
	4,000 mg/kg	Single	Oral	6.85	30	(Crowell et al., 2004b)
Human	25 mg	Single	Oral	0.0071	0.031	(Soleas et al., 2001)
		Single	Oral	0.0079	0.034	(Goldberg et al., 2003)
		Single	Oral	0.0015	0.007	(Almeida et al., 2009)
	50 mg	Single	Oral	0.0066	0.029	(Almeida et al., 2009)
	100 mg	Single	Oral	0.0214	0.094	(Almeida et al., 2009)
	150 mg	Single	Oral	0.0248	0.109	(Almeida et al., 2009)
	200 mg	Single	Oral	0.0249	0.109	(Nunes et al., 2009)
	0.5 g	Single	Oral	0.073	0.318	(Boocock et al., 2007)
		Daily[b]	Oral	0.044	0.19	(Brown et al., 2010)
	1 g	Single	Oral	0.117	0.513	(Boocock et al., 2007)
		Daily[b]	Oral	0.141	0.62	(Brown et al., 2010)
		Single	Oral	0.073	0.320	(Chow et al., 2010)
	2.5 g	Single	Oral	0.268	1.174	(Boocock et al., 2007)
		Daily[b]	Oral	0.331	1.45	(Brown et al., 2010)
	5 g	Single	Oral	0.539	2.361	(Boocock et al., 2007)
		Daily[b]	Oral	0.967	4.24	(Brown et al., 2010)
	5 g[a]	Daily[c]	Oral	1.942	8.5	(Howells et al., 2011)

[a]Micronized formulation. [b]Daily dosing, plasma sampled over 21–28 days. [c]Daily dosing, plasma sampled over 10–21 days.
i.g., intragastrical.

Drug Metabolism Reviews Downloaded from informahealthcare.com by 178.38.226.196 on 07/13/12
For personal use only.

dependent needs to be verified in further studies. It should be noted that a potentially beneficial effect of the modulation of CYP1A1/2 resulting from reduced activation of procarcinogens is controversial (Revel et al., 2003; Chow et al., 2010).

Moderate inhibition of CYP2C9 was also observed in the clinical study by Chow et al. In plasma, resveratrol-3-sulfate reached more than 50-fold higher concentrations than the unconjugated compound. Therefore, the CYP2C9 inhibition may be explained by interactions of CYP2C9 with the metabolite, resveratrol-3-sulfate.

In the study by Chow et al., the metabolic ratios of the concentrations of the metabolite to the parent compound were indicated for several CYPs. The published changes in metabolic ratios (parent compound/metabolites) were 1.70 and 2.71 for CYP2D6 and 2C9, respectively, and 0.84 for CYP1A2. These changes in the metabolic ratios of CYP1A2, 2D6, and 2C9 cannot be translated directly into an absolute value of C_{max} and AUC for the parent compound, because an increase in the numerator (parent compound) can be assumed to be followed in parallel by a decrease in the denominator (metabolite) in the case of enzyme inhibition, assuming that there is only one relevant metabolic pathway. Therefore, an increase in the metabolic ratio by a factor of 2 does not indicate an inhibition of parent drug degradation by 50%. Metabolic ratios therefore display the consequence of enzyme inhibition or induction in a qualitative way. This is in contrast to changes in AUC values, which give a quantitative measure of altered drug exposure. With respect to the study of Chow et al., the changes in metabolic ratios were more dramatic than the changes in the absolute values of C_{max} and AUC. Nevertheless, inhibition of the metabolism of drugs, such as warfarin or sulfonylureas, by resveratrol may be clinically relevant, because these compounds have a very narrow therapeutic range.

While estimating a potential drug-drug interaction for a patient, it must be considered that interindividual differences exist, such as various genetic polymorphism, especially considering CYP2D6 and 2C9 (Meyer, 2000; Weinshilboum, 2003). On the other hand, there are interindividual variances in the expression levels of various CYP isoenzymes (Bebia et al., 2004). These differences are the cause for large variations in baseline metabolic ratios, even without any potential inhibitor. A range of 0.002–7.96 was measured in 38 volunteers as the ratio of the CYP2D6 substrate, dextromethorphan, to dextrorphan (Chow et al., 2010). This variability, combined with a variation of systemic resveratrol concentrations between 0.036 and 1.77 μM after a single dose of 1 g of resveratrol, makes a general conclusion regarding systemic drug-drug interactions difficult. It is conceivable that, in patients reaching high systemic concentrations after oral ingestion of resveratrol, not only intestinal, but also hepatic interactions of CYPs could occur. However, it must be stated that, for doses below several hundred milligrams, the risk of clinically significant drug-drug interactions on the hepatic level is probably minimal.

Potential benefits of resveratrol and side effects in clinical trials

Any inhibition of CYP activity leading to a potential drug-drug interaction must be discussed in the context of the clinically relevant dosing regimens. In the case of resveratrol, potential pharmacological effects are difficult to interpret in a dose- and time-dependent manner. Although work is ongoing evaluating the appropriate dose and clinical use of resveratrol, so far no clinical application has been established (Smoliga et al., 2011; Vang et al., 2011). However, indirect evidence from *in vitro* studies and *in vivo* animal experiments point to potential health benefits, such as cardiovascular protective effects. In addition, preliminary clinical trials using doses that exceeded those provided by resveratrol occurring naturally in red wine induced effects that suggested a contribution to human health (Smoliga et al., 2011). These studies can be summarized as follows.

Life extension has been shown in mice fed with a high-calorie diet when resveratrol was added to the diet (Baur et al., 2006). However, further studies showed that resveratrol does not prolong the lifespan of mice fed with a standard diet (Pearson et al., 2008).

First favorable effects in humans are occurring. Most recently, it has been demonstrated that supplementation with 75 mg of resveratrol twice-daily for 30 days induced metabolic changes that mimic the effect of calorie restriction in obese human volunteers (Timmers et al., 2011).

Resveratrol also possesses cancer-preventive activity in the micromolar range (Jang et al., 1997). Therefore, several attempts were made to achieve micromolar systemic concentrations of resveratrol, despite its extensive first-pass metabolism. High dosages of 5 g of resveratrol per day were well tolerated in healthy volunteers and resulted in plasma concentrations of 2.4 and 4.24 μM after single and multiple dosing for up to 28 days, respectively (Boocock et al., 2007; Brown et al., 2010). Metabolites such as monoglucuronides and resveratrol-3-sulfate exceeded the parent resveratrol considerably in terms of C_{max} and AUC. The secretion of insulin-like growth factor-1, which is associated with higher risk of colorectal cancer (Sandhu et al., 2002), seemed to be inhibited. However, repeated dosing resulted in mild or moderate GI symptoms. Therefore, further clinical studies were suggested to be limited to 1 g per day (Brown et al., 2010; Patel et al., 2011).

Even higher plasma concentrations were achieved in humans by using an altered pharmaceutical formulation. Daily doses of 5 g of micronized resveratrol (Sirtris SRT501) were administrated for 14 days, resulting in high bioavailability and reaching average plasma levels of 8.5 μM of resveratrol with C_{max} values up to 21.4 μM in one individual (Howells et al., 2011). An indication that very high dosages of resveratrol have some drawbacks can be derived from the announcement that a clinical phase II trial using this micronized compound formulation (SRT501) in patients suffering from multiple myeloma was stopped prematurely (Sirtris and GlaxoSmithKline,

Drug Metabolism Reviews Downloaded from informahealthcare.com by 178.38.226.196 on 07/13/12
For personal use only.

© 2012 Informa Healthcare USA, Inc.

Drug Metabolism Reviews Downloaded from informahealthcare.com by 178.38.226.196 on 07/13/12
For personal use only.

2011). Details of the study have not been made available yet to the scientific community. It should be noted that rats treated with up to 300 mg/kg b.w. showed no adverse effects, whereas at much higher repeated doses of 3,000 mg/kg b.w., renal toxicity was observed (Crowell et al., 2004a). Further studies concluded a no observed adverse effect level of a nominal 750 mg/kg b.w. level of resveratrol in rats (Williams et al., 2009; Edwards et al., 2011). Extrapolating a dose of 750 mg/kg b.w. in the rat to a human without any safety margin, based on b.w. conversion or body-surface area conversion, leads to doses of 52.5 g per 70 kg or 8.5 g per 70 kg b.w., respectively (FDA, 2005; Edwards et al., 2011).

First human studies also focus on the putative beneficial effects of resveratrol in strengthening endogeneous antioxidant defenses to promote vasodilatiation and cardiovascular health. In a randomized, double-blind, placebo-controlled crossover study, single doses of 250 and 500 mg of resveratrol were shown to modulate cerebral blood flow dose-dependently in healthy volunteers (Kennedy et al., 2010). Promising data on humans were also obtained by administrating unique dosages of 30, 90, or 270 mg of resveratrol to overweight/obese volunteers. In this double-blind, crossover study, a significant increase in flow-mediated dilatation of the brachial artery (FMD) was measured. FMD is an independent indicator of the risk factor for the development of cardiovascular diseases (Wong et al., 2011). Remarkable is the fact that between the 30- and 270-mg dose, only a very weak increase of the FMD was shown, whereas the difference between 30 mg and placebo was already significant. Further studies should verify whether this effect persists over time with continuous resveratrol intake and whether the higher dose of 270 versus 30 mg provides any advantages resulting in clinically measurable effects.

The proposed beneficial effect of low-dose resveratrol, found in several food compositions, and an increase in FMD between 30- and 270-mg doses demonstrates that the general assumption of higher doses equaling better effects is questionable (Calabrese et al., 2010). Indeed, under some experimental conditions, beneficial effects of resveratrol are more pronounced at lower concentrations or doses. This is the case for endothelial progenitor cells (EPCs) *in vitro* and *in vivo* (Gu et al., 2006). *In vitro* concentrations of 1 μM of resveratrol significantly induced EPC proliferation, migration, and adhension capacity, whereas 60 μM significantly inhibited these effects. This is compatible with the observation that 10 mg/kg of oral resveratrol showed a significant increase in circulating EPCs in a rat model of aorta repair, whereas 50 mg/kg was not effective.

Conclusion

Resveratrol is a moderate-to-weak inhibitor of hepatic CYP enzymes only. Concentrations required for *in vitro* CYP inhibition are mostly in the range of 1–100 μM. IC_{50} values of resveratrol for CYP3A4 activity (1–5 μM) are consistently lower than for the other CYPs. Inductive effects can be observed for CYP1A1/2. *In vivo*, resveratrol is rapidly and efficiently conjugated presystemically, and systemic levels of the free resveratrol aglycon are far below concentrations of the conjugates. High plasma protein binding of resveratrol further reduces the risk of any relevant inhibition of "victim" drug clearance. No inhibition of CYPs by resveratrol conjugates has been documented so far. Unpublished data point to an inhibitory potential of resveratrol-3-sulfate toward CYP2C9.

For the ingestion of resveratrol in the range of a few milligrams per day, which corresponds to resveratrol doses contained in an average serving of red wine, the risk of systemic or intestinal resveratrol-drug interactions is minimal when taking into account the low concentrations reached in the gut and systemic circulation. The use of low-milligram doses of resveratrol as a food supplement should not lead to critical interactions with the intestinal metabolism of coadministered drugs.

Interaction studies in rats between resveratrol and diltiazem or nicardipine lead to a more cautious recommendation for higher doses of resveratrol. Although high doses of resveratrol (in the range 1 g/day or above) are well tolerated by healthy volunteers, the administration of such doses can potentially lead to clinically significant resveratrol-drug interactions resulting from inhibition of intestinal CYP3A4 and/or Pgp. This is especially relevant for drugs with a high intestinal first-pass effect, such as certain calcium-channel blockers, sildenafil, midazolam, and nefazodone. Therefore, ingestion of several hundred milligrams per day of resveratrol as a food supplement may be a risk for patients treated with drugs that possess a narrow therapeutic range and undergo extensive intestinal metabolization. In such patients, the risk of drug interactions exceeds the potential health benefits of resveratrol and should be avoided.

To answer the question of whether and to what extent resveratrol can interact with various drugs, appropriate interaction studies in humans are required, for example, with warfarin (CYP2C9 substrate) and with felodipine or midazolam (CYP3A4 substrate with a high presystemic interaction). Such trials should focus on the absolute bioavailability of the parent compound, and not only on the metabolic ratio, to allow for a quantitative assessment of the interaction potential of resveratrol.

Acknowledgments

The continuous support of Dr. Paul Beilstein (DSM Ltd) is acknowledged. The authors thank Mark Inglin for proofreading of the manuscript for this article.

Declaration of interest

P.D. is supported by a public grant for a Ph.D. thesis project awarded by the Senglet Foundation (Basel, Switzerland). The company DSM markets resveratrol as a food supplement under the trade name Resvida®. M.B. is an employee of DSM Nutritional Products Ltd.

References

Almeida, L., Vaz-da-Silva, M., Falcão, A., Soares, E., Costa, R., Loureiro, A. I., et al. (2009). Pharmacokinetic and safety profile of trans-resveratrol in a rising multiple-dose study in healthy volunteers. Mol Nutr Food Res 53(Suppl 1):S7–S15.

Asensi, M., Medina, I., Ortega, A., Carretero, J., Baño, M. C., Obrador, E., et al. (2002). Inhibition of cancer growth by resveratrol is related to its low bioavailability. Free Radic Biol Med 33:387–398.

Bailey, D. G., Malcolm, J., Arnold, O., Spence, J. D. (1998). Grapefruit juice-drug interactions. Br J Clin Pharmacol 46:101–110.

Baur, J. A., Pearson, K. J., Price, N. L., Jamieson, H. A., Lerin, C., Kalra, A., et al. (2006). Resveratrol improves health and survival of mice on a high-calorie diet. Nature 444:337–342.

Bebia, Z., Buch, S. C., Wilson, J. W., Frye, R. F., Romkes, M., Cecchetti, A., et al. (2004). Bioequivalence revisited: influence of age and sex on CYP enzymes. Clin Pharmacol Ther 76:618–627.

Blanchard, N., Richert, L., Coassolo, P., Lavé, T. (2004). Qualitative and quantitative assessment of drug-drug interaction potential in man, based on Ki, IC50, and inhibitor concentration. Curr Drug Metab 5:147–156.

Bogaards, J. J., Bertrand, M., Jackson, P., Oudshoorn, M. J., Weaver, R. J., van Bladeren, P. J., et al. (2000). Determining the best animal model for human cytochrome P450 activities: a comparison of mouse, rat, rabbit, dog, micropig, monkey, and man. Xenobiotica 30:1131–1152.

Boocock, D. J., Faust, G. E. S., Patel, K. R., Schinas, A. M., Brown, V. A., Ducharme, M. P., et al. (2007). Phase I dose escalation pharmacokinetic study in healthy volunteers of resveratrol, a potential cancer chemopreventive agent. Cancer Epidemiol Biomarkers Prev 16:1246–1252.

Brown, V. A., Patel, K. R., Viskaduraki, M., Crowell, J. A., Perloff, M., Booth, T. D., et al. (2010). Repeat dose study of the cancer chemopreventive agent resveratrol in healthy volunteers: safety, pharmacokinetics, and effect on the insulin-like growth factor axis. Cancer Res 70:9003–9011.

Calabrese, E. J., Mattson, M. P., Calabrese, V. (2010). Resveratrol commonly displays hormesis: occurrence and biomedical significance. Hum Exp Toxicol 29:980–1015.

Canistro, D., Bonamassa, B., Pozzetti, L., Sapone, A., Abdel-Rahman, S. Z., Biagi, G. L., et al. (2009). Alteration of xenobiotic metabolizing enzymes by resveratrol in liver and lung of CD1 mice. Food Chem Toxicol 47:454–461.

Casper, R. F., Quesne, M., Rogers, I. M., Shirota, T., Jolivet, A., Milgrom, E., et al. (1999). Resveratrol has antagonist activity on the aryl hydrocarbon receptor: implications for prevention of dioxin toxicity. Mol Pharmacol 56:784–790.

Chan, W. K., Delucchi, A. B. (2000). Resveratrol, a red wine constituent, is a mechanism-based inactivator of cytochrome P450 3A4. Life Sci 67:3103–3112.

Chan, W. K., Nguyen, L. T., Miller, V. P., Harris, R. Z. (1998). Mechanism-based inactivation of human cytochrome P450 3A4 by grapefruit juice and red wine. Life Sci 62:PL135–PL142.

Chang, T. K., Chen, J., Lee, W. B. (2001). Differential inhibition and inactivation of human CYP1 enzymes by trans-resveratrol: evidence for mechanism-based inactivation of CYP1A2. J Pharmacol Exp Ther 299:874–882.

Chang, T. K., Yeung, R. K. (2001). Effect of trans-resveratrol on 7-benzyloxy-4-trifluoromethylcoumarin O-dealkylation catalyzed by human recombinant CYP3A4 and CYP3A5. Can J Physiol Pharmacol 79:220–226.

Choi, J.-S., Choi, B.-C., Kang, K. W. (2009). Effect of resveratrol on the pharmacokinetics of oral and intravenous nicardipine in rats: possible role of P-glycoprotein inhibition by resveratrol. Pharmazie 64:49–52.

Chow, H.-H. S., Garland, L. L., Hsu, C.-H., Vining, D. R., Chew, W. M., Miller, J. A., et al. (2010). Resveratrol modulates drug- and carcinogen-metabolizing enzymes in a healthy volunteer study. Cancer Prev Res (Phila) 3:1168–1175.

Chun, Y. J., Kim, M. Y., Guengerich, F. P. (1999). Resveratrol is a selective human cytochrome P450 1A1 inhibitor. Biochem Biophys Res Commun 262:20–24.

Ciolino, H. P., Yeh, G. C. (1999). Inhibition of aryl hydrocarbon-induced cytochrome P-450 1A1 enzyme activity and CYP1A1 expression by resveratrol. Mol Pharmacol 56:760–767.

Crowell, J. A., Korytko, P. J., Morrissey, R. L., Booth, T. D., Levine, B. S. (2004a). Resveratrol-associated renal toxicity. Toxicol Sci 82:614–619.

Crowell, J. A., Levine, B. S., McCormick, D. L. (2004b). Resveratrol: drug development for cancer prevention (abstract no. 356) In: Abstracts of the 10th International Congress of Toxicology, July 11–15, 2004, Tampere, Finland. Toxicol Appl Pharmacol 197:218.

Delcò, F., Tchambaz, L., Schlienger, R., Drewe, J., Krähenbühl, S. (2005). Dose adjustment in patients with liver disease. Drug Saf 28:529–545.

Edwards, J. A., Beck, M., Riegger, C., Bausch, J. (2011). Safety of resveratrol with examples for high purity, trans-resveratrol, resVida®. Ann N Y Acad Sci 1215:131–137.

Evans, D. C., Watt, A. P., Nicoll-Griffith, D. A., Baillie, T. A. (2004). Drug-protein adducts: an industry perspective on minimizing the potential for drug bioactivation in drug discovery and development. Chem Res Toxicol 17:3–16.

Galetin, A., Gertz, M., Houston, J. B. (2010). Contribution of intestinal cytochrome p450-mediated metabolism to drug-drug inhibition and induction interactions. Drug Metab Pharmacokinet 25:28–47.

Gill, M. T., Bajaj, R., Chang, C. J., Nichols, D. E., McLaughlin, J. L. (1987). 3,3′,5′-Tri-O-methylpiceatannol and 4,3′,5′-tri-O-methylpiceatannol: improvements over piceatannol in bioactivity. J Nat Prod 50:36–40.

Goldberg, D. M., Yan, J., Soleas, G. J. (2003). Absorption of three wine-related polyphenols in three different matrices by healthy subjects. Clin Biochem 36:79–87.

Goosen, T. C., Cillié, D., Bailey, D. G., Yu, C., He, K., Hollenberg, P. F., et al. (2004). Bergamottin contribution to the grapefruit juice-felodipine interaction and disposition in humans. Clin Pharmacol Ther 76:607–617.

Gu, J., Wang, C., Fan, H., Ding, H., Xie, X., Xu, Y., et al. (2006). Effects of resveratrol on endothelial progenitor cells and their contributions to reendothelialization in intima-injured rats. J Cardiovasc Pharmacol 47:711–721.

Gusman, J., Malonne, H., Atassi, G. (2001). A reappraisal of the potential chemopreventive and chemotherapeutic properties of resveratrol. Carcinogenesis 22:1111–1117.

He, K., Iyer, K. R., Hayes, R. N., Sinz, M. W., Woolf, T. F., Hollenberg, P. F. (1998). Inactivation of cytochrome P450 3A4 by bergamottin, a component of grapefruit juice. Chem Res Toxicol 11:252–259.

Hebbar, V., Shen, G., Hu, R., Kim, B.-R., Chen, C., Korytko, P. J., et al. (2005). Toxicogenomics of resveratrol in rat liver. Life Sci 76:2299–2314.

Hong, S.-P., Choi, D.-H., Choi, J.-S. (2008). Effects of resveratrol on the pharmacokinetics of diltiazem and its major metabolite, desacetyldiltiazem, in rats. Cardiovasc Ther 26:269–275.

Howells, L. M., Berry, D. P., Elliott, P. J., Jacobson, E. W., Hoffmann, E., Hegarty, B., et al. (2011). Phase I randomized, double-blind pilot study of micronized resveratrol (SRT501) in patients with hepatic metastases—safety, pharmacokinetics, and pharmacodynamics. Cancer Prev Res (Phila) 4:1419–1425.

Ingelman-Sundberg, M. (2004). Human drug metabolising cytochrome P450 enzymes: properties and polymorphisms. Arch Pharmacol 369:89–104.

Jang, M., Cai, L., Udeani, G. O., Slowing, K. V., Thomas, C. F., Beecher, C. W., et al. (1997). Cancer chemopreventive activity of resveratrol, a natural product derived from grapes. Science 275:218–220.

Kennedy, D. O., Wightman, E. L., Reay, J. L., Lietz, G., Okello, E. J., Wilde, A., et al. (2010). Effects of resveratrol on cerebral blood flow variables and cognitive performance in humans: a double-blind, placebo-controlled, crossover investigation. Am J Clin Nutr 91:1590–1597.

Drug Metabolism Reviews Downloaded from informahealthcare.com by 178.38.226.196 on 07/13/12
For personal use only.

© 2012 Informa Healthcare USA, Inc.

Drug Metabolism Reviews Downloaded from informahealthcare.com by 178.38.226.196 on 07/13/12
For personal use only.

Kondratyuk, T. P., Park, E.-J., Marler, L. E., Ahn, S., Yuan, Y., Choi, Y., et al. (2011). Resveratrol derivatives as promising chemopreventive agents with improved potency and selectivity. Mol Nutr Food Res 55:1249–1265.

Kopp, P. (1998). Resveratrol, a phytoestrogen found in red wine. A possible explanation for the conundrum of the "French paradox"? Eur J Endocrinol 138:619–620.

Kupferschmidt, H. H., Ha, H. R., Ziegler, W. H., Meier, P. J., Krähenbühl, S. (1995). Interaction between grapefruit juice and midazolam in humans. Clin Pharmacol Ther 58:20–28.

Lilja, J. J., Kivistö, K. T., Backman, J. T., Lamberg, T. S., Neuvonen, P. J. (1998). Grapefruit juice substantially increases plasma concentrations of buspirone. Clin Pharmacol Ther 64:655–660.

Marier, J.-F., Vachon, P., Gritsas, A., Zhang, J., Moreau, J.-P., Ducharme, M. P. (2002). Metabolism and disposition of resveratrol in rats: extent of absorption, glucuronidation, and enterohepatic recirculation evidenced by a linked-rat model. J Pharmacol Exp Ther 302:369–373.

Martignoni, M., Groothuis, G. M., de Kanter, R. (2006). Species differences between mouse, rat, dog, monkey and human CYP-mediated drug metabolism, inhibition and induction. Expert Opin Drug Metab Toxicol 2:875–894.

McLaughlin, L. A., Dickmann, L. J., Wolf, C. R., Henderson, C. J. (2008). Functional expression and comparative characterization of nine murine cytochromes P450 by fluorescent inhibition screening. Drug Metab Dispos 36:1322–1331.

Meyer, U. A. (2000). Pharmacogenetics and adverse drug reactions. Lancet 356:1667–1671.

Mikstacka, R., Gnojkowski, J., Baer-Dubowska, W. (2002). Effect of natural phenols on the catalytic activity of cytochrome P450 2E1. Acta Biochim Pol 49:917–925.

Mugford, C. A., Kedderis, G. L. (1998). Sex-dependent metabolism of xenobiotics. Drug Metab Rev 30:441–498.

Nebert, D. W., Roe, A. L., Dieter, M. Z., Solis, W. A., Yang, Y., Dalton, T. P. (2000). Role of the aromatic hydrocarbon receptor and [Ah] gene battery in the oxidative stress response, cell cycle control, and apoptosis. Biochem Pharmacol 59:65–85.

Nunes, T., Almeida, L., Rocha, J.-F., Falcão, A., Fernandes-Lopes, C., Loureiro, A. I., et al. (2009). Pharmacokinetics of trans-resveratrol following repeated administration in healthy elderly and young subjects. J Clin Pharmacol 49:1477–1482.

Offman, E. M., Freeman, D. J., Dresser, G. K., Munoz, C., Bend, J. R., Bailey, D. G. (2001). Red wine-cisapride interaction: comparison with grapefruit juice. Clin Pharmacol Ther 70:17–23.

Ozdemir, M., Aktan, Y., Boydag, B. S., Cingi, M. I., Musmul, A. (1998). Interaction between grapefruit juice and diazepam in humans. Eur J Drug Metab Pharmacokinet 23:55–59.

Patel, K. R., Scott, E., Brown, V. A., Gescher, A. J., Steward, W. P., Brown, K. (2011). Clinical trials of resveratrol. Ann N Y Acad Sci 1215:161–169.

Pearson, K. J., Baur, J. A., Lewis, K. N., Peshkin, L., Price, N. L., Labinskyy, N., et al. (2008). Resveratrol delays age-related deterioration and mimics transcriptional aspects of dietary restriction without extending life span. Cell Metab 8:157–168.

Piver, B., Berthou, F., Dreano, Y., Lucas, D. (2001). Inhibition of CYP3A, CYP1A, and CYP2E1 activities by resveratrol and other non volatile red wine components. Toxicol Lett 125:83–91.

Piver, B., Berthou, F., Dreano, Y., Lucas, D. (2003). Differential inhibition of human cytochrome P450 enzymes by epsilon-viniferin, the dimer of resveratrol: comparison with resveratrol and polyphenols from alcoholized beverages. Life Sci 73:1199–1213.

Piver B, Fer M, Vitrac X, Merillon J-M, Dreano Y, Berthou F, Lucas D. (2004). Involvement of cytochrome P450 1A2 in the biotransformation of trans-resveratrol in human liver microsomes. Biochem Pharmacol 68:773–782.

Potter, G. A., Patterson, L. H., Wanogho, E., Perry, P. J., Butler, P. C., Ijaz, T., et al. (2002). The cancer preventative agent resveratrol is converted to the anticancer agent piceatannol by the cytochrome P450 enzyme CYP1B1. Br J Cancer 86:774–778.

Raucy, J. L. (2003). Regulation of CYP3A4 expression in human hepatocytes by pharmaceuticals and natural products. Drug Metab Dispos 31:533–539.

Regev-Shoshani, G., Shoseyov, O., Kerem, Z. (2004). Influence of lipophilicity on the interactions of hydroxy stilbenes with cytochrome P450 3A4. Biochem Biophys Res Commun 323:668–673.

Revel, A., Raanani, H., Younglai, E., Xu, J., Rogers, I., Han, R., et al. (2003). Resveratrol, a natural aryl hydrocarbon receptor antagonist, protects lung from DNA damage and apoptosis caused by benzo[a] pyrene. J Appl Toxicol 23:255–261.

Sale, S., Verschoyle, R. D., Boocock, D., Jones, D. J. L., Wilsher, N., Ruparelia, K. C., et al. (2004). Pharmacokinetics in mice and growth-inhibitory properties of the putative cancer chemopreventive agent resveratrol and the synthetic analogue trans 3,4,5,4′-tetramethoxystilbene. Br J Cancer 90:736–744.

Sandhu, M. S., Dunger, D. B., Giovannucci, E. L. (2002). Insulin, insulin-like growth factor-I (IGF-I), IGF binding proteins, their biologic interactions, and colorectal cancer. J Natl Cancer Inst 94:972–980.

Sergent, T., Dupont, I., Van der Heiden, E., Scippo, M.-L., Pussemier, L., Larondelle, Y., et al. (2009). CYP1A1 and CYP3A4 modulation by dietary flavonoids in human intestinal Caco-2 cells. Toxicol Lett 191:216–222.

Sirtris, GlaxoSmithKline. (2011). A clinical study to assess the safety and activity of SRT501 alone or in combination with bortezomib in patients with multiple myeloma. In: ClinicalTrials.gov [Online]. Bethesda (MD): National Library of Medicine (US). Available at: http://clinicaltrials.gov/show/NCT00920556 NLM Identifier: NCT00920556. Accessed on December 2, 2011.

Smoliga, J. M., Baur, J. A., Hausenblas, H. A. (2011). Resveratrol and health—a comprehensive review of human clinical trials. Mol Nutr Food Res 55:1129–1141.

Snyder, S. A., Gollner, A., Chiriac, M. I. (2011). Regioselective reactions for programmable resveratrol oligomer synthesis. Nature 474:461–466.

Soleas, G. J., Yan, J., Goldberg, D. M. (2001). Ultrasensitive assay for three polyphenols (catechin, quercetin and resveratrol) and their conjugates in biological fluids utilizing gas chromatography with mass selective detection. J Chromatogr B Biomed Sci Appl 757:161–172.

Stervbo, U., Vang, O., Bonnesen, C. (2007). A review of the content of the putative chemopreventive phytoalexin resveratrol in red wine. Food Chem 101:449–457.

Timmers, S., Konings, E., Bilet, L., Houtkooper, R. H., van de Weijer, T., Goossens, G. H., et al. (2011). Calorie restriction-like effects of 30 days of resveratrol supplementation on energy metabolism and metabolic profile in obese humans. Cell Metab 14:612–622.

Todesco, L., Bodmer, M., Vonwil, K., Häussinger, D., Krähenbühl, S. (2009). Interaction between pivaloylcarnitine and L-carnitine transport into L6 cells overexpressing hOCTN2. Chem Biol Interact 180:472–477.

Trusov, N. V., Guseva, G. V., Aksenov, I. V., Avren'eva, L. I., Kravchenko, L. V., Tutelyan, V. A. (2010). Effects of combined treatment with resveratrol and indole-3-carbinol. Bull Exp Biol Med 149:213–218.

Tsunoda, S. M., Harris, R. Z., Christians U., Velez, R. L., Freeman, R. B., Benet, L. Z., et al. (2001). Red wine decreases cyclosporine bioavailability. Clin Pharmacol Ther 70:462–467.

U.S. FDA (2005). Guidance for industry: estimating the maximum safe starting dose in initial clinical trials for therapeutics in adult healthy volunteers. [Online]. Silver Spring, Maryland, USA: FDA. Available at: http://www.fda.gov/downloads/Drugs/GuidanceComplianceRegulatoryInformation/Guidances/ucm078932.pdf. Accessed on 06 December 2011.

Vang, O., Ahmad, N., Baile, C. A., Baur, J. A., Brown, K., Csiszar, A., et al. (2011). What is new for an old molecule? Systematic review and recommendations on the use of resveratrol. PLoS ONE 6:e19881.

Weinshilboum, R. (2003). Inheritance and drug response. N Engl J Med 348:529–537.

Williams, L. D., Burdock, G. A., Edwards, J. A., Beck, M., Bausch, J. (2009). Safety studies conducted on high-purity trans-resveratrol in experimental animals. Food Chem Toxicol 47:2170–2182.

Wong, R. H. X., Howe, P. R. C., Buckley, J. D., Coates, A. M., Kunz, I., Berry, N. M. (2011). Acute resveratrol supplementation improves flow-mediated dilatation in overweight/obese individuals with mildly elevated blood pressure. Nutr Metab Cardiovasc Dis 21:851–856.

Yang, C. S., Pan, E. (2012). The effects of green tea polyphenols on drug metabolism. Expert Opin Drug Metab Toxicology 8:677–689.

Yu, C., Shin, Y. G., Kosmeder, J. W., Pezzuto, J. M., van Breemen, R. B. (2003). Liquid chromatography/tandem mass spectrometric determination of inhibition of human cytochrome P450 isozymes by resveratrol and resveratrol-3-sulfate. Rapid Commun Mass Spectrom 17:307–313.

Yu, W., Fu, Y.-C., Wang, W. (2011). Cellular and molecular effects of resveratrol in health and disease. J Cell Biochem 113:752–759.

Zhang, L., Zhang, Y. D., Strong, J. M., Reynolds, K. S., Huang, S.-M. (2008). A regulatory viewpoint on transporter-based drug interactions. Xenobiotica 38:709–724.

Zhou, S., Yung Chan, S., Cher Goh, B., Chan, E., Duan, W., Huang, M., et al. (2005). Mechanism-based inhibition of cytochrome P450 3A4 by therapeutic drugs. Clin Pharmacokinet 44:279–304.

Zhou, S.-F., Liu, J.-P., Chowbay, B. (2009). Polymorphism of human cytochrome P450 enzymes and its clinical impact. Drug Metab Rev 41:89–295.

Drug Metabolism Reviews Downloaded from informahealthcare.com by 178.38.226.196 on 07/13/12
For personal use only.

© 2012 Informa Healthcare USA, Inc.